UNIVERSITÀ DEGLI STUDI DELL'AQUILA
DIPARTIMENTO DI INGEGNERIA INDUSTRIALE E DELL'INFORMAZIONE E DI ECONOMIA

Dottorato di Ricerca in Ingegneria Industriale e dell'Informazione e di Economia

Curriculum Ingegneria Meccanica, Energetica e Gestionale

XXXIII Ciclo

Titolo della tesi

Cooling of Electric Machines Using Advanced Coolants

SSD ING-IND/10 Fisica Tecnica Industriale

Dottorando

Ali Deriszadeh

Coordinatore del corso

Prof. Giuseppe Ferri

Tutor

Prof. Filippo de Monte

A.A. 2019/2020

Abstract

The aim of this research is to investigate the adaption of advanced coolants and phase change materials for electric machines in electric/hybrid vehicle applications. The study uses Al_2O_3 nanoparticles to enhance the heat transfer ability of liquid cooling systems employing the commonly used cooling jacket approach. Employing advanced coolants to improve the heat transfer performance of cooling systems with minimal changes in their structure can be considered as a cost-effective and practical approach to meet the requirements of vehicle applications. In line with this goal, in this research, both heat transfer and fluid flow behaviors of cooling systems employing nanofluids are investigated. In this way, the feasibility and effectiveness of the cooling system can be justified by taking practical criteria into account. Results of the study are used to find the trade-off between the heat transfer and fluid flow behaviors of the under-study nanofluid coolant to achieve the best possible overall performance. 3D CFD analyses are used to evaluate the cooling systems proposed in this research.

Since the applications considered in this research are electric machines used in electric vehicles, the losses of the electric machine were calculated under standard driving cycles. From the results, it was found that there are frequent peak power demands resulting in several peak losses. Also, it was observed that the values of peak losses are several times the mean value of electric machine losses. Considering this property of heat production in electric machines used in electric vehicle applications and the prominent property of phase change materials that have a high latent heat capacity, in this research a hybrid cooling system consisting of a passive cooling part based on phase change materials and an active cooling part based on liquid cooling method was designed. The results of the analyses showed that the phase change material is able to properly store excess thermal energy and the active cooling part assists the passive cooling part by rejecting the stored thermal energy to prepare the phase change material for the next peak heating cycle.

ACKNOWLEDGMENTS

First and foremost, I would like to express my deep and sincere gratitude to my supervisor, Professor. Filippo de Monte**,** who was of great help and inspiration during the different stages of doing this PhD research. I am also grateful to Professors. Giuseppe Ferri, Marco Villani, Marco Tursini and Roberto Cipollone who gave me valuable help throughout my PhD program. Thanks also go to Dr. Giampaolo D'Alessandro, Dr. Lino Di Leonardo, Dr. Giuseppe Fabri, Dr. Davide Di Battista and Dr. Marco Di Bartolomeo for their precious assistance. Finally, I appreciate my family for their support and patience.

This thesis is sincerely dedicated to my parents, Hasneh Solhamal and Vahab Deriszadeh, who showed me the true love in life and to my loving brothers, Abbas Deriszadeh and Adel Deriszadeh.

CONTENTS

LIST OF TABLES

LIST OF FIGURES

1. INTRODUCTION

1.1 PROBLEM STATEMENT

Manufacturing cost is one of the barriers to the widespread use of Electric Vehicles (EVs). As the electric motor is one of the most important components in the powertrain structure of EVs, their cost can play an important role in the production cost of EVs. Therefore, maximum utilization of electric motor torque production capability is desired for EV applications [1]. This becomes more important when considering the high power/torque demand profile of electric motors used in electric vehicles. The highly dynamic nature of the power/torque demands in electric vehicle applications is the function of the driver's behavior and the number of frequent stops and starts. In these applications, the demanded peak torque can be several times the rated torque of the electric motor.

One of the factors that is effective in sizing the electric motor is the ratio of peak power to rated power. On the other hand, the most important factor involved in the ability of the electric motor to produce peak torque several times greater than its nominal torque is the ability of the electric motor cooling system [2, 3]. Thus, for given peak power and rated power, the electric motor size can be reduced if the electric motor cooling system possesses a high performance.

In addition to the effect of the cooling system on the sizing of electric motors, the performance of the electric motor can be negatively affected by the increase in temperature if the cooling system is incapable of controlling the temperature by dissipating the heat flux generated by the electric motor [4-6]. Therefore, the cooling system is a key factor in satisfying the performance and reliability of electric motors.

Without a high-performance cooling system, enhancement in the torque density cannot be achieved. Appropriate heat removal can lift up limits of maximum current density and repetitive peak powers. This means that for a given volume, greater torque can be generated.

1.2 OBJECTIVES AND THESIS ORGANIZATION

In response to the mentioned requirements, the main goal of this thesis is defined to investigate the trade-off among the performance, practicability, and cost of proposed cooling systems. Therefore, it is tried to investigate solutions that can improve the performance of the cooling system without a significant increase in cost, energy consumption, and complexity. One important factor in the cost reduction is the structural simplicity of the cooling system that can make it a general solution applicable to a wider range of electric machines. In this regard, the cooling jacket approach was chosen. Cooling systems based on the cooling jacket are the most common cooling methods for electric machine applications, in which a coolant absorbs the heat flux generated by the electric motor from the stator outer surface avoiding excessive temperature rising [7-10]. Cooling jackets can be a part of electric machine housing regardless of the internal topology of the electric machine. Modifying the structural geometry and employing advanced coolants can improve the performance of the cooling system. Therefore, in this thesis, improving the overall performance of the cooling system for electric machines is investigated in terms of structural geometry modification and employing advanced coolants.

State of the art review on cooling systems of electric machines is presented in Chapter 2. Properties and evaluation methods of employing nanofluids as

advanced coolants are discussed in Chapter 3. In Chapter 4, heat transfer of Phase Change Materials (PCMs) is studied.

To create a platform for the targeted investigations, several 3D models of the cooling system based on the cooling jacket approach are built. The cooling jacket surrounds the stator and end-winding areas of stator windings. Channels have rectangular and circular cross-sections. In Chapter 5, a set of studies are performed on cooling jackets with rectangular channels. In Chapter 5, coolants are chosen as mixtures of water and Ethylene Glycol with various mixture ratios. Moreover, to investigate the effect of different structural geometries, a various number of channel turns are considered. 3D CFD analyses are performed for each combination of different geometries and mixture ratios. The overall performance of each scenario is investigated on the basis of a defined performance evaluation index.

To improve the cooling performance of the under-study cooling system through employing advanced coolants, the effects of adding nanoparticles into the base fluid are investigated in Chapter 6. In line with this goal, to increase the heat transfer capability of the cooling system and to reduce operating temperatures of the electric machine, Aluminum-oxide nanoparticles are added into the base fluid (pure water). To correctly evaluate the performance of the cooling system, both fluid flow and heat transfer performances are evaluated. Also, the effect of the flow rate of the cooling fluid and turns number of spiral channels of the electric machine cooling jacket on heat transfer capability and fluid flow performance of the cooling system are studied.

Passive cooling techniques are promising in regard to their no energy consumption. In Chapter 7, cooling systems based on employing Phase Changed Materials (PCMs) are studied for electric machine applications. PCM-based cooling systems take advantage of the high latent heat absorbance capability of PCMs during phase change processes. A metal-based PCM that possesses a higher thermal conductivity compared to Paraffin that is a common PCM studied in the literature is selected. Three different cooling systems are investigated in Chapter 7. In the first study, entire the cooling

jacket is filed by PCM creating a completely passive cooling system. In the second scenario, PCM is used in spiral paths with different channel turns. Finally, a combination of the passive PCM-based cooling system and the water-cooling system is investigated. Changes in the temperature of PCM, rotor and stator temperatures, and volume fraction liquid phase of PCM in different geometric arrangements are investigated. In all cases, it was observed that employing PCM in a totally passive cooling system can maintain the electric motor's operating temperature within the allowed range but for a certain amount of time. Actually, after the melting process, the heat transfer capability of the cooling system significantly deteriorated. This makes the PCM-based passive cooling system suitable for short-time heat removal needs. This property of PCM-based cooling systems brings to mind the idea that a combination of passive PCM-based cooling system and active cooling system with an advanced coolant can be a promising choice for electric machine applications. In this way, the PCM-based passive cooling system acts on top of the water-cooling active cooling system. So that the PCM-based part of the cooling system is responsible for absorbing excessive heat generated at repetitive peak power operating points and the spiral channel nanofluid cooling system is responsible for removing the heat generated by more frequently operating modes of the electric motor at rated power or lower.

2. LITERATURE REVIEW

2.1 INTRODUCTION

State of the art on cooling system techniques for electric machines is reviewed in this chapter. The literature review covers various categories of electric machine cooling system topologies.

2.2 THE NEED FOR HEAT MANAGEMENT OF ELECTRIC MACHINES

Overheating reduces the performance and durability of electric machines. This increases the need to use and improve the performance of thermal management systems. Especially that the tendency of manufacturers and consumers of electric machines is to build and use electric machines with high performance and reliability. Therefore, to prevent damage caused by overheating, special attention should be paid to the design of thermal management systems.

From the point of view of reducing costs as well as adapting electric machines for applications with size constraints, manufacturers intend to decrease the size of electric machines. It means that the trend is to increase the power density of electric machines. An increase in power density indicates that designing an efficient cooling system for the safe performance of electric

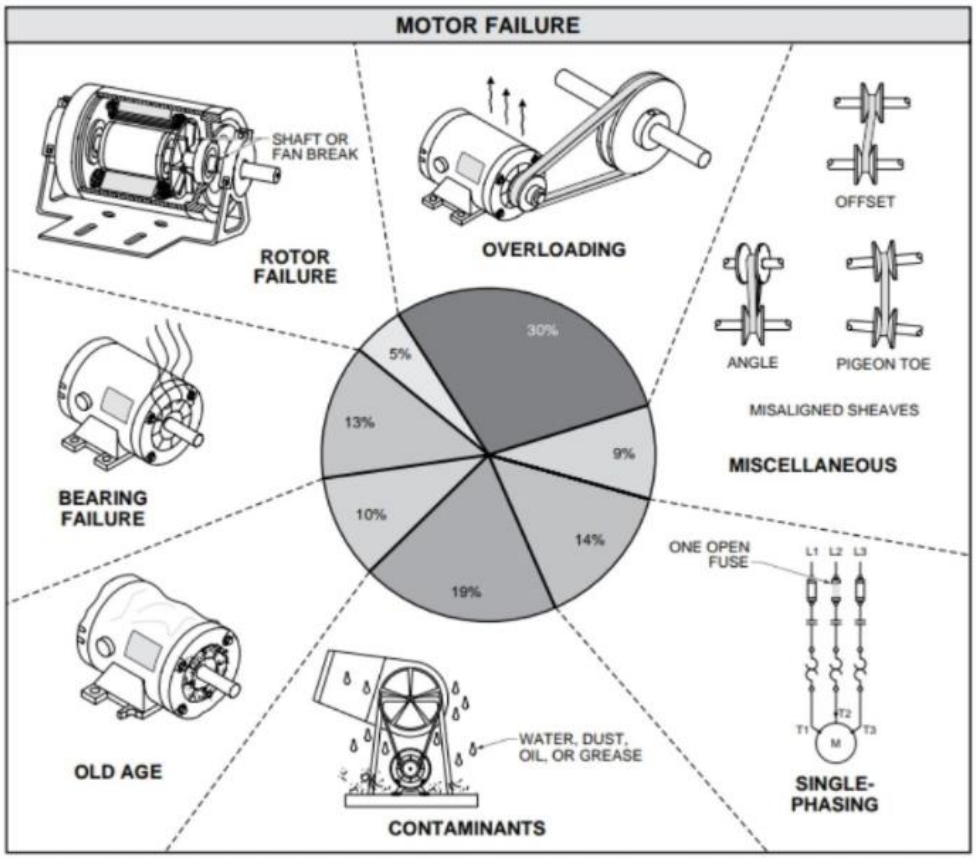

Figure 2. 1. Reasons for defects in electric machines [12].

machines with high power density is necessary and thermal management plays a critical role in their developments [11].

Several reasons including overheating, wrong mechanical coupling, voltage unbalance, exposure to contaminants, etc. can lead to failure of electric machines (Figure 2.1) [12]. Among them, overheating is the major factor in damaging electrical machines [12].

In general, for all electric/electronics devices, damages such as perforation, moving metal devices caused by inserted momentum from electrons, and intermetallic growth are related to overheating effects. In fact, the rate of such damages increases significantly with the increase of temperature. Even if overheating does not cause any of the mentioned failures, it can interfere with the normal operation of the device. For example, as the result of overheating, the movement of free electrons inside semiconductors increases leading to noises in signals [13].

The normal operation of electric machines as power conversion devices consumes energy and generates heat. Therefore, electric machines are designed for a specific operating temperature range depending on their type of operation. To prevent failures, it is necessary to keep the temperature of electric machines within the allowable range to prevent a drop in performance and damage to the electric machine. As a result, thermal management for electric machines is of high importance. In general, according to RESEARCH AND MARKETS, the global market of thermal management materials and devices is predicted to worth $16 billion by 2024 [14].

The commonest method for cooling electrical motors is through the obligatory movement of the air. This method may not be practical and effective for applications of new electrical machines due to reasons such as reliability, weight, and noise. Consequently, designing efficient cooling systems for countering this challenge is of high importance and affects the performance of electric machines directly [15].

2.3 HEAT MANAGEMENT SYSTEMS FOR ELECTRIC MACHINES

Heat can be generated in different parts of an electric machine. The generated heat can be transferred to the outer surface of the electric machine by various heat transfer mechanisms and through adjacent parts. There are several methods to transfer heat and cooling an electric machine.

In general, cooling methods are divided into two categories of active and passive methods according to the mechanism of heat transfer to the environment. Passive cooling methods are based on the natural movement of heat transfer and without consuming any energy. On the contrary, active cooling methods need energy consumption and an active external system of thermal desorption such as forced air movement, cooling with liquid, refrigeration system, etc. [16].

2.3.1 ACTIVE COOLING SYSTEMS

Active methods are used for high heat desorption from electric machines. Active cooling methods have high cooling capacities [17]. Employing active cooling systems, the temperature can be controlled and even kept below the environment temperature. In order to justify the adoption of active cooling systems, their reliability, power consumption, and maintenance requirements must be considered. Forced cooling with airflow or liquid, liquid or air-jet, thermoelectric cooling, and refrigeration system are examples of active cooling systems [18,19].

A common kind of active cooling systems is the movement of airflow by employing a fan. In comparison with natural transfer used in passive cooling methods, the coefficient of heat transfer is higher in active methods, and this coefficient increases with the increase of airflow rate. The major drawback of employing the forced air-cooling system is the decrease in reliability and increase of sound regarding the use of moving components.

Among the many other methods of active cooling, cooling systems based on the Peltier effect employ semiconductors for thermal management. These cooling systems have advantages such as high cooling capacity, small size, having great service life and, not having moving components. In a Peltier device, electric current flows through a pair of semiconductors. The side having a negative charge becomes cooler and the side having a positive charge becomes hotter. The negative electrode is attached to the surface that must become cold, while the positive electrode will be attached to the surface that transfers heat to the environment. High expenses and low electro-thermal efficiency are disadvantages of employing Peltier devices for thermal management [20].

Liquid cooling is another common active cooling method. In this method, heat is desorbed from the electric machine by pumping liquid. These systems include a pump, heat exchanger, and cooling plates. Liquid flow absorbs heat from cooling plates and transfers them to a heat exchanger where heat is transferred to the environment. Because of the high thermal capacity of liquid

and lower thermal resistance between the heated surface and liquid compared to air, liquid cooling systems are able to desorb high heat flux. The main disadvantages of liquid cooling systems are high expenses and complexity [21].

2.3.2 PASSIVE COOLING SYSTEMS

Compared to active cooling systems, passive cooling systems have no moving parts and also do not require energy consumption. These reduce the manufacturing cost of the cooling system, reduce its maintenance requirements, and increase its reliability. Although the cooling capacity of passive cooling systems is less than that of active cooling systems, they are very popular due to the mentioned advantages and are widely used in applications that do not require high cooling capacity. In these applications, employing passive cooling systems is the superior option. Air cooling based on the natural movement of air and phase changed material cooling systems are among the passive cooling systems [22].

Employing Finned housing for electric machines allows the implementation of passive cooling. In this case, cooling is achieved through the natural movement of the air between fins installed on the housing of the electric machine. Advantages include low cost, simple structure, and high reliability. However, it should be noted that the cooling capacity is low regarding the size of the electric machine due to the use of natural convection. Material, space, number, height, distance between fins, thickness, and orientation (vertical, horizontal, or radial) of fins are the factors that affect the performance of natural cooled electric machines. In the end, adopting the natural cooling method leads to increased reliability at the cost of building a heavier electric machine with a low current density [23].

Employing heat pipes can improve the heat transfer performance of passive cooling systems. Heat pipes do not desorb heat but transfer it to another place. Heat pipes are used as a part of thermal management systems of electric machines to distribute and transfer the generated heat effectively. Employing heat pipes in passive cooling systems improves the heat transfer ability of the

system leading to a smaller and lighter passive cooling system. In these systems, heat pipes transfer the heat to the surface of the stator in a passive way to be dissipated from the stator surface by means of natural convection [24].

2.4 ELECTRIC MOTOR COOLING SYSTEM CATEGORIES

Various cooling techniques for electric machines can be categorized into the following categories.

2.4.1 HEAT REMOVAL FROM THE SURFACE OF ELECTRIC MACHINES

The generated heat from different sources inside the electric machine is conducted to the external housing of the electric machine. The transferred heat is a significant part of the internally generated heat. Integrated heat extraction fins and ducts improve the heat transfer to the housing. Also, externally mounted fins provide a larger surface for the sake of heat removal. The conducted heat to the external surface can be removed by means of external cooling systems or through natural convection.

2.4.1.1 NATURAL CONVECTION (FREE COOLING)

In the case of natural cooling, two types of fins can be employed to improve the performance of the cooling system. Integrated heat extraction fins/ducts enhance heat transfer from inside the electric machine to its housing. On the other hand, the transferred heat is dissipated by means of convection and radiation heat transfers from the external surface of the electric machine housing. Usually, the housing external surface is smooth. There is a possibility to increase the convection surface with the help of external fins mounted on the housing. In this way, external fins increase the convection surface between the housing and environment air leading to increased heat removal. It should be noted that orientation, length, and spacing between fins significantly affect the convection heat transfer process of passive natural

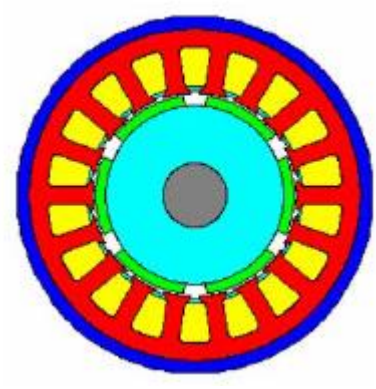

(a)

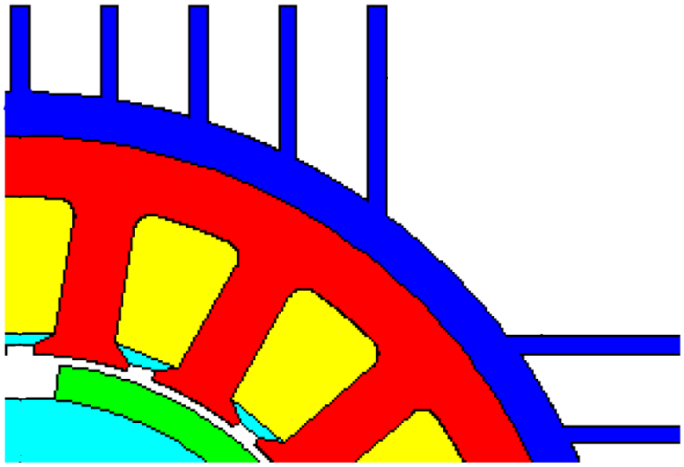

(b)

Figure 2. 2. Electric machine housings for natural convection cooling, (a) smooth housing, (b) housing with perpendicular fins [27, 28].

convection cooling [25]. Fins must be mounted in a way not reducing the natural airflow [26]. To achieve that, in the case of employing fins, they must be mounted perpendicular to the electric machine rotor shaft. Figure 2.2 depicts an example of the smooth housing and the housing with fins mounted perpendicular to the external surface of the electric machine housing. Since the thermal resistance between solid surfaces and the air is very large, the heat transfer capability of the natural convection cooling method is limited. Therefore, the natural convection method is suitable for low-power electric machines or very large electric machines with a substantial convection surface allowing an enhanced heat transfer through the convection heat transfer process [27].

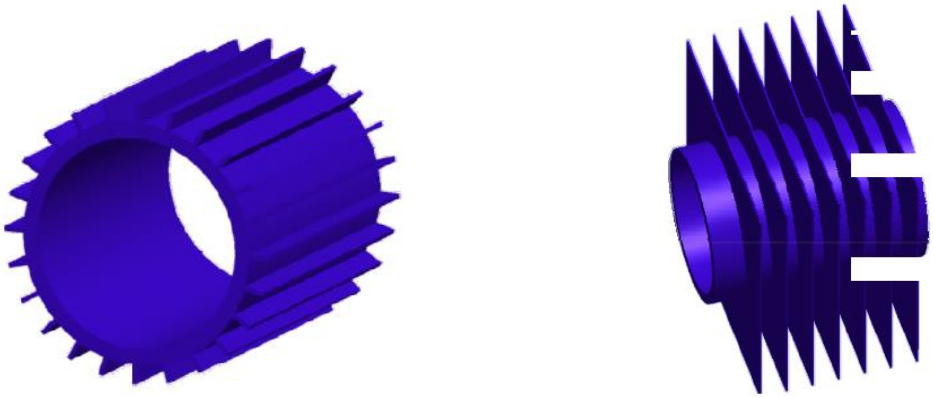

Figure 2. 3. Axial (left) and radial (right) fins [30].

The usage of the natural convection method for a 12 KW 5-phase Brushless DC motor was reported in [29]. In this design, radial fins were mounted on the external surface of the electric machine. After optimization of the electric machine, it was found that the housing with radial fans is a significant portion of the whole electric machine size. In [30], a permanent magnet synchronous machine was designed for aerospace actuation applications. In this study, the natural convection cooling performances of housing with axial fins and housing with radial fines were evaluated in terms of the heat transfer performance and volume of the cooling system. It was found that in the case of employing radial fines, the convection heat transfer is greater and the volume of the cooling system is smaller. This is because radial fins are mounted vertically and not reduce the natural airflow that is critical for the heat removal from the surface in natural convection cooling systems. Both examined fins configurations are shown in Figure 2.3.

An optimization method based on 2D analysis without using lumped thermal networks was proposed in [31]. It is shown that design parameters such as the height of fins, the distance between adjacent fins, the width of fins, and their orientation significantly affect the heat transfer performance of the cooling system. Using the proposed 2D model, it is possible to speed up the selection process among various possible fins arrangements prior to 3D CFD analysis. Various housing structural designs were compared in [32]. The evaluated housing structures are shown in Figure 2.4. It was found that the housing with Square and standard frames have a larger heat transfer coefficient compared

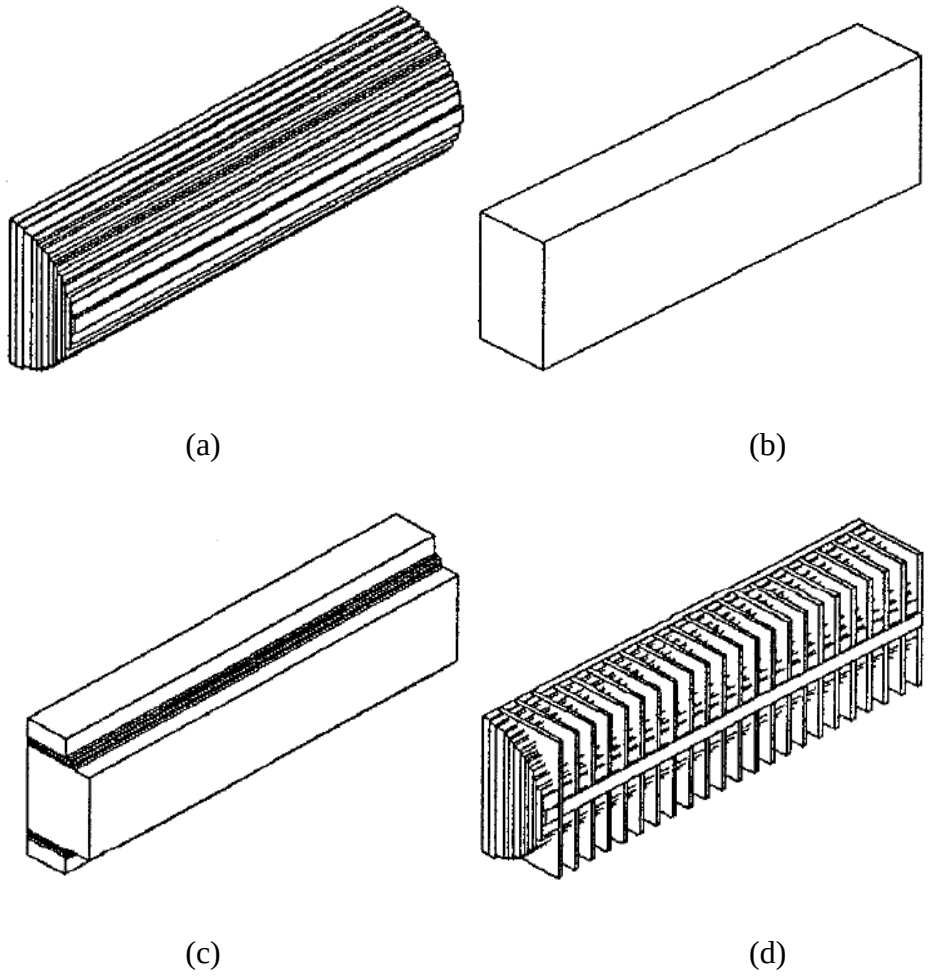

Figure 2. 4. Modelled housing types, (a) cylindrical, square, standard, with mounted radial fins [32].

to the cylindrical housing frame. Also, the housing with radial fines has a heat transfer coefficient of 2 to 3 times of housings without fines. Again, these results confirm that mounting fins can lead to an improved heat transfer performance if they do not disturb the natural airflow.

The possibility of adapting the natural convection cooling for a permanent magnet synchronous machine for airliner high lift actuator was investigated in [33]. It was found that in order to fulfill lifetime and reliability requirements, in the case of adopting the natural cooling method, the length of the electric machine must be increased significantly making the natural cooling inappropriate for this application. An axial permanent magnet

machine for wind turbine application was designed [34]. In this design natural cooling was chosen. It was concluded as the speed of the electric machine is low, the natural cooling method leads to a proper heat removal and successful thermal management of the electric machine.

2.4.1.2 SELF-COOLING AND EXTERNAL COOLING

In this cooling technique, heat removal is carried out by fluid flow receiving its flow power from the electric machine itself. In this way, rotation of the electric machine shaft is exploited to move fluid without any external power [35]. This can be achieved by installing a fan on the shaft [36] or a pump directly driven by the shaft [37]. In the case of generator applications, a fan or a pump can be directly powered from the generated electrical energy by the electric machine itself. In the case of using the fan driven by the shaft, its heat transfer performance is limited by the shaft speed so that at low speeds flow rate of the fluid reduces leading to a reduced heat transfer performance. According to the International Protection (IP) 54 or NEMA, fan-cooled electric motors are recommended for applications with the rated power up to 300 KW [38]. Figure 2.5 shows a structure of an electric machine employing the forced-air cooling system by installing an internal fan on the shaft [36].

Another way of forced air-cooling system is to employ an external fan. The cooling system in this method consists of fans or pumps driven independently by means of their own electric motor [39]. Therefore, the heat transfer performance of external cooling systems is not limited by the shaft speed of the electric machine.

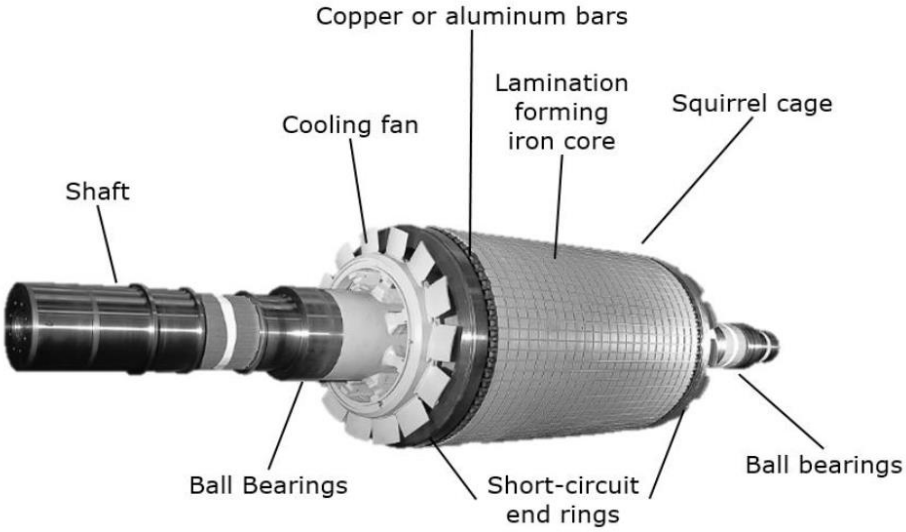

Figure 2. 5. Forced-air cooling by an internal fan [36].

Self-cooling techniques were evaluated for large induction machines with 2-15 MW [40]. The evaluation experimental results showed that the self-ventilated cooling system is feasible for high-power applications. In this study, modifying the geometrical structure of the cooling system, the stator temperature rise was reduced by 10%. Modified fan blades were developed for self-cooling large electric motors [41]. The goal of the modification was to reduce ventilation resistance to increase the flow rate and heat transfer capability of the cooling system. It was observed that the modified fan can increase the airflow by 80% and reduce the stator average temperature by 30%. In [42], a totally enclosed electric machine with an internal fan was designed for traction applications. As the designed motor is enclosed so can reduce the dust-intake and reduce acoustic noise. Experimental tests under the continuous rated load depicted that the temperature rise of the motor is maintained below the defined temperature limits. Another modified blade configuration for self-cooling systems using an internal fan was proposed in [43]. It was shown that the modified fan can improve the flow rate by 90% while noise is reduced. Moreover, because the ventilation resistance is

reduced, the modified fan is derived by 50% less power compared to the conventional internal fan leading to an increased efficiency of the electric machine. CFD analysis of a radial internal fan for electric machine applications was reported in [44]. According to the analysis, the flow rate can be maximized when there is no counter-pressure. The derived relationships of the analysis can be used for the sizing of the internal fan. A self-cooling permanent magnet machine was designed in [45]. Applying some modifications such as vent holes in the rotor structure, it was demonstrated that more uniform cooling performance is achieved through the rotor. The results showed that the temperature rise of permanent magnets can be reduced by up to 20%. A self-cooling system for an 11 KW induction machine was designed in [46]. The design goal was to increase heat transfer of the cooling system in the end-winding area. Using a combination of stirrers mounted on the shaft with direct control of the end-winding porosity, it was reported that the thermal resistance between the end-winding area and frame can be reduced by 12% leading to the increased heat transfer performance in the end-winding area. Another investigation about the cooling of end-winding regions was performed in [47]. According to the results, it was suggested that for a self-cooling electric machine to achieve an adequate heat transfer at the end-winding area, high air velocities on the end shield and direct airflow into the end-winding area are required.

The thermal performance of a 1.65 MW permanent magnet synchronous machine employing forced-air cooling with an external fan was investigated [48]. It was concluded that the number of ventilation holes on the frame significantly affects the consistency of the air flow distribution so that larger numbers of ventilation holes lead to a more uniform air flow distribution. The uniform airflow distribution leads to a uniform heat removal.

2.4.2 CLOSED-CIRCUIT COOLING

Closed-circuit cooling methods consist of two parts. In each part, the cooling fluid flows in a closed circuit. The first part of the cooling system transfers the generated internal heat of the electric machine to an outer surface to the second part of the cooling system. Then, heat removal is carried out by the

secondary cooling system. Closed-circuit cooling systems have an extended heat transfer performance compared to the previous categories mentioned above. Therefore, closed-circuit cooling systems are preferred for high power density electric machines. Various cooling systems are included under this category. The secondary cooling system can be integrated into the electric machine or installed separately. Most of the closed-circuit cooling systems exploit the high heat transfer capability of liquid coolants in their secondary cooling system part.

The heat transfer performance of a water-cooling cooling system for permanent magnet retarder applications was investigated in [49]. The thermal performance of the designed retarder was compared to an air-cooled retarder with the same structure. Experimental results showed that the water-cooled retarder could reach a temperature balance after operating at 1500 RPM after 4 minutes and its temperature remains below 100 ˚C. But, under the same load, the temperature of the air-cooled counterpart reached 500 ˚C after 3 minutes.

A direct oil cooling for electric machines used in traction applications was designed in [50]. The cooling system includes oil channels in the stator and in the housing. It was shown that although the existence of oil ducts in the stator reduces the produced torque by 1%, the oil cooling system can reduce the average temperature rise by 50%, compared to the cooling system without direct oil channels in the stator. A water-cooling system for a permanent magnet linear machine was designed in [51]. The structure of the machine and its cooling system are shown in Figure 2.6 According to the results, it was demonstrated that employing the water-cooling system, the temperature rise is remarkably reduced. It was found that employing the water-cooling system, the thrust density of the linear electric motor can be improved by 176% while the operating temperature remains to belove its limit of 155 ˚C.

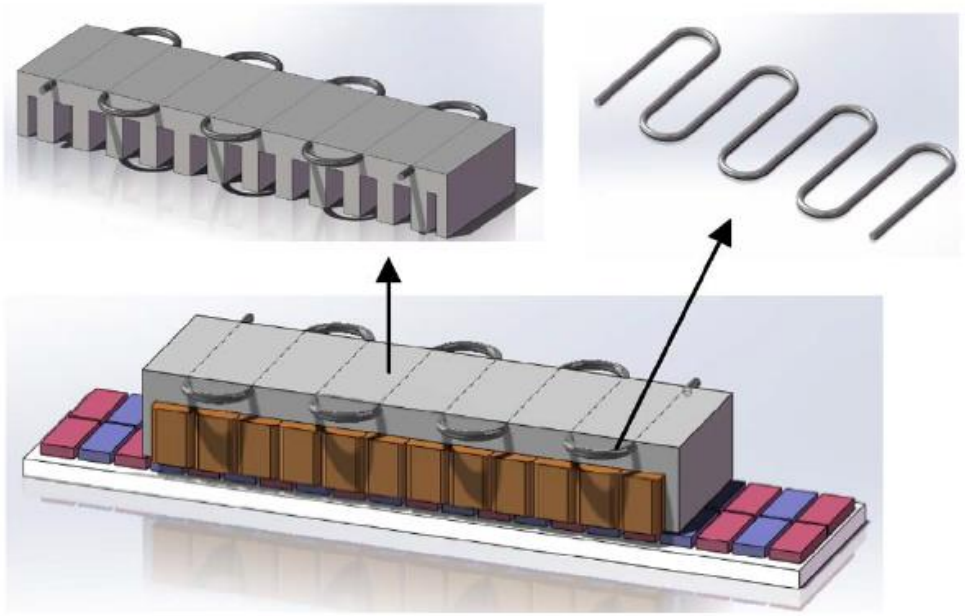

Figure 2. 6. Linear electric machine and its cooling system [51].

Employing a water-cooling system with fluid channels in the stator showed 13 ˚C temperature reduction for an electric machine used in hybrid electric vehicle applications [52]. 47% stator winding temperature reduction of a small synchronous machine when a water-cooling system is used compared to the air-cooling system was reported in [53].

An electric machine employing a cooling jacket for formula E applications was designed in [54] and shown in Figure 2.7. Optimizing the material of the machine, geometries of the stator and the cooling jacket, it was reported that the average winding temperature is reduced by 20%.

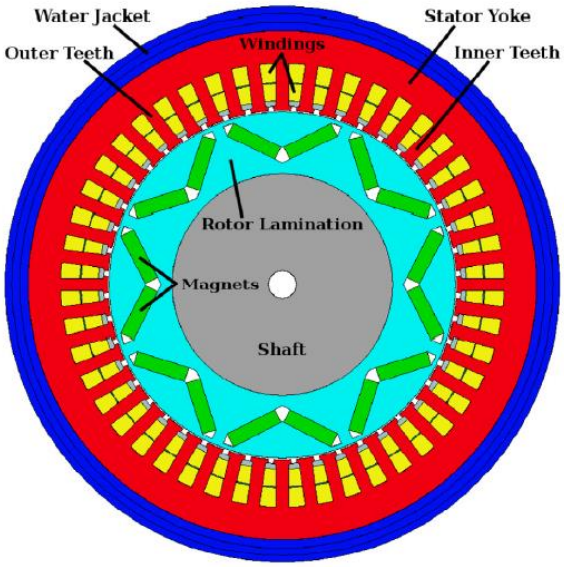

Figure 2. 7. Radial schematic view of the electric machine and the cooling jacket [54].

A water-cooling system consisting of several water-cooled plates inserted into the stator core laminations of a permanent magnet synchronous machine was proposed in [55]. It was demonstrated by experimental tests that using the proposed cooling method, the maximum stator winding temperature can be reduced by 20%.

2.5 DISCUSSION

There are many researches reported in the literature on the thermal analysis of various cooling systems for electric machine applications. As reported in this chapter, most of the studies dealing with the thermal analysis of electric machines in terms of heat transfer performance of the cooling system. These one-dimensional evaluations of the cooling system performance fail to give the designers a clear picture of the overall performance of the cooling system and practical criteria to select a proper cooling system topology. In fact, the heat transfer performance of a cooling system is only one part of the overall performance of the system. It is clear that employing an over-designed cooling system can lead to a significant reduction in the temperature of the electric machine, but certainly increases the cost of production of the product to an unnecessary amount. Therefore, from an engineering design point of view, the optimal design of the cooling system for electric machines is crucial.

This research aims at providing a comprehensive analysis of electric machine cooling systems in terms of their heat transfer performance and other parameters affecting energy consumption and cost of the cooling system such as structural geometry and fluid flow performance.

3. HEAT TRANSFER OF NANOFLUIDS

3.1 INTRODUCTION

Since the heat transfer performance of a cooling system directly is affected by the thermophysical properties of its working fluid, its enhancement can be achieved by employing an advanced coolant. This can lead to a more compact and energy-efficient cooling system. As an advanced heat transfer medium, nanofluids have received much attention to be used in high-performance cooling systems because of their heat transfer performance improvement potentials. Employing nanofluids as high-performance coolants can passively enhance the heat transfer performance of cooling systems even without altering the geometries of the cooling system. Dispersion of nanoparticles in the base fluid increases the thermal conductivity of the coolant and intensifies its turbulence. In this context, this chapter describes the interdependent and interrelated properties of nanofluids contributing to the enhancement of the cooling system heat transfer performance.

3.2 NANOTECHNOLOGY

The prefix "nano" derives from the Greek word “Nanos” and, in the metric system, means "one billionth" of a meter. One nanometer is a factor of 10^{-9} meters. To realize the dimensions in the nanoscale, it should be noted that the diameter of a human hair is, on average, about 50,000 nanometers and a bacterial cell has a diameter of several hundred nanometers. The smallest objects visible to the unaided eye are about 10,000 nanometers in size. In general, nanotechnology deals with nanoscale structures. Such assemblies are referred to as nanostructures.

Nanotechnology is the application of these structures in nanometer-sized equipment and devices. Nanotechnology is the efficient production of materials, devices, and systems by control over materials at the nanometer range and utilizing newly emerged properties and phenomena developed at the nanoscale.

Nanotechnology is among the emerging technologies worldwide and shows unique properties with applications in many fields of science and technology. The interdisciplinary application of nanotechnology has led to the creation of new applications that could not previously be implemented. This universality of nanotechnology has made it pervasive in most fields of science and engineering.

In the field of heat transfer technology, the development of nanotechnology has provided new solutions and development opportunities. In general, nanotechnology is used in most cases to reduce the size of heat transfer systems by increasing the heat transfer capacity obtained with the help of nanotechnology.

What makes nanotechnology suitable for heat transfer applications, is the high surface-to-volume ratio of nanomaterials. This is known as one of the most critical properties of nanomaterials. This property of nanoparticles makes nanomaterials have special thermal properties. The main reason for these special properties is the increase in the surface to volume ratio of

nanomaterials. However, some other unique properties of nanomaterials are also involved in changing the thermal behavior of nanomaterials compared to conventional materials.

Nanofluids are produced by adding metallic or non-metallic nanoparticles to base fluids. As mentioned, due to the enhanced thermophysical properties of nanoparticles, the thermal properties of nanofluids improve compared to the base fluid. In fact, the presence of nanoparticles suspended in the base fluid improves the thermal properties of the resulted nanofluid [56]. Improving the thermal properties of nanofluids occurs in the form of enhanced thermal conductivity and heat transfer coefficient.

Among the special thermal properties of nanofluids, thermal conductivity is a key property that even by adding a small volume fraction of nanoparticles to the base fluid, the thermal conductivity of the resulting nanofluid is significantly higher than the thermal conductivity of the base fluid. The thermal conductivity of nanofluids is affected by the type of nanoparticles, thermophysical properties of the base fluid, size and the shape of nanoparticles, concentration of nanoparticles, etc. It is demonstrated that by adding metallic nanoparticles such as Al_2O_3 and CuO to a base fluid, the thermal conductivity increases significantly compared to adding ceramic nanoparticles. This is because the thermal conductivity of metallic nanoparticles is several times higher than the thermal conductivity of ceramic nanoparticles. Therefore, to obtain the desired thermal properties, the choice of nanoparticles is of utmost importance.

In general, nanofluids can be produced by adding metal, oxide, and carbon nanotube nanoparticles into a base fluid. The addition of nanoparticles to a fluid impacts its thermal conductivity and other physical properties such as the heat capacity and viscosity of the fluid. The chain of alterations in the thermophysical properties of the fluid causes an increase in the thermal conductivity, as well as a remarkable increase in the coefficient of heat transfer in convection heat transfer pathways. As mentioned, in addition to the type of nanoparticles, the size of the nanoparticles is also very effective in the physical and thermal properties of the nanofluid. For this reason,

researchers have paid special attention to studying the effect of nanoparticle size and shape on the physical and thermal properties of nanofluids.

Since nanofluids are a mixture of nanoparticles suspended in a base fluid, the issue of nanofluid stability is of particular importance in the practicality of industrial applications of nanofluids. In this regard, much research has been done on the stability of nanofluids, and the precipitation of nanoparticles during the working process of nanofluids. Precipitation and instability cause a decrease in the thermal properties of nanofluids and cause the phenomenon of agglomeration. Depending on the type of nanoparticles, the issue of stability and deposition in nanofluids varies. Based on morphology and chemical properties, widely used nanoparticles are divided into the following categories.

- **Ceramic:** Hydroxyapatite (HA), Zirconia (ZrO_2), Silica (SiO_2), etc.
- **Metallic:** Gold (Au), Silver (Ag), Copper (Cu), Zinc (Zn), Aluminium (Al), Cobaslt (Co), etc.
- **Carbon-based:** SilFullerenes, Carbon nanotubes, Graphene, etc.
- **Semiconductors:** GaN, GaP, inP, ZnO, etc.
- **Polymeric:** PCL, PLA, PLGA, etc.
- **Lipid-based:** Liposomes, SLN, NLC, etc.

Regarding common base fluids, the fluids widely used as base fluid are as follows and shown in Figure 3.1 [57]:

Water, biofluids, oils, polymer solutions, etc.

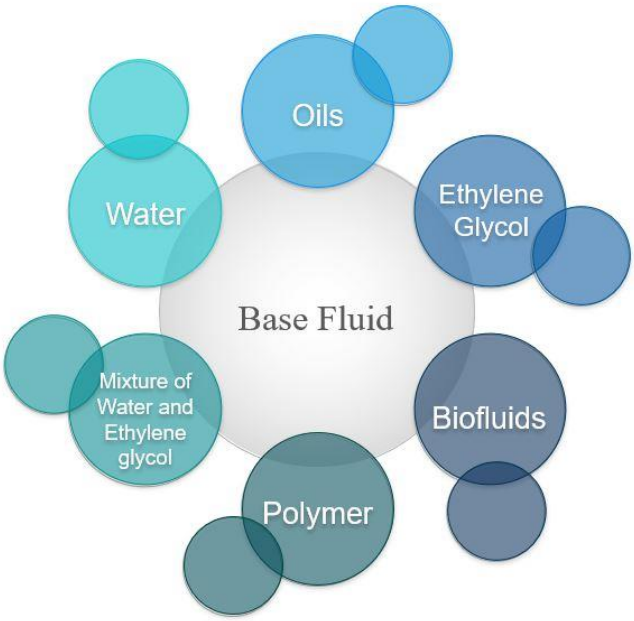

Figure 3. 1. Commonly used base fluids.

3.3 APPLICATION AREAS OF NANOFLUIDS

As mentioned in the previous section, adding nanoparticles to a base fluid changes the physical and thermal properties of the resulting fluid. Depending on the application, some of these properties are desirable. Therefore, the type of nanoparticles and their other properties are selected in order to obtain the targeted properties. The sheer variety of nanoparticles allows them to be used in a wide variety of applications. These applications range from medical science and pharmacy as smart drug carriers to use in cooling systems as advanced coolants. However, Since the subject of this thesis is the cooling of electric machines and since the most significant reinforced feature of nanofluids is their high heat transfer performance, in this section the applications of nanofluids due to their superior heat transfer properties are investigated.

The improved heat transfer performance of nanofluids leads to reduced size heat transfer equipment and on the other hand, reduces the amount of energy consumption. The use of nanofluids in heat exchangers in large industries where water is used as a coolant can reduce water consumption and reduce wastewater production. Also, in applications with size constraints, the use of

nanofluids is very promising because it increases the heat transfer performance of cooling systems.
Another application of nanofluids, which has been created due to their improved heat transfer performance, is the use of nanofluids to transfer heat from the earth's crust to the surface to generate electricity. The use of geothermal energy as clean energy has been considered for many years. Nanofluids can play an important role in reducing energy loss and also increasing the efficiency of geothermal power plants.

In the automotive industry, nanofluids are widely used as a coolant. The improved heat transfer performance of nanofluids reduces the size of the radiator used in vehicles, which improves the aerodynamic shape of the vehicle and reduces fuel consumption. Also, the use of nanofluids as a coolant in vehicles reduces friction and corrosion in pumps and compressors. These are due to the low kinetic energy generated during the collision with surfaces. These nanofluid properties reduce energy consumption by pumps and compressors and also increase their service life.

Other examples of the use of nanofluids in the automotive industry include the use of nanofluids in enhancing the thermal performance of brake fluid and strengthening the braking system of vehicles. Nanofluids increase heat transfer in the vehicle brake system and prevent the brake fluid from boiling and evaporating. This improves the safety of cars. Aluminum-Oxide Brake Nanofluid (AOBN) and Copper-oxide Brake Nanofluid (CBN) are examples of nanofluids used in vehicle brake systems.

One of the design challenges of microelectronic circuits is the optimal dissipation of heat generated by microelectronic chips. The very small cross-section of the fluid-containing channels in the case of using liquid-cooled cooling systems requires special properties for the coolant. The ability to absorb and transfer large amounts of heat flux on a very small surface and special properties of fluid flow that prevent clogging of channels with a very small cross-section containing cooling fluid are among the desired features. These requirements have made nanofluids superior choices as a coolant in microelectronics applications [58].

In general, high thermal conductivity, high critical heat flux, and high heat transfer ability in one-phase have created different contexts for the application of nanofluids in heat transfer systems in various industries.

3.4 EMPLOYING NANOFLUID IN COOLING SYSTEMS

The mixture of ethylene glycol and water is commonly used as a coolant in the automotive industry. This mixture has a lower thermal conductivity compared to water. For this reason, the enhancement of the thermal conductivity of this mixture by adding nanoparticles to it has been considered [59]. Adding nanoparticles to the mixture of ethylene glycol and water improves the heat transfer performance of the coolant. Therefore, by strengthening the heat transfer performance of the coolant, the cooling system of the vehicle can be made smaller. As mentioned earlier, smaller vehicle radiators improve the vehicle's aerodynamic shape and thus reduce fuel consumption. Also, because the weight of the components is very effective in fuel consumption, the cooling system with higher efficiency, in addition to reducing the size, also makes the cooling system lighter. This is another reason to reduce fuel consumption. On the other hand, the use of nanofluids as a coolant reduces the amount of coolant required, which reduces the pumping capacity and makes it possible to use a smaller pump. Therefore, the use of nanofluids in the cooling system of vehicles leads to increasing the heat transfer efficiency of the cooling system, making the cooling system smaller and lighter, and generally reducing the cost of manufacturing the cooling system. These features are especially important for vehicles with internal combustion engine, hybrid, and electric vehicles. In the case of hybrid vehicles, a more efficient cooling system reduces the operating temperature of the environment surrounding the vehicle's electrical and power electronics systems. As a result, the cooling effort required for electrical components decreases [60].

Although researchers have studied the performance of various nanofluids for the use of automotive cooling systems, considering other criteria such as cost and maintenance requirements of the system, nanofluids based on pure ethylene glycol with nanoparticles have been more promising. Pure ethylene glycol has a higher boiling point than a mixture of ethylene glycol and water and can operate below atmospheric pressure. However, due to the fact that it has a lower heat transfer coefficient than the mixture of ethylene glycol and water, this defect must be eliminated in order to take advantage of the mentioned properties. By adding nanoparticles to pure ethylene glycol, the heat transfer coefficient of the fluid can be increased. Therefore, the resulting fluid, in addition to having a high heat transfer coefficient, has a very high boiling point, which causes more heat to be absorbed by the coolant and desorbed through the cooling system [61, 62]. In [63], it was found that the use of nanofluids in radiators could reduce the front cross-section of the vehicle by 10%. Such a reduction in aerodynamic drag can lead to a 5% reduction in fuel consumption.

3.5 INFLUENTIAL PROPERTIES OF NANOFLUIDS ON HEAT TRANSFER PERFORMANCE

Specific properties of nanofluids that affect their heat transfer performance are: [64]:

- High Specific Surface Area (SSA) leading to an improved heat transfer between the base fluid and the nanoparticles
- Stable fluid with a steady scattering because of the dominant Brownian motion of the particles
- Reduction in the thickness of the thermal boundary layer
- Low cooling channel obstruction compared to other solutions

Improving the performance of nanofluids can be achieved due to various factors. The most important of them are [65]:

1. Heat transfer in nanofluid on the increased heat transfer surfaces because of suspended particles.
2. Elevated effective thermal conductivity by the activity of suspended nanoparticles and interactions between nanoparticles and base fluids.
3. Intensified turbulence of the flow caused by the movement of nanoparticles in the fluid.
4. Reduced thickness of the thermal boundary layer because of the dispersion of nanoparticles leading to altering the temperature gradient of the fluid.
5. Mass transfer of the nanoparticles caused by the temperature gradient [66].

3.6 POTENTIAL BENEFITS OF NANOFLUIDS

Nanofluids improve the efficiency of heat exchange systems. Therefore, nanofluids can be effective in reducing carbon in the strategic vision of industries. According to Polaris Market Research, it is anticipated that the global heat transfer fluids market reaches $4.56 billion by 2026. Since the application of nanofluids can increase heat transfer performance, which is desirable for the industry, the demand for nanofluids is expected to increase in the near future. Some of the potential benefits and capabilities of nanofluids are as follows [67].

3.6.1 IMPROVED HEAT TRANSFER AND STABILITY

As mentioned before, the main reason for the increase in nanofluid heat transfer coefficient is due to the fact as a result of nanoparticles suspended in the base fluid, the surface to volume ratio of particles that interact with the base fluid and the heat absorption and dissipation surface increases

significantly. In other words, the effective heat transfer surfaces are increased by adding nanoparticles to the base fluid.

The total surface area of particles per unit of mass is called Specific Surface Area (SSA). Therefore, the SSA of nanoparticles is about 1000 times SSA of particles with micrometer dimensions. Thus, in a nanofluid, more surfaces of nanoparticles are in contact with heat transfer surfaces. These contact surfaces are very effective in heat transfer and therefore the use of nanofluids increases the heat transfer performance of the fluid.

On the other hand, the very small size of the nanoparticles greatly reduces the sedimentation problem that exists in other solutions with suspended particles. Therefore, nanofluids are more stable. Sedimentation occurs when suspended particles with Brownian motion reach a certain speed. This change in the velocity of the suspended particles is caused by an external field, mainly gravity, and causes the suspended particles to settle in the fluid. The rate of sedimentation depends directly on the size of the particles and their mass. Solutions with smaller suspended particles are less likely to settle and are more stable. [68,69].

3.6.2 REDUCED ENERGY TO PUMP THE FLUID

One of the effective factors in fluid heat transfer performance is the fluid velocity, which is measured by the Reynolds number. In order to increase the heat transfer performance of the fluid, the Reynolds number and consequently the velocity of the fluid must be increased. This requires increasing the pumping power of the fluid, which leads to an increase in energy consumption by the pump. Since nanofluids have improved heat transfer coefficient, less fluid velocity is required to dissipate certain heat when using nanofluids. Therefore, in general, it can be said that the amount of energy consumed by the pump using nanofluids is reduced. In [70], It was demonstrated that compared to Al_2O_3, the use of water as a working fluid requires 20% more pumping energy to obtain the same heat transfer rate. Therefore, employing nanofluids can lead to reduced pump energy consumption resulting in increased system efficiency [71].

3.6.3 REDUCED SEDIMENTATION AND OBSTRUCTION OF DUCTS

Solutions containing suspended particles with Brownian motion are exposed to the sedimentation problem caused by the force of gravity or other external fields. Sedimentation can quickly lead to duct obstruction. Sedimentation and consequently obstruction depend directly on the size of the suspended particles. Nanofluids take advantage of the fact that the suspended particles in them are very small and in nanometer sizes. Therefore, nanofluids are less likely to clog ducts than other solutions. Also, due to the small size of nanoparticles, the impact of nanoparticles on the walls of the ducts causes less wear. Friction due to the wear of particles to the walls of the ducts can cause a drop in pressure as well as damage to the pumps. This phenomenon is especially complicated in applications where microchannels are used for heat transfer. Therefore, nanofluids can be used in a wider range of applications and increase heat transfer performance while reducing damage to the system. Finally, it can be said that employing nanofluids instead of other solutions in heat transfer systems reduces maintenance costs [72].

3.6.4 REDUCED SIZE HEAT TRANSFER SYSTEMS

Due to the fact that the use of nanofluids improves the performance of heat transfer systems, so for a given application, the size of the system can be reduced by employing nanofluids. Today, in many applications such as automotive, aerospace, and microelectronics, component size is very important because of their size constraints. Therefore, the use of nanofluids for such applications is very promising. [73].

3.6.5 REDUCED COSTS

Increasing the heat transfer efficiency obtained by using nanofluids reduces the cost of manufacturing cooling systems by reducing the overall volume and size of the system and its components, such as pumps. On the other hand, reducing problems such as clogged ducts, wear, and damage to pumps leads to reduced maintenance costs of the cooling system.

Also, as mentioned, by using nanofluids, the energy consumption of the pumps and as a result, the energy cost is reduced.

3.7 HEAT TRANSFER MECHANISMS OF NANOFLUIDS

Some of the mechanisms involved in the thermal transfer performance of nanofluids are discussed in this section. There are several reasons behind the heat transfer enhancement achieved by adding nanoparticles into fluids. In general, and as the most effective factor in enhancing the heat transfer process of fluids, the addition of nanoparticles to fluids increases their thermal conductivity [74]. Compared to metallic materials, conventional working fluids in heat transfer systems such as water, ethylene glycol, and oil have lower thermal conductivity. Therefore, to enhance the thermal transfer performance of heat transfer fluids their thermal conductivity must be improved. The addition of metallic or oxide particles into the fluids is an effective way leading to increased thermal conductivity. Conventionally, suspensions made of metallic or oxide particles in millimeters or micrometer scales added into conventional heat transfer working fluids were studied. As mentioned in the previous sections, there are several practical issues associated with employing these suspensions such as instability of particles in fluids, sedimentation, obstruction, abrasion, and erosion of ducts. The development of nanotechnology made it possible to employ particles on nanometer-scale instead of millimeters or micros scale particles to build suspensions with improved thermal conductivity. This way, the problems mentioned above can be alleviated or eliminated.

As effective factors in enhancing the heat transfer performance of nanofluids as a result of improving the thermal conductivity, four mechanisms have been investigated in [75]. These mechanisms include Brownian motion, layering at the solid/liquid interface, phonon transport, and clustering.

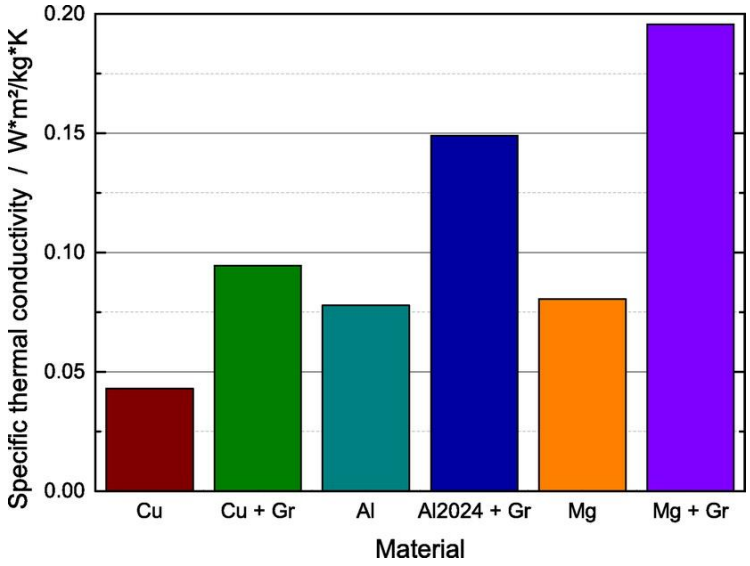

Figure 3. 2. Thermal conductivity of some materials [77].

The impact of some mechanisms on thermal conductivity improvement of nanofluids was investigated in [76]. The studied mechanisms are liquid interfacial layering between nanoparticles and base fluid, particles agglomeration, and Brownian motion. It was demonstrated that the effectiveness of each mechanism depends on the size of the nanoparticles and the liquid boundary layer around the particles. For example, the effect of the Brownian movement is influential where the nanoparticle sizes are in the molecular range. For nanoparticle sizes of 1 to 100 nm, liquid layering and agglomeration have the most influential mechanisms. Finally, for larger particles agglomerations plays a key role in the thermal conductivity enhancement of nanofluids.

Free electrons in metallic solids and lattice vibrations (thermal vibration of atoms) in insulating solids play a key role in carrying heat [77]. As a result of these intrinsic mechanisms, the thermal conductivity of metallic and metal oxide materials is several times of liquids like water and oil that are used as a heat transfer working fluid in heat transfer systems. Figure 3.2 shows the thermal conductivity of few solids. To better understand the difference between the value of thermal conductivity of metals and water, it should be considered that the specific thermal conductivity of water at 25˚C is 0.00059 $Wm^2/Kg\ K$.

3.7.2 BROWNIAN MOTION

There are conflicting views on the importance of the Brownian motion effect on the thermal conductivity of nanofluids. Researchers who believe that the Brownian motion of nanoparticles is not among the main effective factors in increasing the thermal conductivity of nanofluids argue that as the typical size of nanoparticles is two times larger than the base fluid molecular diameter, the effect of nanoparticles Brownian motion is at least half of that of the base fluid [78].

On the other hand, some researchers believe that the Brownian motion of nanoparticles plays a significant role in enhancing the thermal conductivity of nanofluids. One of the studies that support this theory is reported in [79]. In this study, a model of a heated sphere surrounded by a cold fluid was used to describe the effect of the Brownian motion of particles on the thermal conductivity of the suspension. The results of experimental tests also confirmed the results obtained from the model. One drawback to this investigation is that in this study, the velocity of the surrounding fluid was assumed to be equal to the average Brownian velocity of the particles. Also, the temperature of the heated particles was considered constant and the heat transfer between the particles and the fluid was ignored. In general, most recent researches support the theory that the Brownian motion of nanoparticles is unlikely to significantly contribute to the thermal conductivity enhancement of nanofluids.

3.7.3 THERMAL TRANSPORT BY PHONONS

Phonons are quantized lattice vibrations. Heat in crystalline solids mostly is carried by phonons. The thermal conductivity of solids strongly depends on the mean free paths of phonons. This factor explains why the thermal conductivity of crystalline solids decreases with increasing temperature. In fact, at high temperatures, because of phonon-phonon scatterings, the mean free paths of phonons decrease [80]. In general, phonons play a significant role in the thermal conductivity of nanoparticles and consequently thermal conductivity enhancement of nanofluids [81].

3.7.4 EFFECTS OF NANOPARTICLE CLUSTERING

Clustered nanoparticles are formed by the action of gravitational Wonder-Waltz forces. Such a phenomenon results in less thermal resistance for heat transfer. However, the phenomenon of clustering can exert a negative impact on nanofluids. It also can cause the instability of the suspension by forming large masses, as well as reduce the heat transfer by creating empty areas of nanoparticles in the liquid and increasing the heat resistance. Clustering enhances the volume percentage and, as a rule, the higher volume fractions of nanoparticles will result in the greater thermal conductivity of the nanofluid, mainly due to the thicker clusters and the increase in the effective volume fraction [82].

A unique feature of nanofluids is that the expansion in the convection heat transfer coefficient is usually greater than the growth of the effective thermal conductivity. Contrary to the mechanism of boosting thermal conductivity, mechanisms involved in the enhancement of nanofluid transfer coefficient remain unclear. Much research has so far been done on heat transfer in nanofluids confirming the effect of adding nanoparticles on increasing heat transfer. The extent of this effect and the mechanism governing it is still a subject of interest for researchers. All of these works, however, confirm that the convection heat transfer coefficient increases with rising Reynolds number, decreasing nanoparticle diameter, increasing fluid temperature, and increasing nanoparticle concentration [83].

Nanofluids can be used in a variety of settings, but there are some challenges. These include the deficiency in determining the suspension properties of nanoparticles, the lack of appropriate models and theories to investigate the change in nanofluid properties and the inconsistency of experimental results in various experiments. Here are some reasons for appearing different research results [84].

Clustering: It has been confirmed that nanoparticles show a great tendency for rapid aggregation, which affects the thermal conductivity and viscosity of nanofluids. This factor, however, has been excluded in many empirical and numerical studies.

Size of nanoparticles: The size of nanoparticles has been largely ignored by researchers, which affects the results.

Theoretical disputes: Researchers dissent on which heat transfer mechanism is more important and dominant, and how to use these mechanisms in computations. Such differences lead to different analyses and, consequently, inconsistent results.

Different methods of nanofluid preparation: Nanoparticles are differently distributed in fluid depending on the nanofluid preparation method.

3.8 THERMAL CONDUCTIVITY COEFFICIENT OF NANOFLUIDS

The higher the thermal conductivity of a fluid, the higher its heat transfer performance. Therefore, thermal conductivity is an important indicator in evaluating the heat transfer performance of fluids. If a fluid has a low thermal conductivity, it is possible to improve the thermal conductivity of the fluid by adding nanoparticles. In particular, the addition of metallic nanoparticles to fluids can significantly increase their thermal conductivity. In general, the thermal conductivity of nanofluids depends on the type, size, shape, and concentration of the nanoparticles as well as the thermophysical properties of the base fluid [85 - 87]. Factors influencing the thermal conductivity of nanofluids are shown in Figure 3.3 and described in the following.

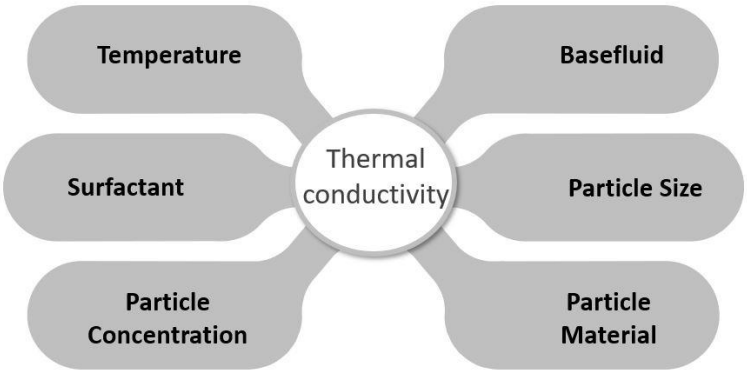

Figure 3. 3. Parameters influencing thermal conductivity of nanofluid.

3.8.1 EFFECTS OF NANOPARTICLE CONCENTRATION ON THE THERMAL CONDUCTIVITY OF NANOFLUIDS

Increasing the concentration of nanoparticles can increase the thermal conductivity of nanoparticles. Depending on the type of base fluid and the type, size, and shape of the nanoparticles, the rate of increase in thermal conductivity varies with the increasing concentration of nanoparticles. In fact, the increase in thermal conductivity is a function of the thermal conductivity of the base fluid and nanoparticles. Figure 3.4 shows the changes in the thermal conductivity with increasing nanoparticle concentration for three different types of nanoparticles. As can be seen, increasing the nanoparticles concentration, Alumina-CuO/water shows the highest rate of thermal conductivity increase [88]. The effect of base fluids types on the thermal conductivity of nanofluids was studied experimentally in [89]. Thermal conductivity of carbon nanotubes–ethylene glycol suspension and carbon nanotubes–synthetic engine oil suspension was measured at various carbon nanotubes concentrations. It was shown that the increase of nanotubes concentration in ethylene glycol suspension shows leads to a higher increase of thermal conductivity.

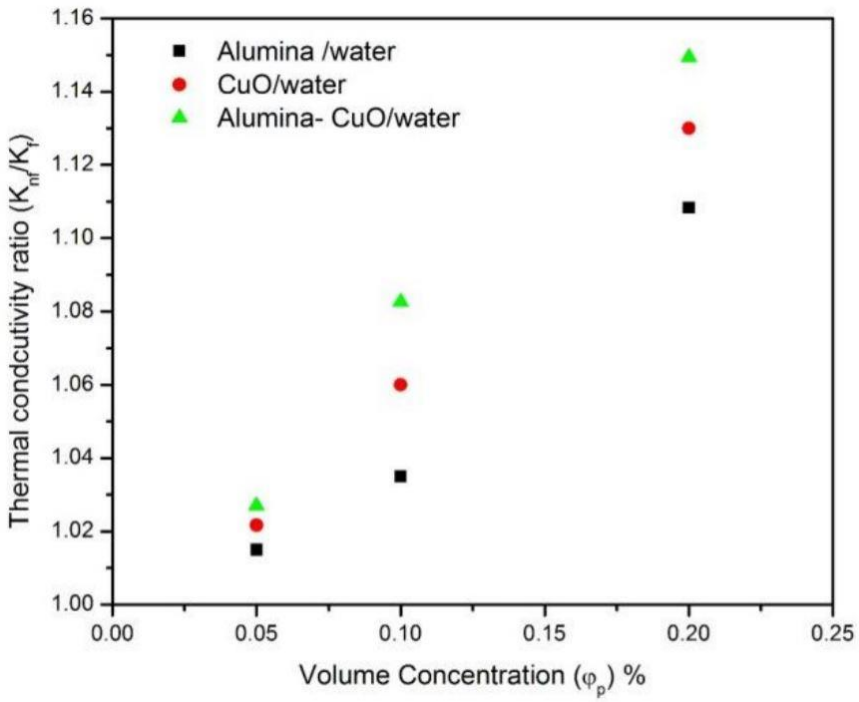

Figure 3. 4. Effects of the concentration of nanoparticles on the thermal conductivity of the fluid [88]

3.8.2 EFFECTS OF TEMPERATURE ON THE THERMAL CONDUCTIVITY COEFFICIENT OF NANOFLUIDS

The temperature has an effect on changes in the thermal conductivity of fluids. As the temperature increases, the thermal conductivity increases. In fact, increasing the temperature increases the movement of nanoparticles within the base fluid, which increases the interaction between the particles. This increases the thermal conductivity of nanofluids at high temperatures. This property of nanofluids is a factor that promotes the use of nanofluids in cooling systems. The principle of increasing the motion of suspended particles in solutions under the influence of temperature increases is true for all solutions, but in the case of nanofluids due to the nano-scale size of suspended particles, the increase in nanoparticles movement under the influence of temperature is much greater than solutions with larger suspended particles. Therefore, in the case of nanofluids, the thermal conductivity coefficient increases significantly with increasing temperature.

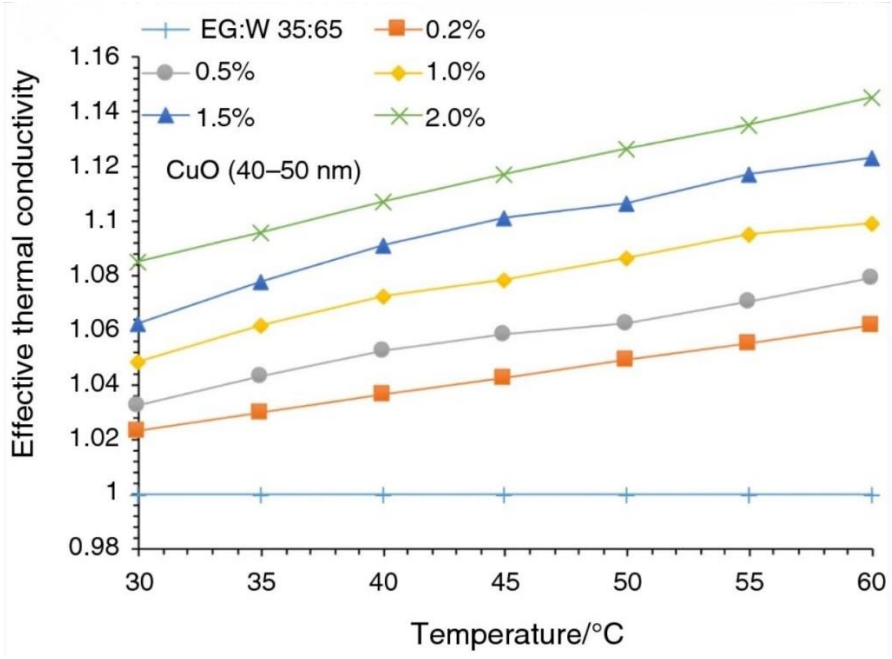

Figure 3. 5. Variations in the thermal conductivity of nanofluids by temperature [90].

This property of nanofluids is especially remarkable at high temperatures when the Brownian motion of the particles is greater. Changes in thermal conductivity due to temperature changes for Ethylene Glycol:Water-CuO nanofluid have been studied [90]. Figure 3.5 shows the diagram of these changes for nanofluids with different concentrations. As can be expected, the rate of increase in thermal conductivity is higher for nanofluids with higher concentrations of nanoparticles at high temperatures. There is also a significant difference between changes in thermal conductivity and temperature changes between the base fluid and the nanofluid.

As demonstrated, the gradient of the corresponding curve increases by temperature, indicating that the higher temperatures will result in the greater effect of nanoparticle concentration on the thermal conductivity.

3.8.3 EFFECTS OF THE SIZE OF NANOPARTICLES ON THE COEFFICIENT OF THERMAL CONDUCTIVITY OF NANOFLUID

In the section describing the effect of temperature on the thermal conductivity of nanofluids, it was mentioned that due to the acceleration of nanoparticles movements with increasing temperature, the thermal conductivity of nanofluids increases. Also, because nanoparticles are in nanoscale, this acceleration of nanoparticles is more remarkable with increasing temperature than other types of particles with larger sizes. Therefore, the size of nanoparticles is effective in increasing the thermal conductivity of nanofluids by affecting the velocity of particles. The variation of thermal conductivity with respect to the diameter of nanoparticles for various nanoparticles is shown in Figure 3.6 [91].

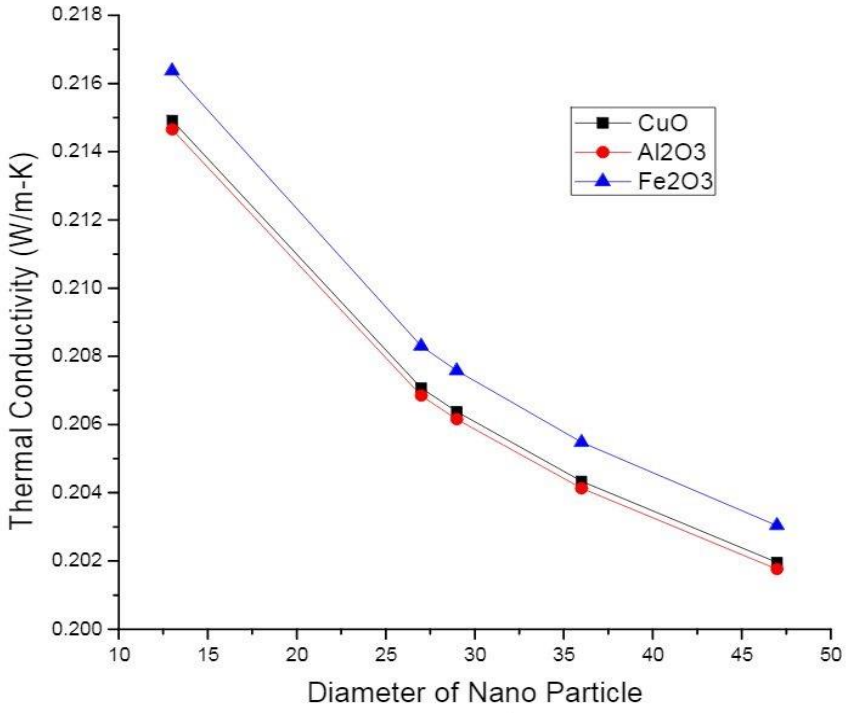

Figure 3. 6. Variation of thermal conductivity with respect to the diameter of nano particles for various nano particles [91].

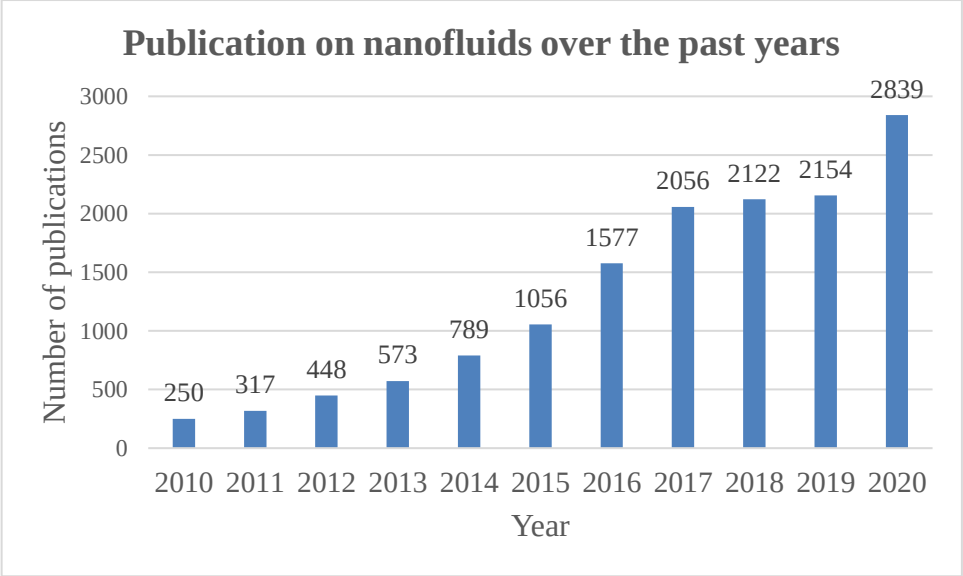

Figure 3. 7. Increasing research on nanofluids over the past years.

3.9 INCREASING RESEARCH ON NANOFLUIDS

Due to the promising properties of nanofluids and the possibility of using nanoparticles in various applications and various sciences, extensive research has been done on nanoparticles. As the use of nanoparticles expands and new applications are found, these researches are further developed so that the volume of research on nanotechnology is growing. Regarding the application of nanoparticles in heat transfer systems, due to the potential of nanoparticles in improving the thermal performance of fluids, research in this field is increasing. The number of studies published in the literature (only in the ScienceDirect database) over the past years on nanofluids is shown in Figure 3.7

3.10 RESEARCH ON THE HEAT TRANSFER COEFFICIENT OF NANOFLUIDS

The main factor in estimating fluid performance in heat transfer systems is the ability of fluids to transfer thermal energy. In fact, by moving the fluid from the place of heat production to the place where heat can be dissipated and exchanged with the environment, thermal energy is transferred [92]. The fluid heat transfer coefficient is the main indicator in determining the ability of fluid in thermal energy transfer [93]. Also, by knowing the heat transfer coefficient, the amount of area required for heat dissipation and its exchange with the environment can be calculated. For this purpose, mathematical relationships are required to perform calculations and design heat transfer systems. Given that the use of fluids in heat transfer systems has a long history, these relationships are already well established for conventional fluids and their use to perform calculations and design heat transfer systems is straightforward [94].

However, in the case of nanofluids, due to the novelty of nanofluids applications and the existence of multiple factors affecting the heat transfer coefficient of nanofluids, the relationships required for the analysis and design of heat transfer systems are not common. In fact, various factors such as heat transfer coefficient, thermal conductivity, nanofluid viscosity, nanoparticle concentration, heat capacity, etc. affect the heat transfer performance of nanofluids [95].

Among all these factors, the heat transfer coefficient is the most important indicator in estimating the heat transfer performance of nanofluids [96]. In general, increasing the heat transfer coefficient is considered an effective approach to reduce the volume of heat transfer systems or increase the performance and capacity of heat transfer systems with the same volume [97, 98]. Therefore, the heat transfer coefficient is the basis of calculations and design of heat transfer systems.

In this regard, extensive research has been conducted on methods for estimating and calculating the heat transfer coefficient of nanofluids [99, 100]. Due to the fact that the addition of nanoparticles to fluids affects both thermal and fluid flow properties, so in addition to heat transfer coefficient, the performance of nanofluid flow should also be considered. This increases the complexity of estimating the overall performance of nanofluids.

The effect of adding Al_2O_3 nanoparticles in Ethylene Glycol-water base fluid on heat transfer coefficient has been investigated [101]. In this study, the effect of Brownian diffusivity to thermophoretic diffusivity ratio on nanofluid heat transfer coefficient has been assessed. It was shown that with increasing this ratio, the heat transfer coefficient of nanofluid increased to 22.7%. According to the results, the heat transfer coefficient of the nanofluid changes significantly by changing the ratio of the Brownian diffusivity to the thermophoretic diffusivity. In [102], a predictive model for the heat transfer coefficient of nanofluid aerosol cooling was proposed. The results showed that the measurement error is 7.26%.

In [103], estimation of heat transfer coefficient obtained by adding SiO_2 and Al_2O_3 nanoparticles to Ethylene Glycol-water base fluid has been studied using CFD analysis. This study was performed for nanofluids at different temperatures and nanoparticles concentrations. The results showed that the addition of nanoparticles to the Ethylene Glycol-water base fluid significantly increases the heat transfer coefficient. The effect of the base fluid on the heat transfer coefficient of the nanofluid has also been investigated. For this purpose, different ratios of water and Ethylene Glycol have been considered. In the first case, a mixture of 60% Glycol and in the second case, 40% Glycol in water are considered. The results showed that the effect of adding nanoparticles with a concentration of 1% in the base fluid on increasing the heat transfer coefficient in a mixture of 40% Glycol in 60% water was greater.

The heat transfer coefficient of water and Al_2O_3 nanofluids has been investigated for the cooling systems of microscale electronic systems [104]. As mentioned in the previous sections, due to the very small dimensions of these systems and the high heat to surface ratio in them, the use of nanofluids

in order to improve the performance of cooling systems in these applications is very promising. The results of practical experiments showed that with increasing the concentration of nanoparticles as well as increasing the velocity of the fluid, the heat transfer coefficient increases. Also, as the diameter of the pipes containing the cooling fluid decreases, the heat transfer coefficient increases.

In [105], the thermal coefficient of Al_20_3 / Ethylene Glycol-Carbon nanotube nanofluids in different nanoparticles concentrations and under varying fluid flow conditions has been studied. In this study, the effect of fluid flow conditions on heat transfer coefficient is investigated. Based on the results, at low concentrations of nanotubes, the effect of adding Al_2O_3 nanoparticles on increasing the heat transfer coefficient is greater.

The CuO / water nanofluid heat transfer coefficient used in the car radiator is investigated [106]. It was shown that the heat transfer coefficient increases with increasing nanoparticle concentration from 0 to 4%. Also, increasing the temperature from 50 to 80 degrees Celsius has reduced the heat transfer coefficient. Based on the results, the addition of surfactant regulates the pH of the nanofluid and leads to a slight increase in the heat transfer coefficient.

Heat transfer coefficient and fluid flow performance for CuOWater nanofluids have been studied [107]. In this study, nanoparticle concentrations of 0.0625%, 0.1255, 0.25, 0.5, 1%, 1.5 and 2% were used. According to the results of the study, in all cases, the heat transfer coefficient increases with the addition of nanoparticles to the base fluid. As the Reynolds number increases, the amount of heat transfer coefficient resulting from the increase in nanoparticle concentration decreases. From the point of view of nanofluid flow performance, the pressure drop increases with the addition of nanoparticles to the base fluid. Also, the nanofluid pressure drop is greater at smaller Reynold numbers. The highest increase in heat transfer coefficient was obtained when the nanoparticle concentration is 2%, which is equal to 57% increase in heat transfer coefficient.

The heat transfer performance of Aluminum oxide and Copper oxide nanofluids in Ethylene Glycol base fluid has been investigated [108]. In this study, the effect of nanoparticle concentration and temperature on the heat transfer coefficient of nanofluids have been investigated. Based on the results, the studied nanofluids improve the heat transfer coefficient by up to 50%. In general, increasing the nanoparticles concentration and temperature has increased the heat transfer coefficient. The highest improvement in heat transfer coefficient was observed at 75 °C and nanoparticles concentration of 1%.

The effect of TiO_2 / water nanofluid flow properties on its heat transfer coefficient has been studied [109]. In this study, the effect of adding tape inserts that causes changes in nanofluid flow on the heat transfer coefficient of nanofluid has been investigated. It was reported that this change in the structure of the heat transfer system could lead to a 23.2% increase in heat transfer coefficient. Also, compared to the base fluid, the heat transfer coefficient has been improved up to 81.1% by using twisted tubes and at greater Reynolds numbers.

In [110], the heat transfer coefficient of Al_2O_3 nanofluid was estimated by practical experiments. Based on the results, it was shown that the Gleninsky equation used for conventional fluids cannot be applied to nanofluids. At Reynolds number 9000 and by adding nanoparticles with a concentration of 0.1%, the heat transfer coefficient was 23.7% higher than the base fluid, while at lower Reynolds numbers the rate of increase in heat transfer coefficient was significantly reduced. Also, by changing the structure of the pipes and adding twisted tapes in the pipes, the heat transfer coefficient at the Reynolds number 9000 increased by 44.7%.

Heat transfer coefficient as an indicator of nanofluid heat transfer performance and pressure drop as an indicator of fluid flow performance for Al_2O_3, SiO_2, and CNT nanofluids in a horizontal tube were investigated [111]. In this study, it was shown that the Gnilinsky equation can be used to estimate the heat transfer coefficient of nanofluids in a turbulent flow regime. The use of the Colebrook – White relationship to estimate the coefficient of friction

was also investigated. Based on the result, this relationship can be used with acceptable accuracy to estimate the coefficient of friction of nanofluids. Regarding the fluid flow performance of nanofluids, nanofluids showed lower performance at the same pumping power compared to the base fluid.

In [112], the heat transfer coefficient and transport properties of ZnO nanoparticles added in ethylene glycol – water base fluid was investigated. This study compares the experimental results with results obtained in other studies reported in the literature. Based on the comparisons, a good agreement was observed among the experimental results and estimated parameters using analytical models.

Different models have been investigated to estimate the heat transfer coefficient of nanofluids based on their thermophysical properties [113]. To estimate the heat transfer coefficient using these models, thermophysical properties of nanofluids such as specific heat, thermal conductivity and so on are required. It is clear that the accuracy of measuring and determining these thermophysical properties affects the accuracy of estimating the heat transfer coefficient. In this study, TiO_2-water nanofluid was studied. Based on the result, it was shown that at low concentrations of nanoparticles, the heat transfer coefficient obtained from all models is almost equal to each other.

A numerical correlation is proposed to estimate the heat transfer coefficient of Al_2O_3-water nanofluid used in the square array subchannel [114]. The proposed correlation uses a correction factor that is a function of the nanoparticle concentration. With this method, it is reported that the proposed correlation is more accurate than conventional relationships.

In [115], the boiling heat transfer coefficient of TiO_2-water nanofluid was studied. In this study, it was confirmed that increasing the Reynolds number increases the boiling heat transfer coefficient of the nanofluid. It was also observed that increasing the concentration of nanoparticles increases the boiling heat transfer coefficient. In this study, using the results obtained from experiments, a numerical correlation was proposed to estimate the heat transfer coefficient of the studied nanofluid.

Heat transfer properties of different nanofluids were studied [116]. The nanoparticles used include Cu, Fe_3O_4, MWCNT and Graphene. In this study it has been shown that the heat transfer coefficient of nanofluids can be up to 20% higher than the base fluid (water). Considering the overall performance of the studied nanofluids, it was concluded that the addition of copper nanoparticles to the base fluid leads to the best performance. In [117], heat transfer and fluid flow properties of Graphene Oxide-DeIonized water (GO-DI) nanofluids were studied. The results of experiments showed that the addition of GO nanoparticles to the base fluid increases the heat transfer coefficient. On the other hand, the studied nanofluid has 71% higher coefficient of friction than the based fluid (water). In this study, a numerical correlation is proposed to calculate the nanofluid heat transfer coefficient.

3.11 MODELING OF NANOFLUIDS

As mentioned in the previous sections, due to the new applications of nanofluids and in order to justify their use, it is necessary to be able to estimate the heat transfer and fluid flow performances of nanofluids. For this purpose, nanofluid behavior modeling is needed. Due to the mixture of nanoparticles and base fluid, these models are two-phase models [118]. However, for simplification, the two-phase model is sometimes reduced to a single-phase model. In this case, the effect of adding nanoparticles to the base fluid is considered indirectly by changing the thermophysical properties of the nanofluid [119]. But to more accurately estimate the performance of nanofluids, especially when the addition of nanoparticles alters the hydrodynamic properties of the resulting fluid, it is necessary to use a two-phase model. The use of single-phase models is possible only in cases where the effect of adding nanoparticles on the fluid flow properties of the nanofluid can be ignored.

3.11.1 SINGLE-PHASE MODELING

Single-phase models have been developed based on single-phase fluid equations. As mentioned, for simplicity in some cases, the single-phase model can be used to analyze nanofluids.

In this method, nanofluid which is a combination of nanoparticles and base fluid can be considered as a single-phase fluid and single-phase fluid properties can be considered as the average properties of nanoparticles and base fluid properties [120]. The key assumption in this simplification is that the relative motion of the nanoparticles and the base fluid is zero. Also, the nanoparticles and base fluid have the same velocity and temperature with thermal and hydrodynamic equilibrium. Considering these assumptions, the rules for single-phase flow are then applied. To increase the accuracy of single-phase models, it is important to measure the thermophysical properties of the nanofluid resulting from the addition of nanoparticles to the base fluid [121, 122]. These properties are defined as the combined mixture properties. Governing equations of the single-phase modeling approach are as follows:

Continuity equation :

$$\nabla.\left(\rho_{nf}V_m\right) = 0 \qquad (3.1)$$

Momentum equation:

$$\nabla.\left(\rho_{nf}V_mV_M\right) = -\nabla P + \nabla.\left(\mu_{nf}\nabla V_m\right) \qquad (3.2)$$

Energy equation:

$$\nabla.\left(\rho_{nf}CV_m.T\right) = \nabla.\left(k_{nf}\nabla T\right) \qquad (3.3)$$

3.11.1.1 HOMOGENEOUS MODELING

The homogeneous model is one of the simplest fluid models. In this modeling approach, the combination of dispersed and continuous phases are considered so the model is established for a new continuous phase. If the homogeneous modeling approach applies to a two-phase fluid, the main assumptions are that velocities of the two phases are equal and two phases are in the full thermodynamical disequilibrium.

A numerical method was proposed in [123] to model phase transitions of fluid flows. the accuracy of the proposed model was verified by numerical experiments. A numerical simulation of liquid-vapor phase change in compressible flows was performed in [124]. The used model was based on a homogeneous model assuming equilibrium between phases.

3.11.1.2 DISPERSION MODELING

The dispersion single-phase modeling approach is based on transport equations involving the thermal dispersion effect. Thus, in this modeling method, the effects of the diffusion mechanism are considered in the energy equation. In [125], Using the dispersion modeling approach, a numerical simulation of a nanofluid was performed. Considering the thermal dispersion, random motion of nanoparticles was accounted for. A single-phase model of nanofluids based on the dispersion modelling approach was proposed in [126]. In the proposed model, the effect of the relative velocity between nanoparticles and the base fluid was accounted in the form of perturbation of the energy equation.

3.11.2 MODELING OF MULTIPHASE FLOWS

Multiphase modeling methods are more accurate in estimating the performance of nanofluids. There are several methods for multiphase modeling. However, the main approaches are the Eulerian-Lagrangian, Eulerian, the volume of fluid, and two-phase mixture modeling methods [127].

Eulerian-Lagrange models are based on solving the Navier-Stokes equations with the time average approach. As its name suggests, in this method, the primary phase is analyzed based on the Eulerian method and the secondary phase based on the Lagrangian method. Due to the small size of nanoparticles, even at low concentrations of nanoparticles, a large number of suspended particles are in the volume fraction of nanofluids, so solving equations by Lagrangian method is time-consuming for them and requires a high volume of computations [128].

The Eulerian modeling method is based on solving the equations of continuity and momentum by the Eulerian method. It should be noted that the continuity and momentum equations must be solved separately for the fluid phases [129]. Therefore, the number of equations that must be solved in this modeling method is very large. For this reason, the Eulerian method and the Eulerian-Lagrange method, despite being very accurate, are less used for modeling nanofluids.

The volume of fluid modeling method is based on solving momentum equations for small volume fractions. In the two-phase mixture modeling method, hybrid momentum equations with averaging properties of phases are considered.

3.11.2.1 VOLUME OF FLUID (VOF) METHOD

In VOF modelling method, a single set of momentum and energy equations is solved by tracing surfaces of two or more immiscible fluids with the unknown layer between phases. In this method, the equations related to the secondary phase are solved by solving the continuity equations of the secondary phase. The required thermophysical properties in the equations are calculated as the average properties of all phases in specific volume fractions [130].

The governing equations of VOF modeling approach are:

Continuity equation:

$$\frac{1}{\rho_q}\left[\frac{\partial}{\partial t}\left(\alpha_q \rho_q\right) + \nabla \cdot \left(\alpha_q \rho_q v_q\right) = S_{\alpha q} + \sum_{p=1}^{n}\left(\dot{m}_{pq} - \dot{m}_{qp}\right)\right] \qquad n\ 3.5)$$

where $S_{\alpha q}$ is considered zero by default, $\dot{m}_{qp}$ is the mass transfer from phase q to phase p and $\dot{m}_{pq}$ is the mass transfer from phase p to phase q. If the number of phases is n, then the volume fraction equation is solved for phase n-1 and the volume fraction of the nth phase is calculated according to the following constraint:

$$\sum_{q=1}^{n} \alpha_q = 1 \qquad (3.5)$$

Momentum equation:

The momentum equation is solved across the domain and the resulting velocity field is available for all phases.

$$\frac{\partial}{\partial t}(\rho v) + \nabla \cdot (\rho v) = -\nabla P + \nabla \cdot [\mu(\nabla v + \nabla v^{T})] + \rho g + F \qquad (3.6)$$

3.11.2.2 THE EULERIAN-EULERIAN METHOD

As mentioned, the Eulerian model is computationally high in terms of the number of equations to be solved. In this model, multiple sets of governing equations including momentum, energy, turbulence, species, and volume fraction equations must be solved for each nanofluid phase. In fact, in the Eulerian-Eulerian method, each phase of the mixture is considered as a separate phase and Eulerian equations of the fluid must be solved for them separately [131].

3.11.2.3 MIXTURE MODELING

External forces such as gravity and centrifugal forces cause velocity differences between the phases of a multiphase mixture. In the mixture model, the basic assumption is that there is a local equilibrium in terms of velocity between the phases of a multiphase mixture. Therefore, the mixture model is not suitable for multiphase mixtures where there is a weak coupling between the phases, such as air and particle mixtures, since the local velocity equilibrium assumption is not true. However, in multi-phase mixtures with a relatively strong coupling between phases such as nanofluids, the mixture model can be used. In the two-phase mixture model of nanofluids, the base fluid is considered as a continuous fluid and nanoparticles as the dispersed phase.

The mixed model includes a continuity equation for each phase and a momentum equation containing an additional term that includes the effect of the velocity difference between the phases in the calculations. In fact, the mixture model of multiphase mixtures is a simplified form of full models that has an acceptable accuracy with a moderate computational effort and a smaller number of variables to be solved [132].

For many applications, compared to single-phase models, the mixture model has a quite acceptable accuracy achieved with a moderate increase in computational volume. In [133], the mixture modeling approach was employed for numerical simulation of Cu-water nanofluid inside a square cavity filled with porous media. Using the established mixture model, the effects of Rayleigh number, nanofluid concentration, and the porous layer thickness on heat transfer performance of the nanofluid were studied.

A 3D two-phase simulation of Proton-exchange membrane fuel cells (PEMFC) by using a multiphase mixture model was carried out in [134]. The proposed model takes interactions between phases into account. The parameters that represent the interactions between phases are considered as the effect of the droplet size, the drag coefficient, velocity, Reynolds number, and the droplet relaxation time. The accuracy of the proposed model was verified by comparing results of experimental tests and simulations based on Fluent software with the results obtained from the proposed model.

A multiphase mixture model for multicomponent transport in capillary porous media was developed [135]. The proposed model consists of conservation equations. In order to reduce the number of equations, algebraic relations were used to describe the relative velocity between phases and the mixture. Using these relationships, it is possible to dynamic properties of phases can be calculated in the post-processing stage after obtaining the convergence of governing equations of the mixture.

3.12 MODELS PREDICTING THERMAL CONDUCTIVITY IN NANOFLUIDS

One of the prominent features of adding nanoparticles to fluids is the increased heat conduction coefficient of fluids. Therefore, in order to design heat transfer systems and in order to select suitable nanoparticles for the intended application, heat transfer coefficient estimation models are needed. Examples of proposed models for estimating the heat transfer coefficient of nanofluids proposed in the literature are listed in Table 3.2.

Table 3. 1. Models proposed for predicting thermal conductivity in nanofluids.

Equations	**Names**
$k_{nf} = k_f \left[\frac{k_p + 2k_f - 2\varphi_v(k_f - k_p)}{k_p + 2k_f + 2\varphi_v(k_f - k_p)}\right]$	Maxwell [136] *(3.7)*
$k_{nf} = k_f \left[\frac{k_p + 2k_f - 2\varphi_v(k_f - k_p)(1+\beta)^3}{k_p + 2k_f + \varphi_v(k_f - k_p)(1+\beta)^3}\right]$	Yu and Choi [137] *(3.8)*
$k_{nf} = k_f \left[\frac{k_p + (n-1)k_f - (n-1)(k_f - k_p)\varphi_v}{k_p + (n-1)k_f + (k_f - k_p)\varphi_v}\right]$	Hamilton and Crosser [138] *(3.9)*
$k_{nf} = k_f \left[1 + \frac{(a+b)(k_p - k_f)}{bk_p + ak_f}\varphi_v\right]$	Timofeeva et al [139] *(3.10)*

There are several theoretical and empirical models for predicting the thermal conductivity of nanofluids. The thermal conductivity of nanofluids is affected by nanoparticles concentrations, size of nanoparticles, shape of nanoparticles, type of nanoparticles, viscosity, pH, temperature, ty of base fluids, and other properties of nanoparticles and base fluid.

Regarding the effect of the size of nanoparticles on the thermal conductivity of nanofluids, smaller nanoparticles have a larger effective surface area leading to enhancing the Brownian motion and increased thermal conductivity. Also, regarding the nanoparticle concentration, the increase in nanoparticles concentration enhances interfacial area between the nanoparticles and the base fluid leading to increased thermal conductivity.

3.13 PHYSICAL AND THERMAL PROPERTIES OF NANOFLUIDS

Nanofluids as fluid nanoparticle suspensions have several thermophysical properties with bilateral effects. These properties determine the heat transfer and fluid flow behavior of nanofluids. Therefore, estimating and measuring the properties of nanofluids is necessary to predict and analyze their

performance and to design heat transfer systems. In this section, density and specific heat that are the most important properties of nanofluids are investigated.

3.13.1 DENSITY OF NANOFLUIDS

As a function of the base fluid and nanoparticles densities, the density of the nanofluid can is expressed as [140]:

$$\rho_{nf} = (1 - \varphi_v)\rho_f + \varphi_v \rho_p \qquad (3.11)$$

where (*f*), (*p*), and (*nf*) indicate the base fluid, nanoparticles, and nanofluids, respectively, and (φ_v) is the volume fraction of the nanoparticles in the fluid.

Equation 3.12 was validated by comparing measured densities of Al_2O_3-water nanofluids with calculated densities [140]. According to the comparison, the maximum deviation of the calculated densities of the nanofluid from the experimentally measured densities was 0.6% at nanoparticles concentration of 31.6% (Figure 3.8)

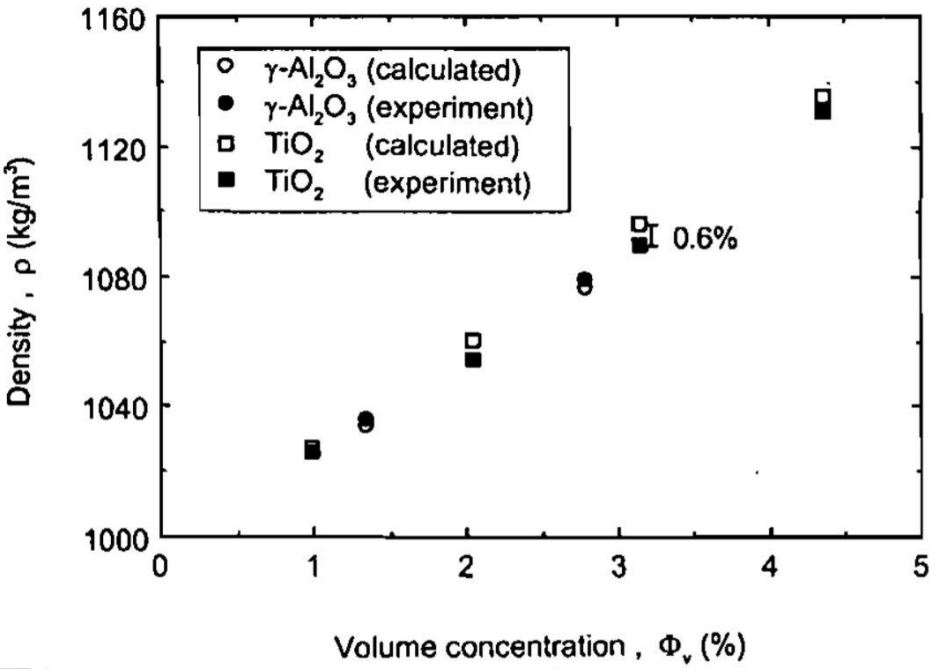

Figure 3. 8. Density variations by the volumetric percentage of nanoparticles at 298 K (comparison of theoretical and experimental values) [140].

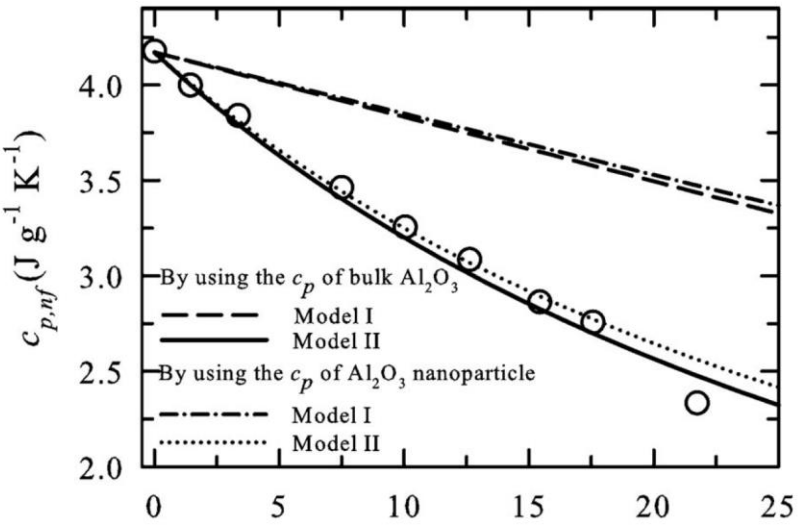

Figure 3. 9. Comparison of theoretical and experimental values of specific heat of Al_2O_3-water nanofluid [142].

3.13.2 SPECIFIC HEAT OF NANOPARTICLES

Determining the specific heat of nanofluids is important in assessing the heat transfer performance of nanofluids and their employment in heat transfer systems. Commonly used equations to calculate the specific heat of nanofluids are listed in Table 3.3. In [142], the specific heat of Al_2O_3-water nanofluid was measured experimentally and calculated using model I and model II equations. Figure 3.9 shows that the model I equation failed to calculate the specific heat of the nanofluid accurately.

Table 3. 2. Existing methods for determining the specific heat of nanofluid.

Methods	**Researchers**
$Model\ I$: $(C_p)_{nf} = (1-\varphi_v)C_{pf} + \varphi_v C_{pp}$	Pak and Cho [140] (*3.12*)
Model II: $(C_p)_{nf} = (1-\varphi_v)C_{pf}\rho_f + \varphi_v C_{pp}\rho_p$	Buongiorno [141] (*3.13*)

3.13.3 RHEOLOGICAL PROPERTIES

Adding nanoparticles to fluids not only alters their heat transfer properties but also affects their rheological properties. The extent of these changes depends on the type and properties of the nanoparticles and the base salad. In some cases, the addition of nanoparticles to a Newtonian fluid results in a non-Newtonian fluid with varying viscosity.

Unlike other suspensions, little research has been carried out on the rheological properties of nanofluids. In addition to the relatively new applications of nanofluids, another reason for the lack of research on the rheological properties of nanofluids is that the heat transfer properties of nanofluids have been more prominent and attractive to researchers.

The interaction between nanoparticles and the base liquid has a great influence on the rheological behavior of nanofluids. shear viscosity, shear thinning and temperature are the most important factors to determine the rheological behavior of nanofluids by affecting the interaction between nanoparticles and the base fluid.

The well-known Einstein equation is adapted for viscosity calculation of nanofluids as follows [143].

$$\mu_{nf} = (1 + 2.5\varphi_v)\mu_f \qquad (3.14)$$

According to equation 3.15, the viscosity of nanofluids increases with increasing nanoparticle concentration. The viscosity of Fe-Si-water nanofluid was experimentally measured in [144]. The experiments were carried out at temperatures from 20 ˚C to 50˚C and nanoparticles concentrations of 0.25% to 1%. According to the results, the highest viscosity was measured at 25 ˚C for nanoparticle concentration of 1%. Therefore, it was experimentally demonstrated that increasing the nanoparticle concentration leads to increased viscosity.

Einstein equation (equation 3.15) was developed for non-interacting suspensions of spherical particles and is not able to predict the viscosity of

Table 3. 3. Models to calculate the effective viscosity of particle suspensions.

Model	Researcher
$\mu_{nf} = \frac{\mu_f}{(1-\varphi_v)^{2.5}}$	Brinkman [146] (*3.15*)
$\mu_{nf} = \frac{9}{8}\mu_f \left[\frac{(\varphi_v/\varphi_m)^{1/3}}{1-(\varphi_v/\varphi_m)^{1/3}}\right]$	Frankel and Acrivos [147] (*3.16*)
$\mu_{nf} = \mu_f \left[1-\frac{\varphi_v}{\varphi_m}\right]^{-[\mu]_1\varphi_m}$	Krieger–Dougherty [148] (*3.17*)
$\mu_{nf} = \mu_f[1+2.5\varphi_v+6.5{\varphi_v}^2]$	Batchelor [149] (*3.18*)

nanofluids with acceptable accuracy, especially at larger nanoparticle concentrations [145]. Therefore, other equations were proposed to properly indicate the effect of nanoparticle concentration on the viscosity. Some of the nanofluid viscosity equations are listed in Table 3.4.

In [150], comparing experimental test results with calculated viscosities for nanofluids, it was concluded that Einstein's equation is suitable for viscosity calculation of nanofluids with nanoparticle concentrations smaller than 0.001. For nanofluids with nanoparticle concentrations from 0.001 to 0.1, the viscosity calculated by equation 3.19 shows a good agreement with measured viscosities.

3.14 TURBULENT FLOW

Like single-phase and multiphase flow regimes, laminar and turbulent flows are a type of fluid classification based on their fluid flow behavior. A fluid flow is in the laminar flow regime if the fluid particles move in a regular and smooth path. On the other hand, flows in which fluid flow is accompanied by turbulent changes are called turbulent fluid flow regimes. So, the turbulent flow regime is characterized by irregular movements of fluid particles that is indicated by Reynolds number. This irregularity is intensified by increasing the velocity of the fluid [151].

Heat transfer of different nanofluids was studied in [152]. In this study, Al_2O_3, CuO, and ZnO nanoparticles were added into water as the base fluid. In the turbulent fluid flow regime with Reynold numbers ranged from 4000 to 18000, the highest value Nusselt number was found in the case of adding Al_2O_3 nanoparticles to the base fluid because Al_2O_3 nanoparticles have the lowest mass density compared to other nanoparticles leading to high velocity of nanoparticles in the base fluid.

In [153], heat transfer of Al_2O_3 and TiO_2 nanoparticles in water as the base fluid was investigated. Reynolds number was considered in the range of 10000 to 40000. According to experimental results, the highest cooling performance enhancement was shown in the case of employing Al_2O_3-water nanofluids with 2% nanoparticle concentration. Also, for both nanofluids, the heat transfer coefficient increased with increasing in Reynolds number.

The thermal performance of water-TiO_2, Al_2O_3, and CuO nanofluids under a turbulent flow regime was investigated [154]. It was found that the heat transfer coefficient is strongly affected by nanoparticle concentration, type of nanoparticles and Reynolds number. According to results, increasing Reynolds number, the heat transfer increased by 0.7% to 8% for various nanofluids.

Heat transfer characteristics of Alumina and amorphous carbonic nanofluids under laminar and turbulent flow regimes were investigated in [155]. For the

alumina nanofluid, the heat transfer coefficient enhancement under the laminar flow regime was 15% and under turbulent was 20%. So, entering a turbulent flow regime could increase the heat transfer coefficient enhancement of the nanofluid by more than 30%. However, in the case of amorphous carbonic nanofluid, heat transfer coefficient enhancement under the laminar flow regime was 8% and no remarkable further heat transfer coefficient improvement was noticed in the turbulent flow regime.

3.15 GOVERNING EQUATIONS OF THE THREE-DIMENSIONAL TURBULENT FLOW

Governing equations of heat transfer and fluid flow problems including the equations of continuity, momentum, and energy conservation, are expressed in general forms as follows [156].

Continuity equation:

$$\frac{\partial}{\partial X_i}(\rho u_i) = 0 \qquad (3.19)$$

Momentum vector equations:

$$\frac{\partial}{\partial X_j}\left(\rho u_i u_j\right) = -\frac{\partial P}{\partial X_i} + \frac{\partial}{\partial X_j}\left[\mu\left(\frac{\partial u_i}{\partial X_j} + \frac{\partial u_j}{\partial X_i} - \frac{2}{3}\delta_{ij}\frac{\partial u_i}{\partial X_j}\right)\right] + \frac{\partial}{\partial X_j}\left(-\rho\overline{u'_i u'_j}\right) \qquad (3.20)$$

Energy equation:

$$\frac{\partial}{\partial X_i}\left(u_i(E\rho + P)\right) = \frac{\partial}{\partial X_j}\left[\left(\lambda + \frac{Cp\mu_t}{pr_t}\right)\frac{\partial T}{\partial X_j} + u_i\left(\tau_{ij}\right)_{eff}\right] = 0 \qquad (3.21)$$

where (E) is the total energy and $(\tau_{ij})_{eff}$ is the deviator stress tensor, which are defined as follows:

$$E = CpT - (P/\rho) + (u^2/2) \qquad (3.22)$$

$$\left(\tau_{ij}\right)_{eff} = \left[\mu_{eff}\left(\frac{\partial u_j}{\partial X_i} + \frac{\partial u_i}{\partial X_j}\right) - \frac{2}{3}\mu_{eff}\frac{\partial u_i}{\partial X_j}\delta_{ij}\right] \qquad (3.23)$$

The transfer equation for the shear stress transfer model (k-ω) is as follows:

$$\frac{\partial}{\partial X_i}(\rho k u_i) = \frac{\partial}{\partial X_j}\left(\Gamma_k \frac{\partial k}{\partial X_j}\right) + \tilde{G}_k - Y_k + S_k \quad (3.24)$$

$$\frac{\partial}{\partial X_i}(\rho \omega k u_i) = \frac{\partial}{\partial X_j}\left(\Gamma_\omega \frac{\partial \omega}{\partial X_j}\right) + \tilde{G}_\omega - Y_\omega + D_\omega + S_\omega \quad (3.25)$$

where (G_k) denotes the production of turbulent kinetic energy as a result of the mean velocity gradient and G_ω denotes the production of this term from ω.

$$\tilde{G}_k = \min(G_k, 10\beta^* k\omega) \quad (3.26)$$

$$G_k = -\overline{\rho u'_i u'_j}\left(\frac{\partial u_j}{\partial X_i}\right) \quad (3.27)$$

$$G_\omega = \frac{\alpha}{\upsilon_t} G_k \quad (3.28)$$

In the above-mentioned equation, υ_t is the turbulent kinematic viscosity, β^* is the model constant, and the factor α is calculated from the following equation:

$$\alpha = \alpha_\infty \frac{(\alpha^*_0 + Re_t/R\omega)}{(1 + Re_t/R\omega)} \quad (3.29)$$

$R\omega = 2.95$ and the term α is expressed as follows:

$$\alpha_\infty = F_1 \alpha_{\infty,1} + (1 - F_1)\alpha_{\infty,2} \quad (3.30)$$

$$\alpha_{\infty,1} = \frac{\beta_{i,1}}{\beta^*_\infty} - \frac{\kappa^2}{\sigma_{\omega,1}\sqrt{\beta^*_\infty}} \quad (3.31)$$

$$\alpha_{\infty,2} = \frac{\beta_{i,2}}{\beta^*_\infty} - \frac{\kappa^2}{\sigma_{\omega,2}\sqrt{\beta^*_\infty}} \quad (3.32)$$

$$\kappa = 0.41, \beta_i = 0.072, \alpha = \alpha_\infty = 1.0$$

where κ=0.41, and β_i = 0.072. In the above Reynolds numbers, $\alpha=\alpha_\infty=1$.

In (3.26) and (3.27), Γ_ω and Γ_k are effective diffusion of *k* and ω, and are expressed as follows:

$$\Gamma_k = \mu + \frac{\mu_t}{\sigma_k} \quad (3.33)$$

$$\Gamma_\omega = \mu + \frac{\mu_t}{\sigma_\omega} \quad (3.34)$$

σ_ω and σ_κ represent the turbulent Prandtl number in the model (*ω-k*), and are expressed as follows:

$$\sigma_\omega = \frac{1}{F_1/\sigma_{\omega,1}+(1-F_1)/\sigma_{\omega,2}} \quad (3.35)$$

$$\sigma_k = \frac{1}{F_1/\sigma_{k,1}+(1-F_1)/\sigma_{k,2}} \quad (3.36)$$

The μ_t sentence is turbulent viscosity and is expressed by the following equation:

$$\mu_t = \alpha^* \frac{\rho k}{\omega} \quad (3.37)$$

α^* is the attenuator of the turbulent viscosity and is expressed by the following equation:

$$\alpha^* = \alpha^*_\infty \frac{(\alpha^*_0+Re_t/R_k)}{(1+Re_t/R_k)} \quad (3.38)$$

$\alpha* = \alpha*_\infty = 1.0$

$Re_t = k\rho/\omega\mu, R_k = 6, \alpha^*_0 = \beta_i/3, \beta_i = 0.072$

The mixing equation *F1* is equal to:

$$F1 = \tan(\Phi_1^4) \quad (3.39)$$

$$\Phi_1 = \min\left[\max\left(\frac{\sqrt{k}}{0.09\omega y}, \frac{500\mu}{\rho y^2 \omega}\right), \frac{4\rho k}{\sigma_{\omega,2} D_\omega^+ y^2}\right] \quad (3.40)$$

$$D_\omega^+ = \max\left[2\rho \frac{1}{\sigma_{\omega,2}} \frac{1}{\omega} \frac{\partial k}{\partial x_j} \frac{\partial \omega}{\partial x_j}, 10^{-10}\right] \quad (3.41)$$

In equation (3.41), (*y*) is the distance to the next surface of the fluid, (D_ω^+) is the positive part of the diffusion sentence in the cross-section, and (Y_k) and

Table 3. 4. Proofs of k-ω shear stress transfer turbulence model.

$\sigma_{k,1}$=1/176	$\sigma_{k,2}$=1	$\sigma_{\omega,1}$=2	$\sigma_{\omega,2}$=1/168	α_1=0/31	$\beta_{i,1}$=0/075
$\beta_{i,2}$=0/0828	α^*_∞=1	α_∞=0/52	β^*_∞=0/09	β_i=0/072	α_0=1/9
R_β=8	R_k=6	R_ω=2/95	ζ^*=1/5	σ_k=2	σ_ω=2

(Y_ω) represent (k) and (ω) losses, respectively, and are defined as follows concerning turbulence:

$$Y_k = \rho\beta^* k\omega \quad (3.42)$$

$$Y_\omega = \rho\beta\omega^2, \beta^* \& \beta \text{areconstants} \quad (3.43)$$

$$\beta_i = F_1\beta_{i,1} + (1 - F_1)\beta_{i,2} \quad (3.44)$$

(D_ω) represents the diffusion sentence, and S_k and S_ω represent the possible source conditions. Specifically, D_ω equals:

$$D_\omega = 2(1 - F_1)\rho\sigma_{\omega,2}\frac{1}{\omega}\frac{\partial k}{\partial X_j}\frac{\partial \omega}{\partial X_j} \quad (3.45)$$

3.16 BASIC EQUATIONS GOVERNING THE THREE-DIMENSIONAL LAMINAR FLOW

The governing dimensionless equations include the equations of continuity, momentum, and energy, which are solved in a Cartesian coordinate for a steady-state.

Continuity equation:

$$\frac{\partial U}{\partial X} + \frac{\partial V}{\partial Y} + \frac{\partial W}{\partial Z} = 0 \quad (3.46)$$

Momentum equations:

$$U\frac{\partial U}{\partial X} + V\frac{\partial U}{\partial Y} + W\frac{\partial U}{\partial Z} = -\frac{\partial P}{\partial X} + \frac{1}{\rho_{nf}\nu_f}\frac{1}{Re\left(\frac{\partial}{\partial X}\left(\mu_{nf}\frac{\partial U}{\partial X}\right)+\frac{\partial}{\partial Y}\left(\mu_{nf}\frac{\partial U}{\partial Y}\right)+\frac{\partial}{\partial Z}\left(\mu_{nf}\frac{\partial U}{\partial Z}\right)\right)} \quad (3.47)$$

$$U\frac{\partial V}{\partial X} + V\frac{\partial V}{\partial Y} + W\frac{\partial V}{\partial Z} = -\frac{\partial P}{\partial Y} + \frac{1}{\rho_{nf}\nu_f}\frac{1}{Re\left(\frac{\partial}{\partial X}\left(\mu_{nf}\frac{\partial V}{\partial X}\right)+\frac{\partial}{\partial Y}\left(\mu_{nf}\frac{\partial V}{\partial Y}\right)+\frac{\partial}{\partial Z}\left(\mu_{nf}\frac{\partial V}{\partial Z}\right)\right)} \quad (3.48)$$

$$U\frac{\partial W}{\partial X}+V\frac{\partial W}{\partial Y}+W\frac{\partial W}{\partial Z}=-\frac{\partial P}{\partial Y}+\frac{1}{\rho_{nf}\nu_f}\frac{1}{Re\left(\frac{\partial}{\partial X}\left(\mu_{nf}\frac{\partial W}{\partial X}\right)+\frac{\partial}{\partial Y}\left(\mu_{nf}\frac{\partial W}{\partial Y}\right)+\frac{\partial}{\partial Z}\left(\mu_{nf}\frac{\partial W}{\partial Z}\right)\right)} \quad (3.49)$$

Energy equation:

$$U\frac{\partial \theta}{\partial X}+V\frac{\partial \theta}{\partial Y}+W\frac{\partial \theta}{\partial Z}=\frac{1}{\alpha_f\left(C_p\rho\right)_{nf}}\frac{1}{RePr\left(\frac{\partial}{\partial X}\left(K_{nf}\frac{\partial \theta}{\partial X}\right)+\frac{\partial}{\partial Y}\left(K_{nf}\frac{\partial \theta}{\partial Y}\right)+\frac{\partial}{\partial Z}\left(K_{nf}\frac{\partial \theta}{\partial Z}\right)\right)} \quad (3.50)$$

3.17 GOVERNING EQUATIONS TO CALCULATE PROPERTIES OF NANOFLUIDS

In this section, we discuss the equations governing the properties of nanofluids. The equation below is employed to calculate the density of the nanofluid:

$$\rho_{nf}=(1-\varphi)\rho_f+\varphi\rho_s \quad (3.51)$$

The effective heat dissipation coefficient of the nanofluid is calculated by the following equation:

$$\alpha_{nf}=\frac{k_{eff}}{\left(\rho C_p\right)_{nf}} \quad (3.52)$$

The specific heat capacity of the nanofluid is calculated using the equation below:

$$\left(\rho C_p\right)_{nf}=(1-\varphi)\left(\rho C_p\right)_f+\varphi\left(\rho C_p\right)_s \quad (3.53)$$

In turbulent flow, equation is employed to calculate the effective dynamic viscosity of the nanofluid:

$$\mu_{nf}=\mu_f(123\varphi^2+7.3\varphi+1) \quad (3.54)$$

In a laminar flow, equation is adopted to calculate the effective dynamic viscosity of the nanofluid:

$$\mu_{nf}=\frac{\mu_f}{(1-\varphi)^{2.5}} \quad (3.55)$$

The effective thermal conductivity of nanofluids with spherical particles is expressed as [157]:

$$k_{eff} = k_f \left[1 + \frac{k_s A_s}{k_f A_f} + c k_s Pe \frac{A_s}{k_f A_f}\right] \quad (3.56)$$

In equation (3.57), the experimental constant is *c=36000*:

$$\frac{A_s}{A_f} = \frac{d_f}{d_s} \frac{\varphi}{1-\varphi} \quad (3.57)$$

$$Pe = \frac{u_s d_s}{\alpha_f} \quad (3.58)$$

In equations (3.58) and (3.59), the diameter of water molecule and nanoparticle molecule are respectively (d_f) and (d_s), and (u_s) is the Brownian velocity of nanoparticles that is calculated by the following equation:

$$u_s = \frac{2\kappa_b T}{\pi \mu_f {d_s}^2} \quad (3.59)$$

In equation (3.60), the value of k_b=1.3807× 10^{-23} *J/K* is the Boltzmann constant.

3.18 EQUATIONS OF MEASURED PARAMETERS IN A THREE-DIMENSIONAL LAMINAR AND TURBULENT FLOW

Here, the parameters used are defined and the equations employed to calculate the parameters from the simulation results are discussed. The pumping power (PP) is among the parameters to determine the channel performance and is defined as the power required to pump fluid into the channel. The correlation between this parameter and the pressure drop (ΔP) along the channel is obtained from the following equation:

$$PP = u_{in} A_c \Delta P \quad (3.60)$$

where (u_{in}) is the inlet velocity in the channel and (A_c) is the cross-sectional area of the channel. The hydraulic diameter of the channel is also a physical characteristic of the channel and is defined as follows:

$$D_h = \frac{4A_c}{p} \quad (3.61)$$

where (A_c) is the cross-sectional area of the channel and (p) is the wetting environment of the channel.

The Reynolds number is a dimensionless quantity in the study of fluid flow regimes, which is another characteristic of the flow. In fluid mechanics, it indicates the ratio of inertial force to viscous force and is mainly applied to determine whether the fluid flow is laminar or turbulent. This number is also a similarity parameter for two different streams:

$$Re = \frac{u_{ave} D_h}{v} \tag{3.62}$$

The coefficient of friction is another parameter of channel performance, which depends on the parameters of the channel geometry and is calculated from the following equation:

$$f = 2\Delta P \frac{D_h}{L} \frac{1}{\rho {u_{in}}^2} \tag{3.63}$$

A mean Nusselt number is a two-dimensional parameter and in heat transfer, indicates the ratio of convective to conductive heat transfer across a boundary. It is obtained from the following equation:

$$Nu_{ave} = \frac{q'' D_h}{k_f (T_w - T_m)} \tag{3.64}$$

where (T_w) is the channel wall temperature and (T_m) is the average bulk temperature. To evaluate the overall thermal and fluidic performance of a channel, we define the parameter (PEC) as thermal efficiency as follows:

$$PEC = \frac{\left(\frac{Nu_{ave}}{Nu_{ave,s}}\right)}{\left(\frac{f}{f_s}\right)^{(1/3)}} \tag{3.65}$$

The Poiseuille number is calculated from the equation below:

$$C_f = fRe \tag{3.66}$$

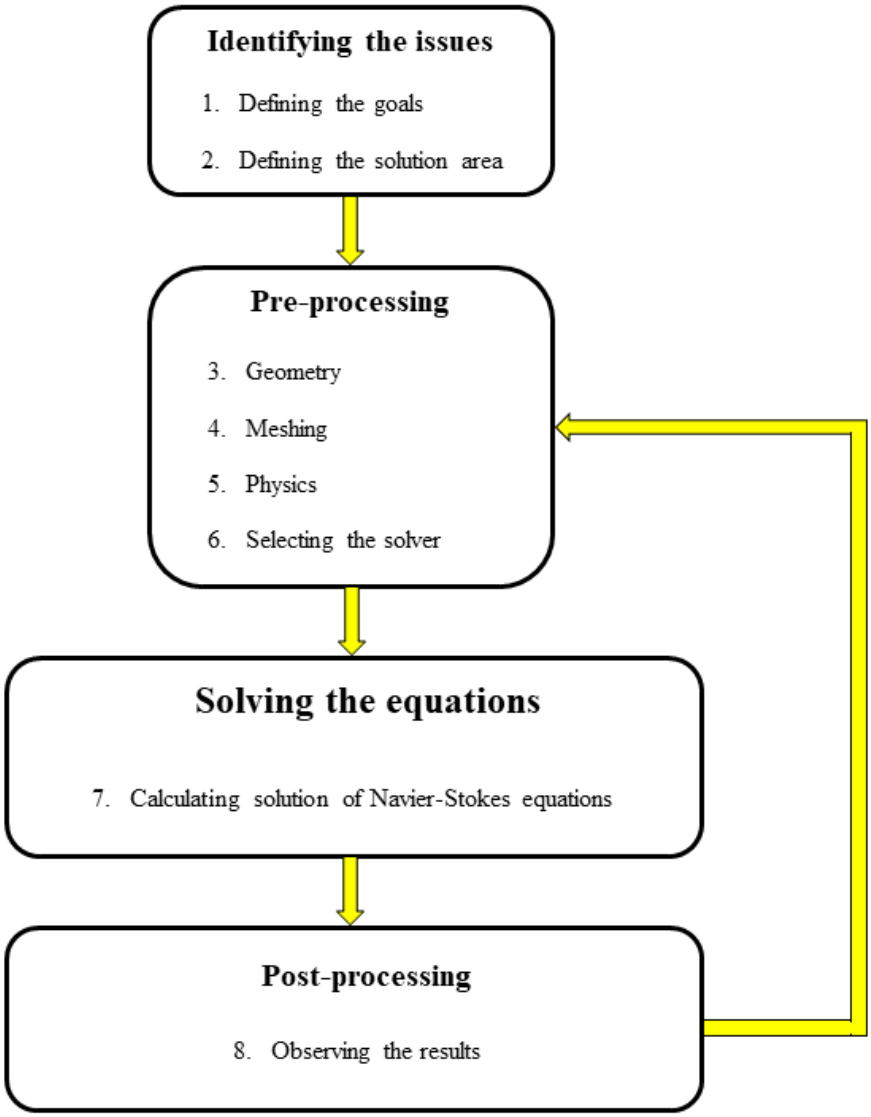

Figure 3. 10. Overview of problem-solving with CFD.

3.19 OVERVIEW OF PROBLEM-SOLVING WITH CFD

For CFD modeling, it is critical first to determine the objectives of the problem and then the scope of the modeling. The solution domain converts into a set of criteria by networking. Then, the problem can be solved by adjusting the physics of the problem (e.g., physical models, material properties, range properties, boundary conditions, etc.) and defining settings

for the solver (e.g., numerical methods, solution controllers, convergence, etc.).

The results are post-processed upon solving the problem. Now, the results can be evaluated, and the necessary modifications made to the model if necessary (Figure 3.10).

4. HEAT TRANSFER OF PHASE CHANGE MATERIAL

4.1 INTRODUCTION

Phase Change Materials (PCMs) can store large amounts of thermal energy when they are liquid at high temperatures and because of their high heat of fusion, can release large amounts of thermal energy when they transform to the solid phase. In fact, their distinctive property is charging and discharging a large amount of thermal energy from a small mass. The potential application of PCMs in cooling systems is to store the excess thermal energy during peak heat generation intervals and desorb it later through the released energy of their phase transformation. This chapter investigates heat transfer mechanisms of PCMs to provide a clear picture of their potential for use in the cooling systems of electric machines, which is the main focus of this thesis.

4.2 THE IMPORTANCE OF HEAT STORAGE

Heat storage systems are required in many applications. In applications where thermal energy is generated or extracted and it is necessary that all the thermal energy produced or part of it be used later, heat storage systems are required [158]. As a simple and basic application, sodium acetate that is a PCM is used in hand warmers. These hand warmers consist of sodium acetate gel in a

plastic bag. The heat stored in sodium acetate gel when it is in the liquid phase is released by changing its phase to the solid phase, causing the hands to warm up.

Another application of phase change materials is their use in building passive heat management systems. In fact, PCMs with low melting temperatures about room temperature are used to insulate walls and ceilings. In this application, excess heat inside the building is stored in the phase change material as latent heat and is released as the environment cools [159].

Renewable energy generation is another application for PCMs. In most cases, the purpose of producing renewable energy is to convert it into electrical energy, but thermal energy plays a role as an energy source or as a medium for energy conversion in these applications. For example, the energy produced by thermal solar panels is thermal energy used to heat water or the environment in residential buildings. On large scale, the generated thermal energy by solar panels is used to generate electric energy. In these systems, solar collectors absorb heat energy from solar radiation. This generated thermal energy is in heaters. Phase change materials are used in solar thermal systems to store thermal energy as well as to increase system efficiency.

On a larger scale, PCMs are used to store thermal energy to balance energy supply and demand in renewable energy plants. The demand for electricity varies greatly throughout the day and seasons. The difference between the demand for electricity at peak times and the times with low consumption is very significant. When using fossil fuels to generate electricity, regulating the amount of electricity generated is a straightforward process. Therefore, depending on the demand for electricity, energy generation can be increased or decreased. But in the case of renewable energy generation, energy generation changes throughout the day and night times and is also a function of the seasons. Therefore, energy storage systems should be used to balance the energy supply with the demand for energy [160]. In general, depending on the type of energy stored, energy storage systems are divided into three main categories, including electrochemical, electromechanical, and thermal energy storage systems. The classifications of various types of energy storage

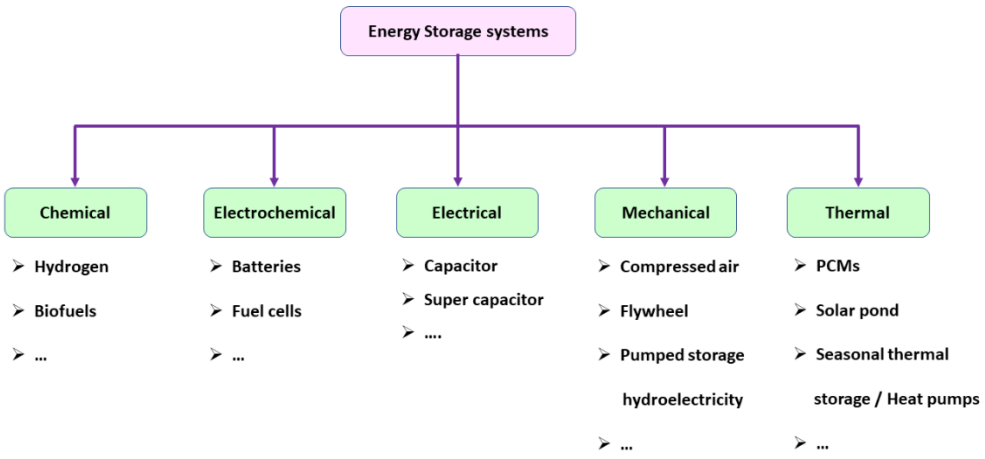

Figure 4. 1. Classification of energy storage systems.

systems are shown in Figure 4.1. Among them, some thermal energy storage systems use PCM materials [161].

It can be said that the largest contribution of PCM materials in energy storage systems is in concentrated solar power plants. In these renewable power plants, using mirrors or lenses, a large amount of sunlight is concentrated onto a receiver part containing solar thermal collectors. The absorbed thermal energy is used to produce steam driving an electric generator [162].

It is clear that it is not possible to generate electricity in these power plants during the night when there is no sunlight. As a solution, a PCM medium is used to store thermal energy during the day and use it at night. In this way, concentrated solar power plants can generate electricity during the day and night whenever there is a demand for energy. According to IRENA, molten-salt energy storage system capacity is expected to reach 870 GWh by 2030 [163].

4.2 PHASE CHANGE MATERIALS (PCMS):

PCMs are employed as storage media to store the thermal energy in the form of latent heat. The most distinctive property of PCMs is their high heat storage capacity in a small mass. The melting/solidification temperatures, thermal energy storage capability, and latent heat of fusion are the most determining properties of PCMs in their thermal performance [164].

Thermal energy storage systems exploit the high latent heat property of PCMs and their ability to store and release thermal energy through phase transformation. The maximum latent heat can be used when the transformation of PCMs is in the form of solid-liquid transformation. However, some PCMs store thermal energy with solid-solid transformation. In this way, heat is stored as a result of the transfer of material from one crystal structure to another. The Solid-solid transfer has less volume change compare to the solid-liquid transfer [165,166].

Other phase change mechanisms of PCMs are solid-gas and liquid-gas phase transformations. Solid-gas and liquid-gas transformations have higher latent heat transfer capacity, but their large volume change during the phase change process causes problems in storage containers and limits their potential applications in thermal storage systems [167]. In this regard, solid-solid PCMs have the smallest volume change leading to increased flexibility in their container design and ease of manufacturing. however, solid-solid and solid-liquid transformations have less latent heat capacity compared to liquid-gas transmission, but smaller volume change. Among various types of PCM phase change mechanisms, solid-liquid transformation is more commonly used in thermal storage systems.

The main components of a thermal energy storage system based on latent heat are as follows.

1. A suitable PCM with desired thermophysical properties, mainly, the heat of fusion and melting/solidification temperatures.

2. A suitable container that fits PCM properties.

3. An appropriate heat exchanger.

Therefore, to design and development a thermal energy storage system based on latent heat, knowledge of PCMs thermophysical properties, container requirements, and heat exchanger requirements are needed [168].

4.3 APPLICATION OF PHASE CHANGE MATERIAL IN COOLING SYSTEMS

According to latent heat properties of PCMs, as a passive cooling system, PCM-based cooling systems have absorbed much attention for electric machine cooling system applications. High latent heat capacity of PCMs can be exploited to absorb a large amount of heat and store it during a limited time based on the specific latent heat capacity of the employed PCM material. Phase changing process of PCMs intensifies their heat storage capability. Then, the stored heat is released through the phase change process of PCMs [169]. Thermal energy is absorbed while its solid form is turned to liquid and is desorbed when its liquid form is turned to solid [170]. The later start of the melting process leads to the larger amount of heat that can be absorbed by PCMs. Several factors such as thermal conductivity of the selected PCM, thermal conductivity of the heat exchanger container, and the thickness of heat exchanger container can affect the duration of PCMs' melting process and consequently latent heat capacity of PCM-based cooling systems. It was demonstrated that the time needed for melting process of PCMs increases with decreasing thermal conductivity of heat exchanger container. [171].

For applications with size and volume constraints, cooling with phase change materials is an effective approach. Actually, employing PCMs in cooling systems can significantly reduce the size of cooling systems. For example, employing PCMs in heat sinks can increase their heat absorption and desorption capability leading to smaller size of heat sinks for a given application [172, 173].

4.4 THERMAL ENERGY STORAGE TECHNIQUES

In some application such as renewable energy generation, there is need to store the generated energy in the form of heat to be used later when it is needed. Thermal energy storage (TES) systems are used to store thermal energy. Storing thermal energy produced from geothermal power plants is an example of TES application. Using TESs, thermal energy can be stored for a short-term or long-term durations. For example, storing heat during summer to be used in winter [174].

Some applications of TES systems are as follows:

1. Storing generated thermal energy from renewable sources to balance the energy supply and demands. In this case, TES systems can bridge the gap between the generated thermal energy and thermal energy demands by storing the generated energy during off-peak demand hours and releasing the stored thermal energy during peak demand hours.

2. Energy efficiency enhancement of buildings. In these applications, PCMs act as TES systems inside walls and sealings.

3. Waste heat reusing in industrial processes.

PCMs are one of the materials used in TES systems. According to their unique properties, many of high-efficiency TES systems are PCM-based storage systems. Phase change process of PCMs can be in various forms such as solid-solid, solid-liquid, solid-gas, liquid-gas, and vice versa. According to application requirements such heat absorption capacity, cost, and size one of the mentioned phase change categories can be adopted. TES systems employing PCMs that transform from liquid or solid phases to gas phase are the least cost-effective TES systems as in these cases there are specific container requirements [175].

4.4.1 VARIOUS THERMAL ENERGY STORAGE SYSTEMS

Thermal energy can be stored by various methods such as sensible heat, latent heat and chemical heat, or a combination of them.

4.4.1.1 SENSIBLE HEAT STORAGE

In sensible heat storage, thermal energy is stored without changing the phase of the medium used for heat storage. In this case, thermal energy is stored by increasing temperature of the storage medium. Storage mediums can be in solid or liquid phases. Actually, these TES systems rely on thermal capacity of materials temperature change during the thermal energy charging and discharging process. The amount of stored heat depends on the specific heat of used materials and can be expressed as follows [176]:

$$Q = \int_{T_i}^{T_f} mC_p dT \qquad (4.1)$$

$$Q = mC_p(T_f - T_i) \qquad (4.2)$$

where (m) is mass, (C_p) is special heat, (T_f) is liquid temperature, and (T_i) is the initial temperature of fluid.

4.4.1.2 LATENT HEAT STORAGE

These TES systems exploit the latent heat capacity of materials used as the storage medium when changing their phase from liquid or solid into gas or vice versa. The storage capacity of the latent heat storage system is defined as follows [177]:

$$Q = \int_{T_i}^{T_m} mC_p dT + ma_m \Delta h_m + \int_{T_m}^{T_f} mC_p dT \qquad (4.3)$$

$$Q = m\left[C_p(T_m - T_i) + a_m \Delta h_m + C_p\left(T_f - T_m\right)\right] \qquad (4.4)$$

where (a_m) is the volume fraction of liquid phase, (Δh_m) is enthalpy change, (C_p) is specific heat capacity, and (T) is fluid temperature.

4.5 ENERGY STORING WITH LATENT HEAT

PCMs are employed in TES systems that are based on latent heat. In these TES systems, thermal energy charging and discharging occurs when material phase changes from one phase to another phase. This kind of transformation is called phase change.

The most common and cost-effective PCM-based TES systems employ PCMs with solid-liquid phase change process. Unlike in sensible heat storage systems, PCMs used in TES systems absorb and release heat at semi constant temperature. Heat storing capacity of PCMs can be several times more than sensible heat storing materials like water [178, 179]. Figure (4.2) shows the heat capacity of different materials [180].

Figure 4. 2. Heat capacity of different materials [180].

4.5.1 FEATURES OF PHASE CHANGE MATERIALS

Phase change materials employed in TES systems must possess specific chemical, thermophysical, and economic features that are listed below [181]:

Thermophysical features:

- High Latent heat

- Fixed melting temperature or in a limited range
- High thermal conductivity
- High heat capacity
- High density
- Low volume change
- No deterioration of thermophysical properties
- Reversible melting and solidification processes

Chemical features:

- Chemical stability
- Compatibility with container material
- Non-toxic
- Non-flammable

Economic features:

- Accessibility
- Low cost

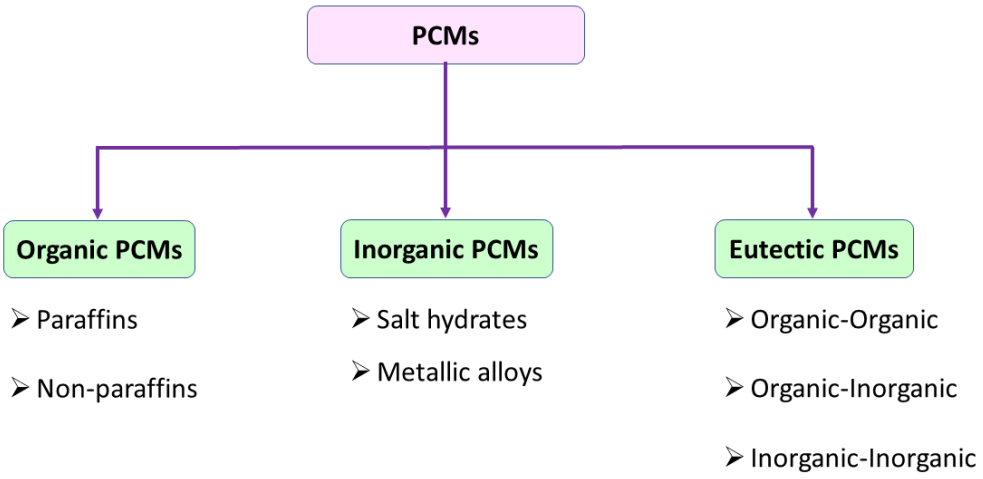

Figure 4. 3. Classification of phase change materials [182].

4.5.2 CLASSIFICATION OF PHASE CHANGE MATERIALS

Phase change materials are classified under organic, inorganic, and eutectic categories. These categories are shown in Figure 4.3.

4.5.2.1 ORGANIC PHASE CHANGE MATERIALS

Organic materials are divided into two groups of paraffin and non-paraffin. Such materials have homogenous melting and are corrosive for materials of their container. Organic phase change materials applied for heating and cooling of buildings have the melting point at 20 to 32 degrees on the Centigrade scale [183, 184].

Paraffins:

Paraffin includes a combination of straight chains. Crystallization of this chain causes the release of a great amount of Latent heat. Melting point and Latent heat increase by increase of chain length. Paraffin is one of the best choices for being used as a phase change material for energy saving due to its extensive accessibility in a wide range of melt temperatures [185].

Regarding economic considerations, only paraffin with industrial purity can be utilized as phase change materials in systems of saving Latent heat. Paraffin is safe, reliable, predictable, noncorrosive, and cheap. It is also

neutral and stable chemically below 500 degrees on the Centigrade scale and does not have much volume change and has low steam pressure in melting [186].

Due to the above-mentioned features, paraffin has a long solidification-melting cycle. In addition to such features, homogenous melt which forms the nucleus is another significant feature of paraffin. Its defects include low conductivity coefficient, slight flammability, and incompatibility with plastic containers. These defects can be removed with a slight change in paraffin wax and saving unit. Table (4.1) provides a list of selected paraffin with melting point and Latent heat.

Non-paraffins:

Organic non-paraffins include numerous materials with changing features. Some researchers have conducted an extensive investigation on organic materials and finally considered some esters, fatty acids, alcohol, and glycols suitable for saving energy. Some of their features include high Latent heat, flammability, coefficient of low thermal conductivity, low flammability point, different degrees of toxin, and incompatibility in high temperatures [188].

Table 4. 1. Melting point and Latent heat of paraffin [187]

Groups	Latent heat (kJ/kg)	Melting point (^{o}C)	Number of carbon atoms
I	228	5/5	14
II	205	10	15
I	237	16/7	16
II	213	21/7	17
I	244	28	18
II	222	32	19
I	246	36/7	20
II	200	40/2	21
II	249	44	22
II	232	47/5	23

II	255	50/6	24
II	238	49/4	25

4.5.2.2 INORGANIC PHASE CHANGE MATERIALS

Inorganic materials are divided into salt and metal hydrates. Inorganic compounds have high Latent heat in units of mass and volume. They are cheap and inflammable in comparison with organic compounds. However, such materials have some defects like decomposition and undercooling (which affects features of phase change) [189].

Salt hydrates:

The general formula of salt hydrates is as follows. Transfer of solid-liquid phase of salt hydrates is indeed dehydrating these materials. Salt hydrates are an important group of phase change materials that possess the following features: Latent heat in volume unit, quite high thermal conductivity, slight changes of volume while melting, being toxic slightly, homogenous melt, density difference of water, and the material combined with it (which causes sedimentation at the bottom of the container) and formation of a weak nucleus which causes undercooling [190].

Metals:

Such materials include metals with low melting points and eutectic metals. Such metals have not been taken seriously in the technology of phase change materials due to their weight. High Latent heat in volume unit and high conductivity coefficient are their features [191].

4.5.2.3 EUTECTICS PHASE CHANGE MATERIALS

Eutectic is a combination of two or several elements with minimum melt. They quite constantly get melted and solidified without being decomposed.

4.6 SPIRAL CANALS HAVING PHASE CHANGE MATERIALS

Phase change materials are used as temperature regulators in different situations. Such materials melt and solidify at a fixed temperature and can store and release a high amount of energy. Thermal energy is absorbed while its solid form is turned to liquid and is desorbed when its liquid form is turned to solid. Furthermore, their consumption power has increased, and their sizes have decreased with the advancement of electronic equipment [192]. As a result, more power is inserted at a lower level. Therefore, heat management has become a significant issue in designing devices such as smartphones, digital cameras, notebooks, and personal ancillary digital equipment. Such devices are not used consistently in the long term. Consequently, cooling systems can be used in such situations based on phase change materials.

Cooling based on phase change materials is a passive cooling method and the cooling process can be divided into three stages depending on temperature (see Figure 4.4). In the first stage, heat is absorbed through an electric motor so that the temperature of solid material reaches melting temperature. In the second stage, phase change material starts to melt at a fixed temperature, and heat is absorbed without temperature increase during the melting process. Size may increase slightly in this stage due to phase change [193].

In the third stage where phase change material is melted, fluid temperature increases if input heat continues. Although phase change materials can absorb a great amount of heat while changing phase, cooling by them may be limited to the necessary time needed for complete melt. Therefore, it is desirable that phase change materials are used in situations where input heat is alternate and sudden [182].

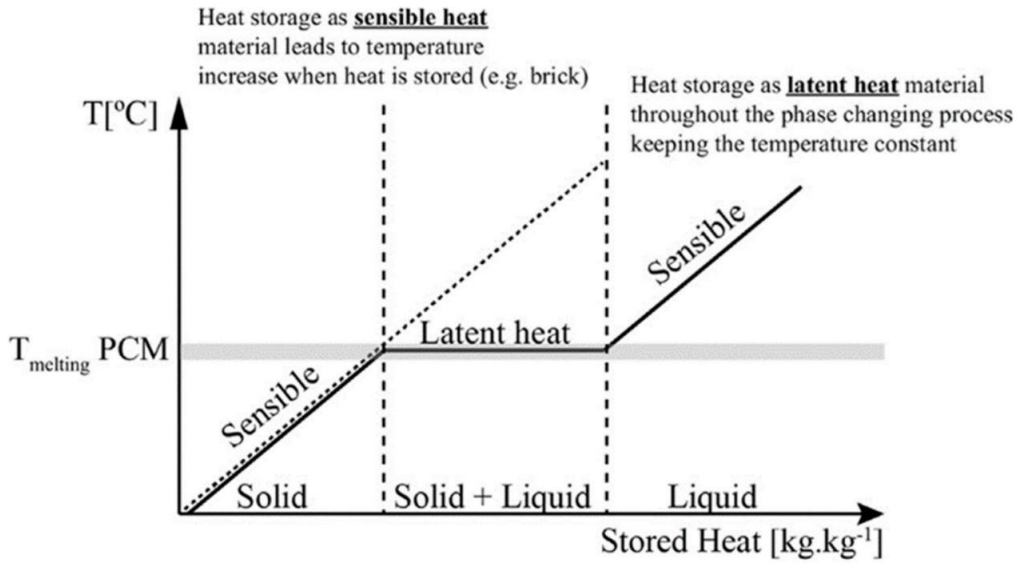

Figure 4. 4. A scheme of temperature changes of phase change materials [181].

Unique features of phase change materials like having Latent heat of high fusion, high thermal capacity, and being non-toxic and noncorrosive have made them suitable for systems of heat management. Phase change materials store energy five to fourteen times more than saving materials of sensible energy.

As a result, researchers have paid attention to them as one of the best resources for saving energy during recent years. They are extensively utilized in engineering systems. They are also used in energy-saving systems, cooling of electrical systems, energy saving in buildings, heat exchangers, and other applications.

However, these materials have the undesirable feature of low thermal conductivity which causes a tough challenge for using them in cooling systems. In order to solve such a problem, it is needed to use materials with high thermal conductivity in systems having phase change materials. This material with such conductivity can be used in different shapes like blades, metal structures, or nanoparticles [194].

4.7 INCREASE OF THERMAL CONDUCTIVITY COEFFICIENT OF PHASE CHANGE MATERIALS

Most phase change materials have a high capacity for heat saving (99 to 330 kilojoules per kilogram). But their basic problem is their low thermal conductivity coefficient (0.2 W/m.K for most paraffin and 0.5 W/m.K for Inorganic salts) [195]. The weak performance of heat transfer is the key limiting factor in employing phase change materials in situations needing quick saving and releasing energy.

Basically, the coefficient of thermal conductivity of phase change materials can increase by employing materials with high conductivity coefficient. This coefficient increase can happen by increasing materials with high conductivity in various methods. These methods include:

- Placing metal compounds and structures in phase change materials
- Distributing particles with high thermal conductivity in phase change materials

Researchers found out that adding particles with high thermal conductivity at micro and nanoscale to phase change materials enhanced thermodynamic features of phase change materials and this resulted in a system performance increase.

Placing phase change materials in spiral pipes is discussed as a technique for increasing the thermal conductivity coefficient of phase change material. It has been observed that placing phase change materials in a spiral pipe leads to a significant decrease of time needed for phase change and consequently system efficiency is improved significantly. Studies of researchers have indicated that all metals were not compatible with phase change materials. For instance, aluminum particles are compatible with paraffin while nickel is not. This caused researchers to seek materials with low density and high thermal conductivity coefficient that were compatible with all phase change materials.

Studies on phase change materials began in 1940 by Telex and Reymond [196], but it did not catch much attention until the late 1970s and the beginning of the 1980s when energy resources decreased. From then on, extensive studies were conducted on various applications of these systems e.g. solar heating systems such as those carried out by Esparrow et al. [197], Morrison and Adel Khalik [198], and Marshal and Dietsche [199].

Some studies were conducted on determining the general behavior of phase change materials in the late 1970s including Stritih [200], Ismail et al. [201] and Agyenim et al. [202] Studies conducted on such materials especially their basic designing, systems, and optimization processes, investigation of transient behavior and performance of these systems also continued. Investigation and development were extensively conducted in the field of dissociation of particular phase change materials and also on problems and limitations of this method and features of new materials.

The main defect in the majority of phase change materials is their low thermal conductivity coefficient which slows down the rate of melting and solidifying in these materials. Development of PCMs concerns comprehending the thermal behavior of these materials when they enter the area of solid-liquid phase change and also designing and selecting containers for preserving and formulating issues related to phase change. Various geometries have been suggested for the container of saving PCM. PCMs are usually preserved in narrow and long heat pipes and cylindrical or rectangular containers. The findings indicated that both rectangular and cylindrical containers had more applications in comparison with other ones.

Hosseini et al. [203] investigated thermal behavior and features of heat transfer of paraffin RT50 as PCM during the melting and solidification process in a shell and tube heat exchanger in a laboratory and numerical test. Their numerical results indicated that the melting zone had appeared in different times and places near fluid pipe of heat transfer and progressed towards the exterior. Laboratory results also indicated that an increase of fluid temperature from 70 to 80 Celsius degrees caused an increase of theory in melting and solidification process up to 4.88 and 4.81 percent respectively.

Rahimi et al. [204] investigated the solidification and melting process of RT35 as PCM in a shell and tube heat exchanger in a laboratory test. Cubic shell contained a pipe in which space between shell was filled with RT35 and water was flowing as working fluid in pipes.

The results indicated that using shell increased the average temperature of it without any consideration of the flow, while a decrease of shell pace had no considerable effect on this parameter. Furthermore, when input fluid temperature increased from 50 to 60 degrees on the Celsius scale melting time decreased more in comparison with the increase from 60 to 70 degrees on the Celsius scale.

Investigation of melting behavior of phase change material was conducted by Hosseini et al. [205] in a shell and tube heat exchanger in a numerical and laboratory test. They found out that the increase in fluid temperature of heat transferor (water) from 70 to 80 degrees on the Celsius scale decreased the general time of melting to 37 percent.

Lieu et al. [206] investigated thermal features of citric acid while melting in a vertical energy-saving system in a laboratory test. They studied the movement of the liquid-solid surface along a radius and the effect of Reynolds number on parameters of heat transfer. The effect of shell length was also reported. Their results indicated that shell in thermal conductivity and also natural movement enhanced the process of heat transfer.

Hosseini et al. [207] investigated the melting and solidification process of PCM in another numerical and laboratory test by using linear shells as thermal conductivity enhancement (TCE) in shell and tube heat exchangers. Their results indicated that using longer shells would cause faster melt and more feasible temperature distribution.

Bathelt and Viskanta [208] investigated heat transfer while a horizontal cylinder was being melted under the pressure of fixed heat flux at a fixed surface temperature and being placed in a para blade in a laboratory test. They reported that the melting behavior of phase exchange material in the upper

half was more visible due to ascending flow of melting material affected by natural movement.

Ettouney et al. [209] studied the melting and solidification process in a shell and tube heat exchanger in a laboratory test. The fluid heat transferor was placed in the interior pipe and paraffin wax as PCM was placed in a shell. The results indicated that processes of melting and solidification were affected by natural movement and conductivity respectively.

Akgün et al. [210] investigated the wax paraffin melting process in a vertical shell and tube heat exchanger in a laboratory test. They focused on the enhancement of heat transfer of thermal storage system containers. Their results showed that the increase in temperature of heat transferor resulted in a decrease of time needed for melting of phase change material. They also reported that less input flow rate was needed for less energy consumption.

Vyshak and Jilani [211] investigated numerically the effect of different geometries of energy-saving systems that had the same volume and level. They carried out a comparative study on the total time needed for melting phase change material placed in three various geometries (rectangular, cylindrical and, shell and tube). Their results indicated shell and tube containers had the least amount of time for an equivalent amount of stored energy which was affected more by increasing mass of PCM in the intended geometry.

Pahamli et al. [212] recently investigated the effect of centrifugal force of the pipe carrying working fluid on the melting process of paraffin RT50 in shell and tube geometry. Their results indicated that an increase of centrifugal force towards the below part could decrease the time needed for complete melt to 64 percent by increasing natural movement.

Pradeep et al. [213] investigated the effect of adding nanoparticles to phase change materials. They studied the effect of adding silver nanoparticles to the capability of energy saving of phase change materials (paraffin) by conducting an experimental test. They added 0.05 and 0.1 percent mass of nanoparticles to paraffin and investigated the melting and solidification

temperature of paraffin. Their results indicated that adding silver nanoparticles to paraffin increased the capability of thermal energy saving.

Kasali et al. [214] investigated the behavior of phase change materials in an electronic diode component. Their findings showed that using phase change materials increased the capability of temperature tolerance of electronic components.

Selvam et al. [215] investigated using phase change materials for temperature management of a thermoelectric and also used COMSOL software for simulation. Their results indicated that using phase change materials decreased the operating temperature of thermoelectric so that phase change materials with 3-millimeter thickness decreased average temperature by 33 %.

According to numerical and experimental studies conducted by researchers, it can be concluded that phase change materials show a reasonable performance. The studies that investigated the performance of phase change materials numerically considered the flow unsteady and changes of other quantities have been provided based on time.

5. ELECTRIC MACHINE COOLING SYSTEMS BASED ON ETHYLENE GLYCOL AND WATER MIXTURE IN SPIRAL CHANNELS

5.1 INTRODUCTION

The overall performance of a cooling system based on the cooling-jacket method employing for the thermal management system of an electrical machine for automotive application is investigated in this chapter. The cooling system is based on the closed-circuit liquid cooling method employing a mixture of Ethylene Glycol and water as its coolant. The overall performance of the cooling system employing Ethylene Glycol and water mixture with different volume fractions is evaluated. Various geometry of the cooling system, and physical characteristics of the coolant fluid are studied. Thermal analyses of the cooling system are performed using computational fluid dynamics and 3D turbulent fluid motion analysis. According to analysis, influence of the critical parameters on the overall performance of the cooling system is studied.

5.2 LIQUID-COOLING SYSTEMS EMPLOYING ETHYLENE GLYCOL AND WATER MIXTURE AS THE COOLANT

Ethylene glycol (C2H6O2) is a colorless and odorless fluid with a low viscosity. Adding Ethylene Glycol to a base fluid, its freezing point is lowered and the boiling point increased. The effect of Ethylene Glycol on freezing and boiling points depends on its concentration in the base fluid. On the other hand, as Ethylene Glycol is substantially toxic, maximum volume fraction of is mixture with a base fluid is limited. The lower limit of the volume fraction is determined by requirements of the desired application. In [216], it was demonstrated that a mixture of 40% Ethylene Glycol and 60% water shows a better performance compared to 50%-50% mixture. Physical properties of Ethylene glycol are listed in Table 5.1 [217]. Thermal conductivity, density, and velocity of the mixture of Ethylene glycol and water at different volume fractions of the mixture are shown in Figure 5.1, 5.2, and 5.3, respectively [218].

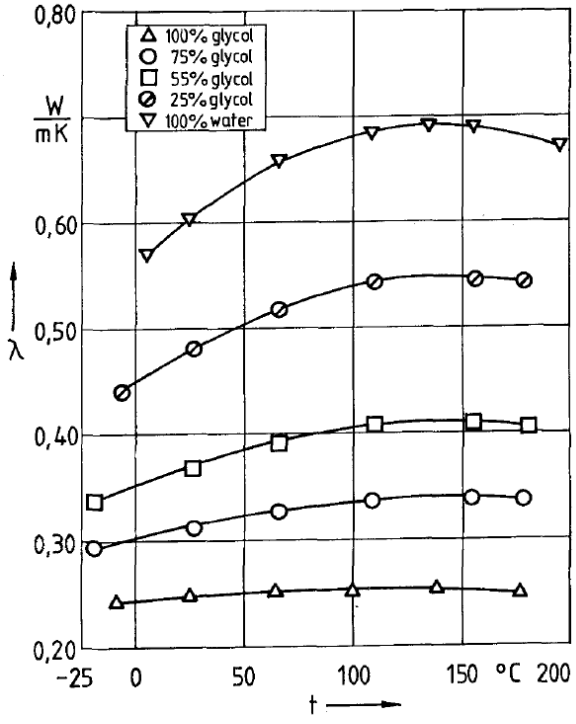

Figure 5. 1. Thermal conductivity of ethylene glycol-water mixtures [218].

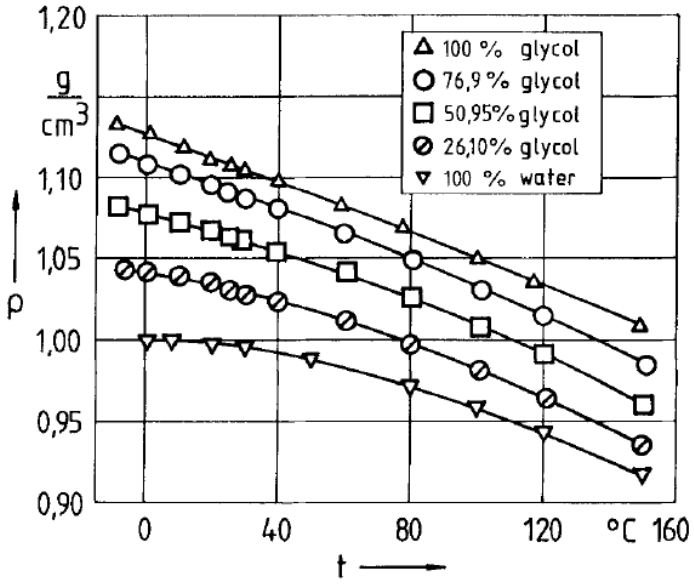

Figure 5. 2. Density of ethylene glycol-water mixtures [218].

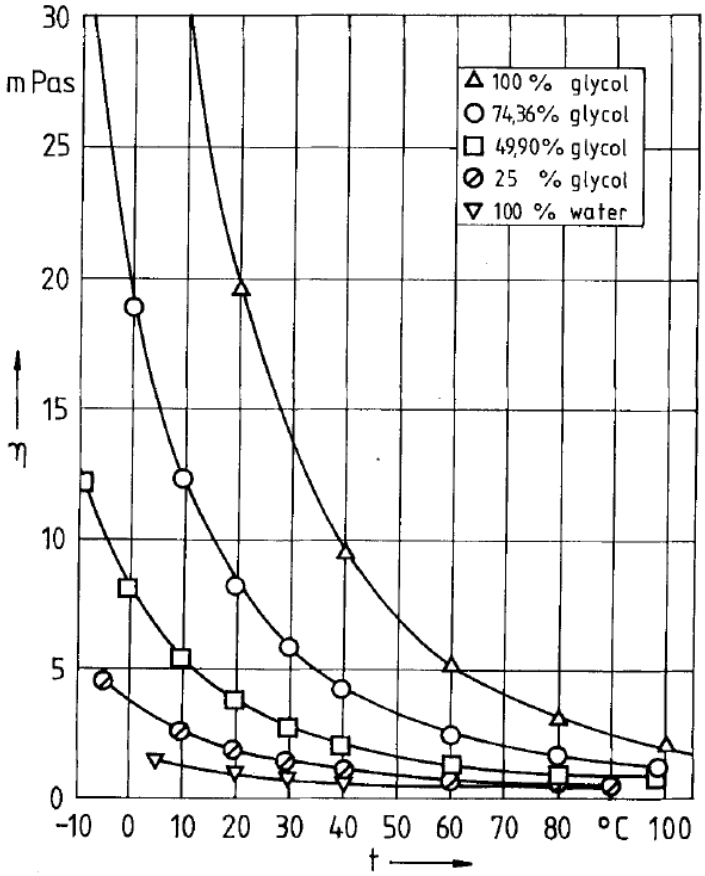

Figure 5. 3. Viscosity of ethylene glycol-water mixtures [218].

Table 5. 1. Physical properties of Ethylene glycol [217]

Auto-ignition temperature	**427.0 °C**
Boiling point at 101.3 kPa	197.6 °C
Critical temperature	446.9 °C
Critical specific volume	19.1×10^{-2} L g^{-1}mol
Cubic expansion coefficient at 20 °C	6.2×10^{-4} K^{-1}
Density at 20 °C	1113.5×10^{-9} g m^{-3}
Flash point, closed cup (Pensky-Martens closed cup ASTM D93)	126.7 °C
Flash point, open cup (Cleveland Open Cup ASTM D92)	137.8 °C
Heat of combustion at 25 °C	-1053.0 kJ g^{-1} mol
Heat of vaporization at 1 atm	53.2 kJ g^{-1} mol
Lower explosive limit	3.2 vol%
Molecular weight	62.1 g mol^{-1}
Normal freezing point	-13.0 °C
Onset of initial decomposition	240.0 °C
Refractive index at 25 °C	143.0×10^{-2}
Specific gravity (20/20 °C)	111.0×10^{-2}
Solubility in water at 20 °C	100 wt%
Solubility of water in ethylene glycol at 20 °C	100 wt%
Surface tension at 25 °C	48.0×10^{-3} N m^{-1}
Upper explosive limit	53.0 vol%
Vapor density (air = 1)	2.1
Vapor pressure at 20 °C	7.5 Pa
Viscosity at 20 °C	19.8×10^{-3} Pa s

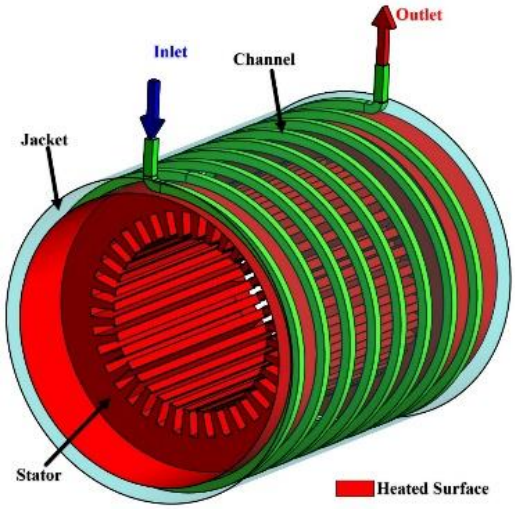

(a)

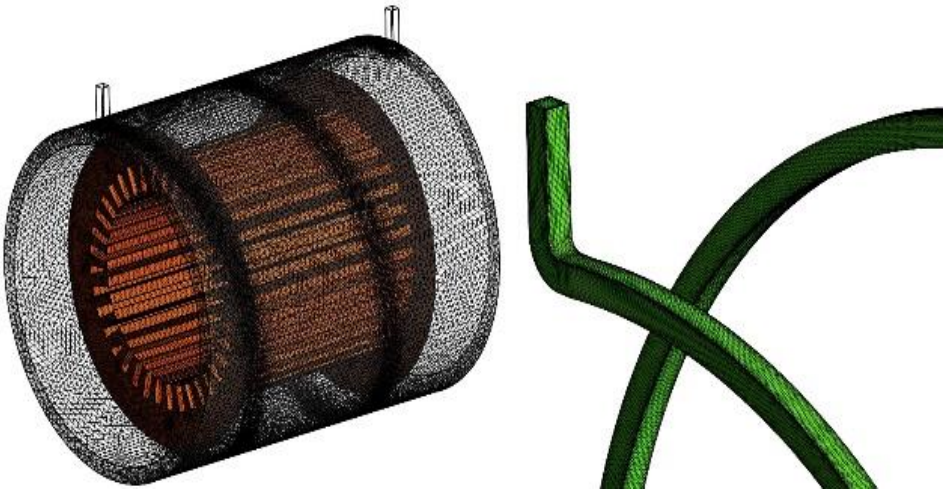

(b)

Figure 5. 4. Problem schematic representations, (a) Stator and cooling system, (b) non-uniform mesh grids.

In this chapter, a spiral channel liquid-cooling system is designed and its overall performance is investigated for various cases such as using different coolant fluids, different structural geometry, and different physical characteristics of the coolant fluid. In the designed cooling system, both sides of end-winding areas are covered by the cooling jacket. Thermal analysis is implemented based on 3D turbulent fluid motion model. Computational fluid dynamics (CFD) analysis is used to compare simulation results and to explain impact of different parameters on performance of the cooling system.

5.3 COOLING SYSTEM MODEL

The implemented cooling system consists of spiral channels in the machine housing, surrounding the stator winding and end-winding regions. Dimensions of the modelled electric machine and the cooling system are listed in Table 5.2. Materials of the external surface of the electric machine and the cooling-jacket are listed in Table 5.3. Figure 5.4.a shows the designed cooling system. The channel has a rectangular cross section with width of 6 mm and height of 6 mm. Under-study coolants are water and different mixtures of water and Ethylene Glycol. Mixing ratios of Ethylene Glycol and water are 20:80, 40:60, and 60:40. Figure 5.4.a shows three different geometrical components of the under-study cooling system and electric motor. It consists of the stator core, aluminum housing, and cooling channel inside the housing. Through the channel, a cooling liquid circulates refrigerating the motor.

In order to reduce computational expenses, simulation of some electrical parts such as windings have been avoided and from a separate thermal analysis, the generated heat flow has been determined. As can be seen in Figure 5.4.a, only outer surfaces of the electric machine and the aluminum jacket have been considered. The inlet coolant temperature is given as 70°C. To have some extra cooling margin for the designed cooling system, it has been assumed that whole the generated heat from the machine is taken away by the aluminum housing. A uniform heat flux of 3500 W/m2 has been applied to outer surface of the stator. Turn number of the spiral channel are 2, 4, 6, and 8 turns. The coolant flow is turbulent and simulation studies are implemented under Reynolds numbers of 2500, 5000, 7500, and 10000. Boundary conditions are listed in Table 5.4. Thermophysical properties of coolant fluids are summarized in Table 5.5.

In this chapter, computational fluid dynamics (CFD) studies are performed using Ansys CFX. The pressure velocity coupling is achieved using Rhie-Chow interpolation technique. The convergence criterion for hydrodynamic

Table 5. 2. Dimensions of the electric machine and the cooling jacket

	Electric Motor	**Water Jacket**
Length	190 mm	210 mm
Width	240mm (with coil)	240 mm
Thickness	_____	10 mm

Table 5. 3. Materials of the electric machine and the cooling jacket

	Material
Stator	Steel
Water Jacket	Aluminum

and thermal parameters is considered to be $1e\text{-}^{6}$. k-W model is used for simulating turbulence inflow conditions.

In simulation of the system, non-uniform meshes are used so that adjacent to the channel walls due to the large gradients, smaller meshes are used. Mesh grids are shown in Figure 5.4.b.

5.4 GOVERNING EQUATION OF 3D TURBULENT FLUID MOTION

Some governing equations of heat transfer and fluid motion are conjugation equations, momentum and energy equations which are described in this section. The Reynolds number in the fluid flow analysis, is another characteristic of the flow which a non-dimensional quantity is representing the ratio of the inertial force to the viscous force. Reynolds number is used to determine whether the fluid flow is laminar or turbulent.

$$Re = \frac{u_{ave} D_h}{v} \quad (5.1)$$

where uave is the speed of the coolant fluid (m/s), v is kinematic viscosity of the fluid (m2/s), and Dh is channel diameter (m). The channel diameter is one of the physical characteristics of the channel and is defined as follows.

$$D_h = \frac{4A_c}{p} \quad (5.2)$$

where, Ac is the cross-sectional area of the channel and p is the duct area.

Another performance evaluating parameter of the channel is the friction coefficient that depends on geometry parameters of the channel and is calculated by the following equation.

$$f = 2\Delta P \frac{D_h}{L} \frac{1}{\rho {u_{in}}^2} \quad (5.3)$$

The average Nusselt number is also a non-dimensional number indicating the heat transferred through the convection to the heat transmitted through the conduction and is obtained from the following equation.

$$Nu_{ave} = \frac{q'' D_h}{k_f (T_w - T_m)} \quad (5.4)$$

where, Tw, is the temperature of the channel wall and Tm is the average bulk fluid temperature. To determine the overall thermal and fluid performance, we define the parameter PEC (Performance Evaluation Criterion) as follows.

$$PEC = \frac{\left(\frac{Nu_{ave}}{Nu_{ave,s}}\right)}{\left(\frac{f}{f_s}\right)^{(1/3)}} \quad (5.5)$$

where, Nuave,s and fs are base parameters and are defined for the base fluid (pure water). Indeed, PEC indicates the ratio of the increase in heat transfer capability to the increase in the pressure drop caused by coolant fluid in comparison with the base fluid.

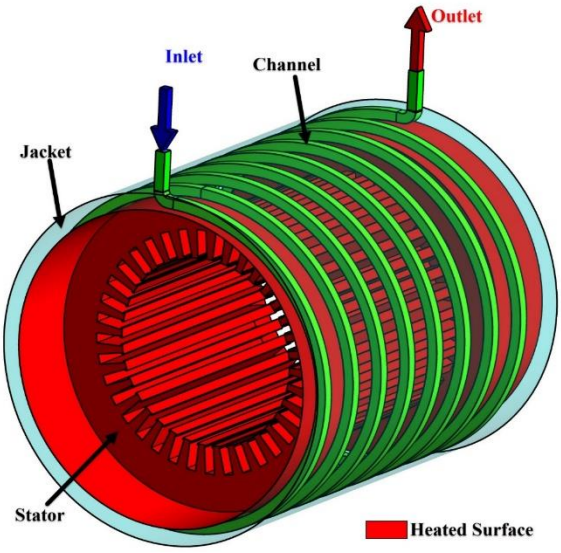

Figure 5. 5. Geometric boundary conditions.

Table 5. 4. Boundary conditions and CFD determinant parameters.

Boundary Conditions	
Re	2500, 5000, 7500, 10000
Number of Turns	2, 4, 6, 8
Working Fluids	Pure Water EG/W 20:80 EG/W 40:60 EG/W 60:40
Inlet Temperature	343.15(K) / 70 (c')
Heat Flux	3500 (W/m^2K)

5.5 BOUNDARY CONDITIONS

Boundary conditions and considered combinations of determinant parameters are listed in Table 5.4. The determinant parameters are Reynolds number, channel turns number, and volume fraction of the Ethylene Glycol-Water mixture. Boundary conditions are temperature of the inlet fluid and the heat flux transferred from internal parts of the electric machine to the cooling jacket. In this study, heat flux is considered as a constant value. Geometric boundary conditions are shown in Figure 5.5.

5.6 RESULT AND DISCUSSION

Average convection heat transfer coefficient and average Nusselt number for different Reynold numbers under different turn number of the spiral channel and at different volume fractions of Ethylene Glycol are shown in Figure 5.6 and Figure 5.7, respectively. As can be seen from Figure 5.6 and Figure 5.7, with increasing the Reynolds number, heat transfer coefficient and Nusselt number increase in all cases.

The main reason behind the increase of the heat transfer coefficient and Nusselt number is that by increasing the Reynolds number, fluid velocity increases and consequently fluid momentum increases resulting in increase of velocity and temperature gradients of the fluid in the near-wall regions. Accordingly, drag caused by the friction of the coolant fluid against the surface of the channel is enhanced and the coolant spends a shorter time contacting with the wall. As a result, heat transfer is significantly improved.

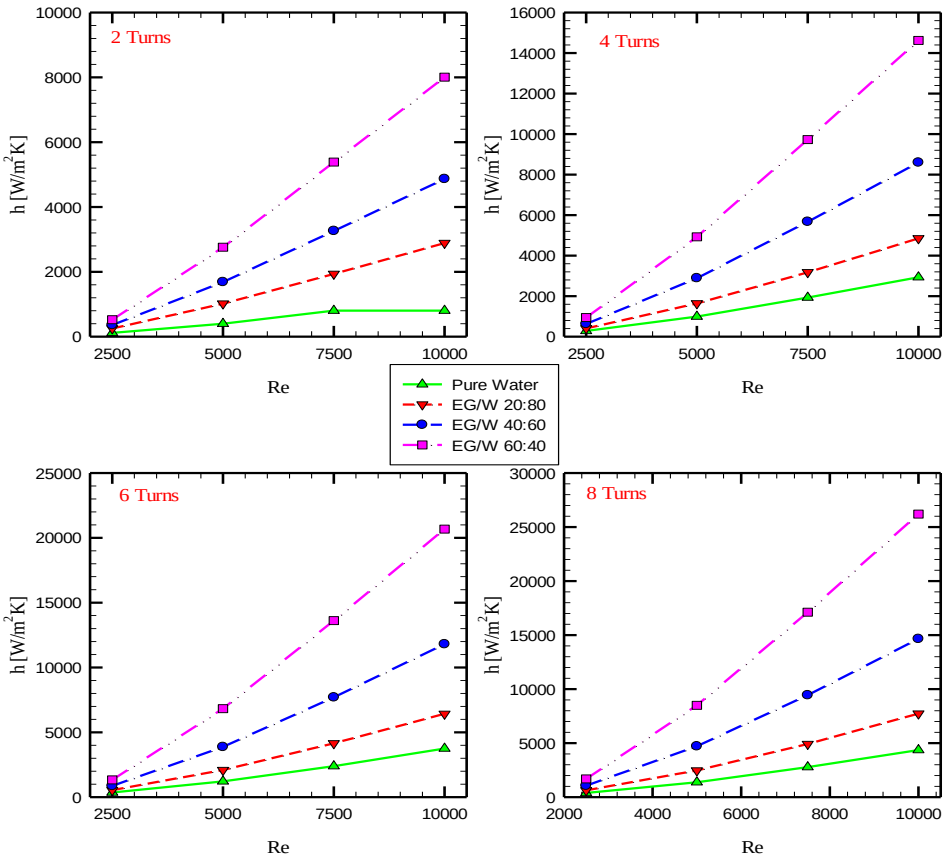

Figure 5. 6. Average convection heat transfer coefficient.

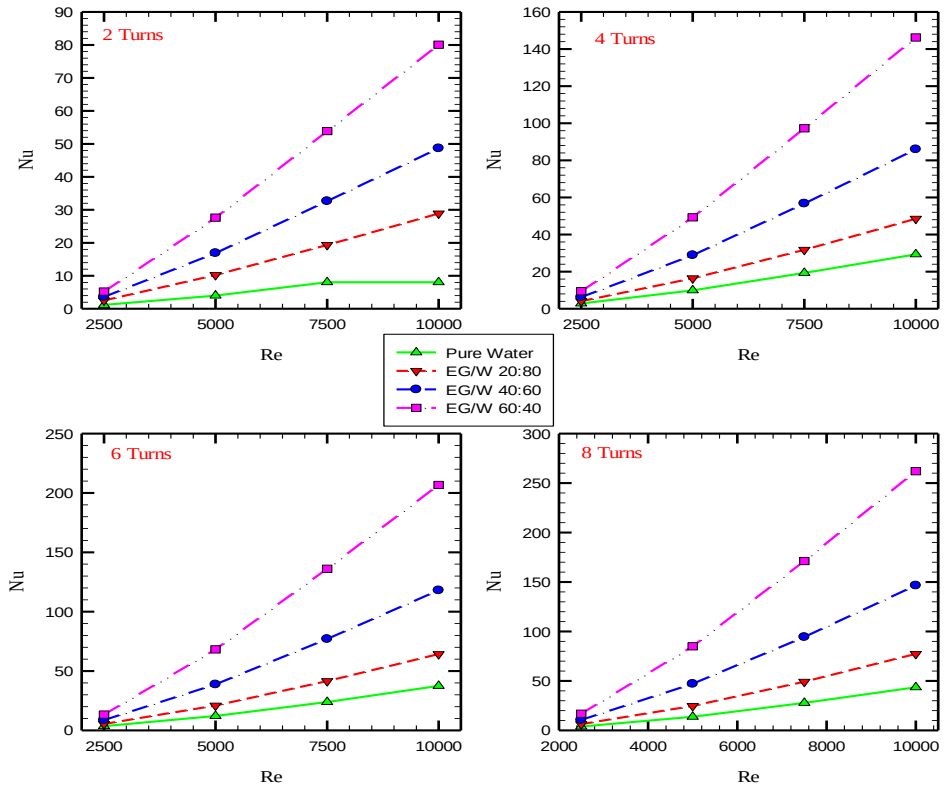

Figure 5. 7. Average Nusselt number.

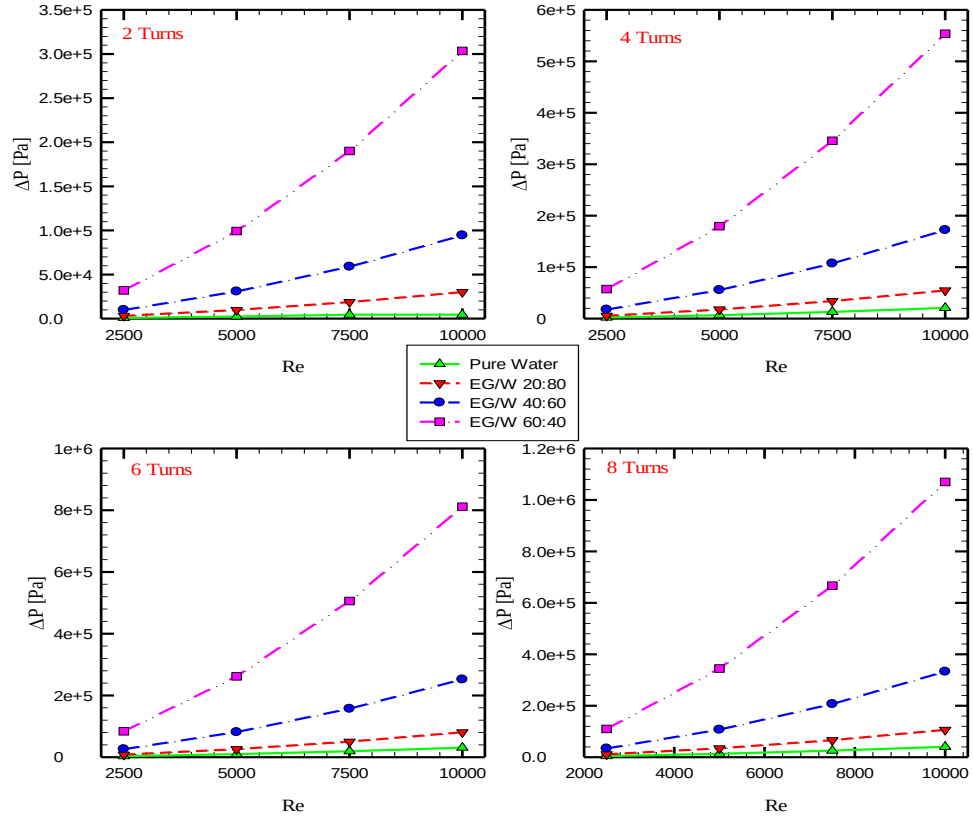

Figure 5. 8. Average pressure drop.

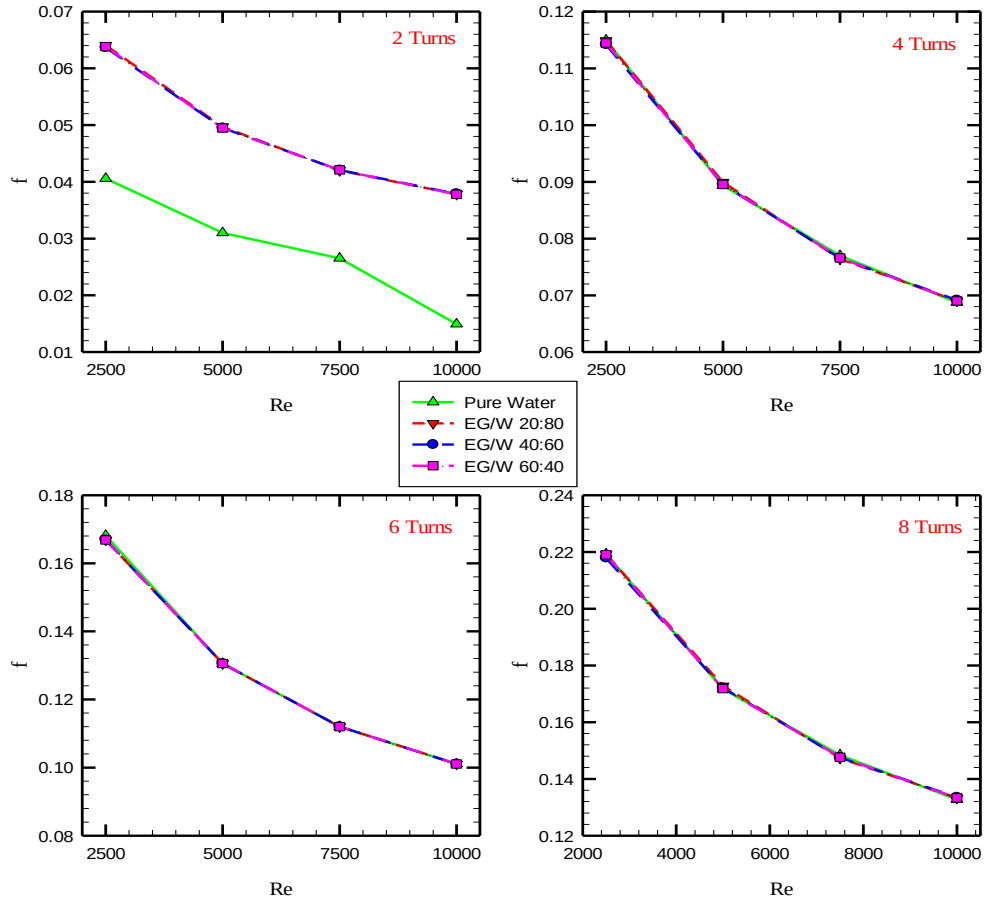

Figure 5. 9. *Average fanning friction factor.*

Moreover, with increasing volume fraction of Ethylene Glycol, heat transfer coefficient and Nusselt number increase. With increasing volume fraction of Ethylene Glycol, ratio of the density to the viscosity decreases, therefore based on (1) velocity increases. This phenomenon is intensified in the cases where volume fraction of Ethylene Glycol is higher. In addition to the Reynolds number and volume fraction of Ethylene Glycol, with increasing turn number of spiral channels, heat transfer coefficient and Nusselt number increase. The reason is that increasing turn number of spiral channel results in increase of the length of the flow path of the fluid which leads to increase of contact level between fluid and the channel. In addition, higher number of turns leads to higher thermal coupling between channels because the channel's spin rate decreases, and the channels become closer to each other enhancing heat transfer with more uniform temperature distribution on the stator and the housing.

Figure 5.8 and Figure 5.9 show average pressure drop and average fanning friction factor under different Reynolds numbers at different number of turns and volume fraction of Ethylene Glycol. From the figures, it can be concluded that with increasing the Reynolds number and number of turns, pressure drop increases. The reason is that the increase in number of turns leads to increase of length of the channel which leads to increase of slippery forces due to the increased fluidity of the coolant due to the increased volume fraction of ethylene glycol.

Figure 5.10 and Figure 5.11 show the performance evaluation criterion, PEC, diagrams relative to pure water and the turn number of 2. It can be seen whether in the case where PEC is relative to pure water and relative to the turn number 2, the PEC values are greater than 1. This means that by increasing the volume fraction of ethylene glycol and the number of turns, the thermal efficiency increases. In other words, the increase in the heat transfer coefficient is more significant than the increase in the pressure drop.

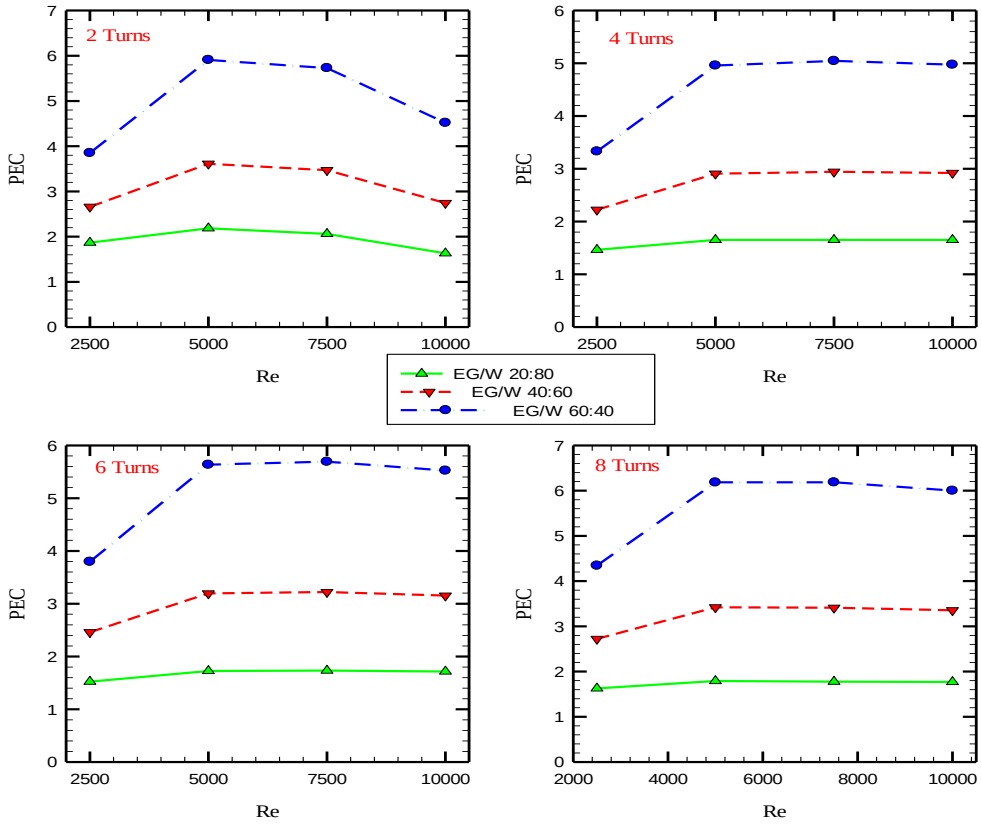

Figure 5. 10. PEC Based on Pure Water.

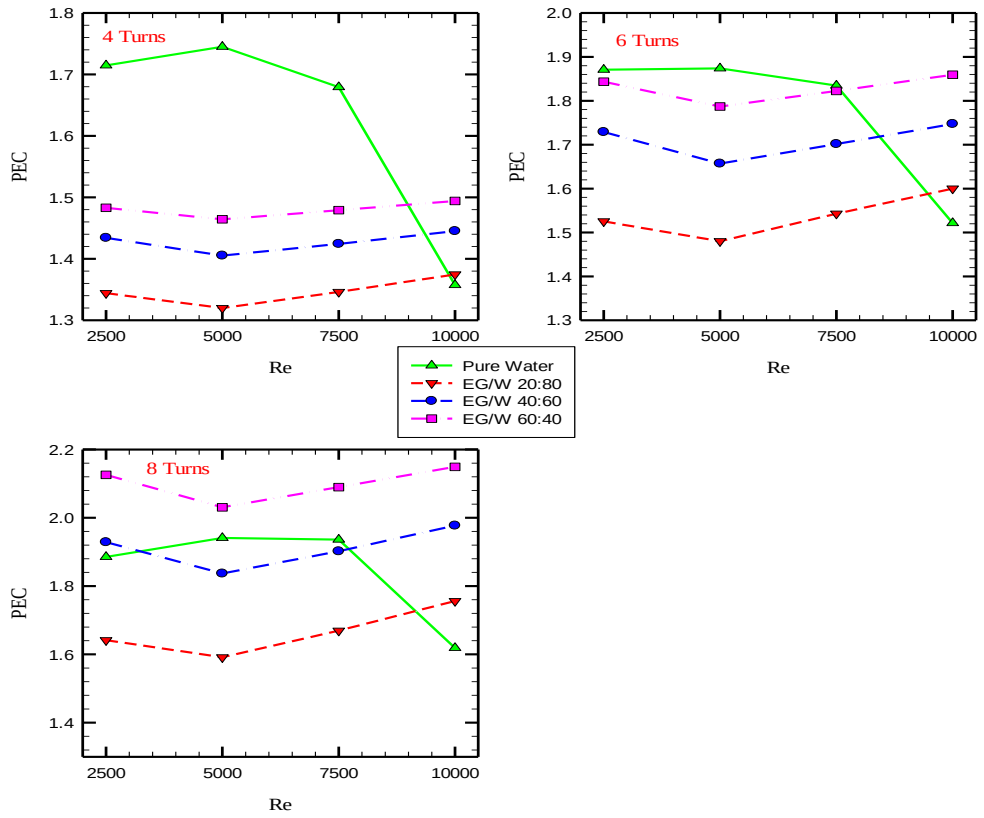

Figure 5. 11. PEC based on 2 Turns.

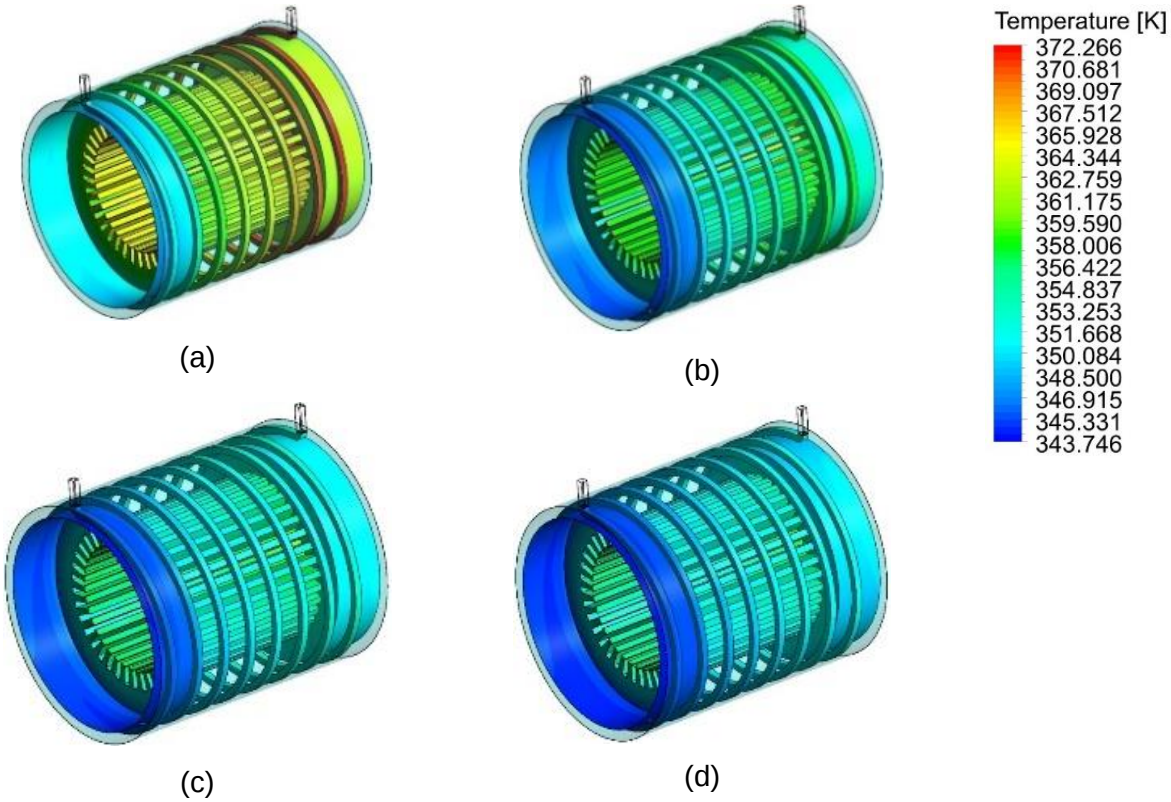

Figure 5. 12. Temperature distribution on heated surfaces and channel walls for (a) Re=2500, (b) Re=5000, (c) Re=7500 and (d) Re=10000.

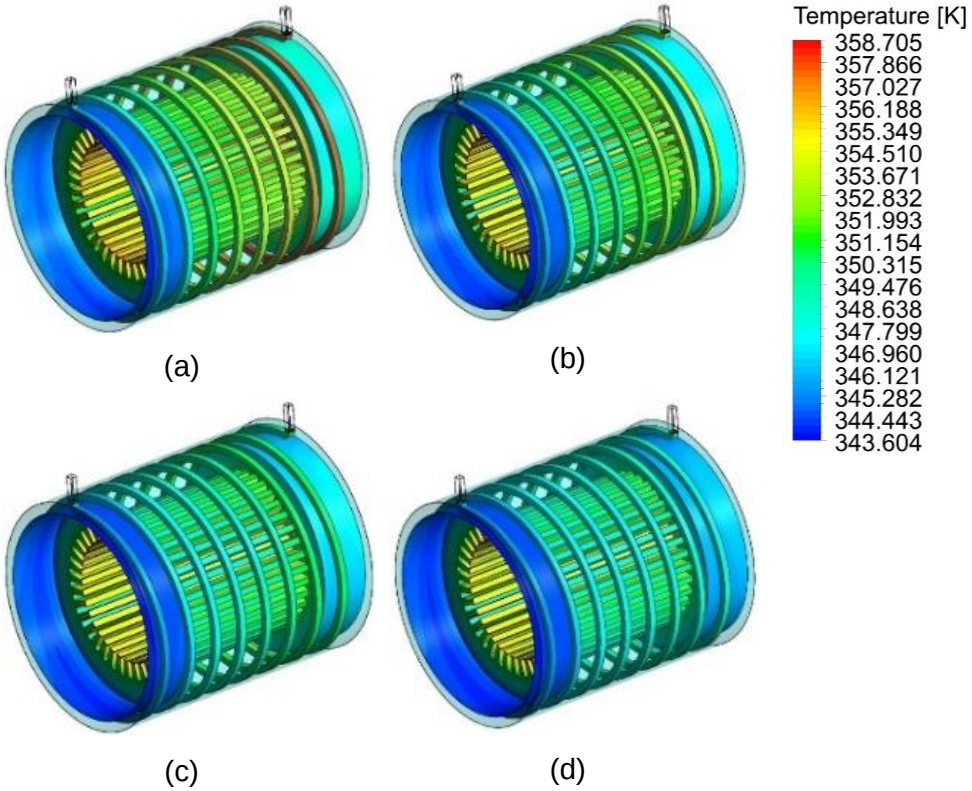

Figure 5. 13. Temperature distribution on heated surfaces and channel walls for (a) Pure Water, (b) EG/W 20:80, (c) EG/W 40:60 and (d) EG/W 60:40.

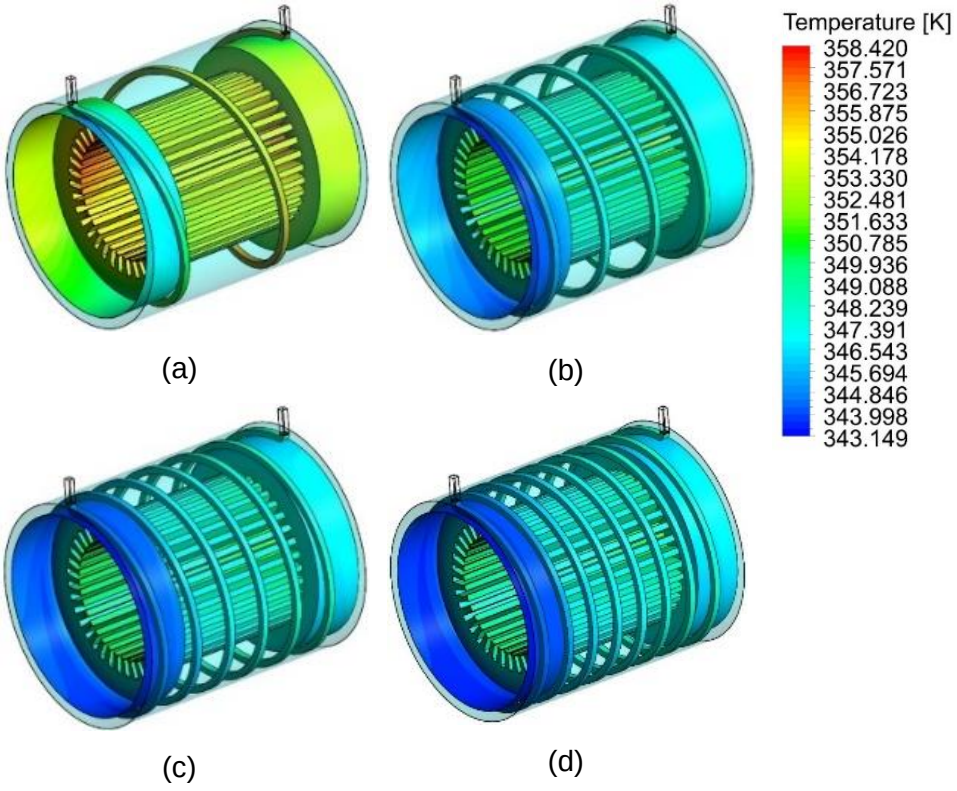

Figure 5. 14. Temperature distribution on heated surfaces and channel walls for (a) 2 Turns, (b) 4 Turns, (c) 6 Turns and (d) 8 Turns.

Figure 5.12, Figure 5.13, and Figure 5.14 show temperature distribution on heated surfaces and channel walls for different Reynolds numbers, for different volume fractions of ethylene glycol, and different number of turns, respectively. Increasing all of the above-mentioned parameters will increase the heat transfer and result in a better cooling performance. This reduces the temperature of the external surface of the electric motor and also makes the temperature distribution more uniform on the outer surface of the electric motor.

5.7 CONCLUSION

In this chapter, a 3D heat transfer and fluid flow of an electric machine cooling system with spiral channels employing mixture of ethylene glycol and water as coolant in the turbulent flow regime were investigated. From CFD analyses, it was observed that increasing turns of channels, the volume fraction of ethylene glycol, and the Reynolds number all increase the heat transfer coefficient. The defined performance evaluating parameter in this study, PEC, was used to evaluate the thermal and fluid flow performance of the cooling system. Higher values of this parameter indicate performance improvement of the designed cooling system. According to the simulation results, it was concluded that in comparison with pure water, with turn number of 8, at volume fraction of 60:40, and at Reynolds number of 5000, the highest PEC can be obtained. Also, regarding turn numbers, compared to the cooling system with 2 turn channels, the highest PEC value was found for channels with 8 turns, volume fraction of ethylene glycol to water of 60:40, and at Reynolds number of Re = 10,000.

6. ELECTRIC MACHINE COOLING SYSTEMS BASED ON NANOFLUID IN SPIRAL CHANNELS

6.1 INTRODUCTION

The overall performance of an electric machine cooling system is examined in terms of heat transfer and fluid flow. The structure of the cooling system is based on the cooling jacket method. The cooling jacket contains spiral channels surrounding the stator and end-windings of the electric machine. Al_2O_3-water nanofluid is used inside the channels as the cooling fluid. The concentration of nanoparticles and the geometric structure of the cooling system have special effects on both aspects of heat transfer and fluid flow. Therefore, in this chapter, the overall performance of the cooling system is evaluated by considering these effects. This study compares the importance of heat transfer and fluid flow performances on the overall performance of the cooling system. Numerical analyses are performed by 3D computational fluid dynamics and 3D fluid motion analysis.

6.2 LIQUID-COOLING SYSTEMS EMPLOYING NANOFLUIDS AS THE COOLANT

Employing advanced coolants such as nanofluids with high heat transfer coefficients and good fluid flow performance is an effective way to improve the heat transfer performance of cooling systems [219]. Recently, the usage of adding nanoparticles to coolant flu-ids has attracted much research attention due to its advantage of increasing the heat transfer capability of cooling systems [220]. Nanoparticles, due to their high thermal conductivity coefficients, increase the heat transfer rate and improve the performance of the cooling system.

Heat transfer performance of SiO2-water nanofluid with different nanoparticle concentrations in an automotive radiator consisting of flattened tubes were studied in [221]. It was reported that maximum increment in convection heat transfer was noticed for highest nanoparticle concentration of SiO2-water nanofluid. However, fluid flow performance was not considered. Thermal performances of Al_2O_3/CNC and Al2O3/TiO2 nanofluid coolants for radiator applications were studied in [222]. According to the results, it was shown that heat transfer parameters such as heat transfer coefficient have a proportional relationship with the volumetric flow rate. Heat transfer improvement in thermoelectric-based auto-motive waste heat recovery systems by using nanofluid was studied in [223]. It was shown that employing nanofluids can effectively improve heat transfer performance of the waste heat recovery system and increase of nanofluid concentration has positive effect on output performance of the system. However, in this study, the effect of increasing the concentration of nanoparticles from the point of view of fluid flow has not been investigated. In [224], the application of nanofluid in the electric motor cooling system has been studied from both aspects of heat transfer and fluid flow. However, the concentration range of nanoparticles has been limited and only the positive effect of adding nanoparticles to the base fluid has been investigated and its negative effect on

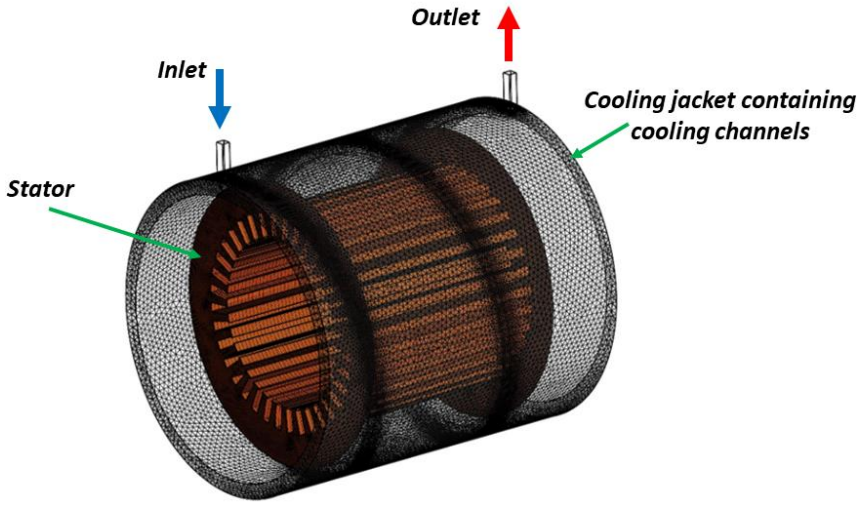

Figure 6. 1. Meshed schematic of the cooling system.

the temperature gradient at channels wall and the increase in diameter of the boundary conditions has not been investigated.

It is worthwhile noting that, although adding nanoparticles to coolants leads to the increase in heat transfer capability of the coolant, due to the increase in the density and viscosity of the fluid because of the addition of nanoparticles, the pressure drops, and the required pumping power in the fluid increases. This is not a desirable fluid flow phenomenon. Therefore, to justify the performance of cooling systems employing nanofluid coolants, both thermal and fluid flow performance analyses are necessary [225].

In this chapter, the thermal performance of an indirect cooling system of the electric motor employing a cooling jacket and Al_2O_3-water nanofluid coolant is investigated. Modeling approaches are described and used to establish a numerical model of the cooling system. Effects of various heat transfer and fluid flow parameters on the heat transfer performance of the cooling system are investigated. The dual effect of adding nanoparticles to the base fluid on heat transfer performance is investigated. Apart from evaluating the overall performance of the cooling system based on both heat transfer and fluid flow aspects, as one of the main contributions of this study, beneficial level of increasing nanoparticle concentration is investigated. To examine overall

performance of the cooling system, a performance evaluation index is defined that is able to determine the pros and cons of using nanofluids in different conditions.

6.3 MODELING

Physical, mathematical, and numerical modeling approaches are employed to establish a model of the problem and provide a platform for the cooling system performance analysis.

6.3.1 PHYSICAL MODEL

The designed cooling system in this chapter consists of a cooling jacket with spiral cooling channels. Figure 6.1 shows a schematic of the cooling system. The cooling jacket is designed with spiral channels extracting heat from stator and end-winding surfaces. The length of the electric machine is 190 mm. The length of the cooling jacket is 210 mm covering stator end-windings. The thickness of the cooling jacket is 10 mm. In this study, three different models of the cooling systems with 4, 6, and 8 channel turns are developed. Cooling channels are filled with Al_2o_3-water nanofluid. Cooling channels carrying nanofluid are made of Aluminum and the material of the electric motor body is steel. Dimensions of the modelled electric machine and the cooling jacket are listed in Table 6.1. Materials of the outer surface of the electric machine and the cooling jacket are listed in Table6.2. 3D schematics of the physical model with different channel turns number are shown in Figure 6.2.

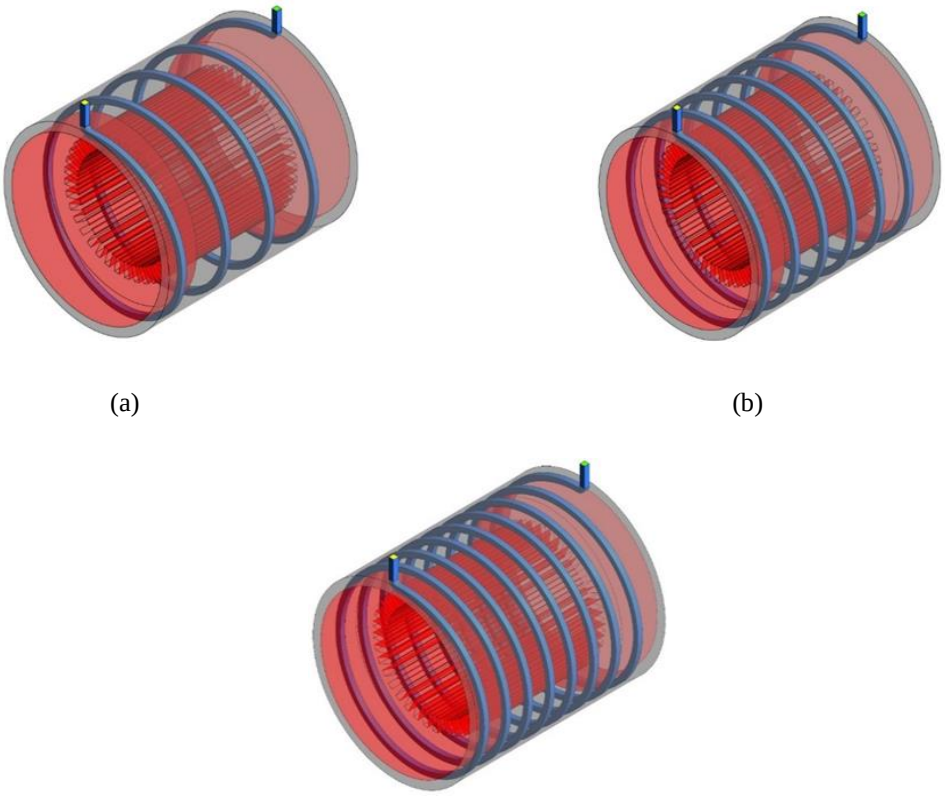

(a) (b)

(c)

Figure 6. 2. Schematic of the cooling system with (a) 4 turns, (b) 6 turns, and (c) 8 turns.

Table 6. 1. Dimensions of the electric machine and the cooling jacket

	Electric Motor	Cooling Jacket
Length	190 mm	210 mm
Width	240mm (with coil)	240 mm
Thickness	_____	10 mm

Table 6. 2. Materials of the electric machine stator and the cooling jacket

	Material
Stator	Steel
Cooling Jacket	Aluminum

6.3.2 MATHEMATICAL MODEL

The mathematical model is employed to solve the fluid flow and heat transfer. In fact, the mathematical model is the basis of the numerical model and numerical analysis. Therefore, in this section, the governing equations for heat transfer and fluid flow are presented.

6.3.2.1 GOVERNING EQUATION FOR LAMINAR NANOFLUIDS

In this chapter, the flow regime is considered laminar. Accordingly, steady-state continuity, momentum, and energy equations for laminar flows in cartesian coordinates are as follows.

The continuity equation is:

$$\frac{\partial(u)}{\partial x}+\frac{\partial(v)}{\partial y}+\frac{\partial(w)}{\partial z}=0 \tag{6.1}$$

where u, v, and w are fluid velocities along x-, y-, and z-axis, respectively.

Momentum equation in x-axis direction is as follows.

$$u\frac{\partial(u)}{\partial x}+v\frac{\partial(u)}{\partial y}+w\frac{\partial(u)}{\partial z}=-\frac{1}{\rho_{nf}}\frac{\partial P}{\partial x}+\nu_{nf}\left(\frac{\partial}{\partial x}\left(\frac{\partial u}{\partial x}\right)+\frac{\partial}{\partial y}\left(\frac{\partial u}{\partial y}\right)+\frac{\partial}{\partial z}\left(\frac{\partial u}{\partial z}\right)\right) \tag{6.2}$$

where ρ_{nf} is density of nanofluid and p is pressure. ν_{nf} is coefficient of nanofluid Kinematic viscosity.

Momentum equation in y-axis direction is expressed by:

$$u\frac{\partial(v)}{\partial x}+v\frac{\partial(v)}{\partial y}+w\frac{\partial(v)}{\partial z}=-\frac{1}{\rho_{nf}}\frac{\partial P}{\partial x}+\nu_{nf}\left(\left(\frac{\partial}{\partial x}\left(\frac{\partial v}{\partial x}\right)+\frac{\partial}{\partial y}\left(\frac{\partial v}{\partial y}\right)+\frac{\partial}{\partial z}\left(\frac{\partial v}{\partial z}\right)\right)\right) \tag{6.3}$$

The Momentum equation in z-axis direction is:

$$u\frac{\partial(w)}{\partial x}+v\frac{\partial(w)}{\partial y}+w\frac{\partial(w)}{\partial z}=-\frac{1}{\rho_{nf}}\frac{\partial P}{\partial x}+\nu_{nf}\left(\frac{\partial}{\partial x}\left(\frac{\partial w}{\partial x}\right)+\frac{\partial}{\partial y}\left(\frac{\partial w}{\partial y}\right)+\frac{\partial}{\partial z}\left(\frac{\partial w}{\partial z}\right)\right) \tag{6.4}$$

Energy equation for nanofluids is:

$$\rho_{nf}\,C_{p,nf}\left(u\frac{\partial(T)}{\partial x}+v\frac{\partial(T)}{\partial y}+w\frac{\partial(T)}{\partial z}\right)=K_{nf}\left(\frac{\partial}{\partial x}\left(\frac{\partial T}{\partial x}\right)+\frac{\partial}{\partial y}\left(\frac{\partial T}{\partial y}\right)+\frac{\partial}{\partial z}\left(\frac{\partial T}{\partial z}\right)\right) \tag{6.5}$$

where T is temperature. $C_{p,\,nf}$ and K_{nf} are nanofluid specific heat and thermal conductivity, respectively.

6.3.2.2 Formulations for Physical Properties of Nanofluids

Using valid empirical relationships for parameters such as density, specific heat capacity, thermal conductivity coefficient, and Nanofluid viscosity, determination of thermophysical properties to determine flow behavior and heat transfer at different volume fractions of nanofluid are implemented as follows.

The density of nanofluid is expressed as:

$$\rho_{nf} = (1-\varphi)\rho_{fb} + \varphi\rho_p \tag{6.6}$$

where ρ_f and ρ_p are density of base fluid and nanoparticles, respectively. φ refers to the volume fraction of nanoparticles.

Specific heat of nanofluid is:

$$(\rho C_p)_{nf} = (1-\varphi)(\rho C_p)_{fb} + \varphi(\rho C_p)_p \tag{6.7}$$

Effective thermal conductivity of nanofluid is calculated as [226]:

$$\frac{k_{eff,nf}}{k_{fb}} = \frac{k_p + 2k_{fb} + 2\varphi(k_p - k_{fb})}{k_p + 2k_{fb} - \varphi(k_p - k_{fb})} \tag{6.8}$$

where $K_{eff,nf}$ is effective thermal conductivity of nanofluid. K_p and K_{fb} are thermal conductivities of nanoparticles and base fluid, respectively.

According to the numerical model of dynamic viscosity obtained from experimental studies in [227], viscosity is given by:

$$\mu_{nf} = \mu_{fb}(123\varphi^2 + 7.3\varphi + 1) \tag{6.9}$$

where μ_{nf} and μ_{fb} are viscosities of nanofluid and base fluid, respectively.

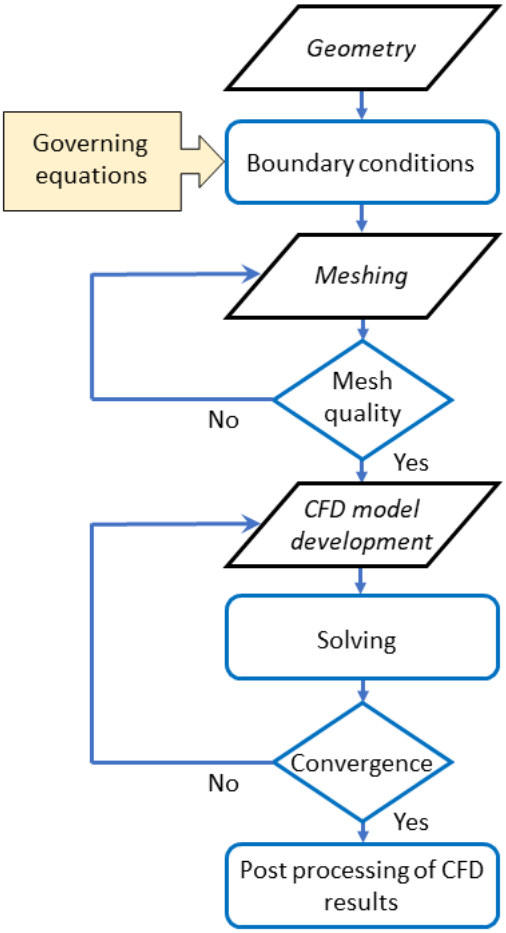

Figure 6. 3. CFD solution flowchart.

Reynolds number is defined by

$$Re = \frac{\rho_{nf} u_{in} D_h}{\mu_{nf}} \tag{6.10}$$

where u_{in} is inlet velocity and D_h is hydraulic diameter.

Heat transfer coefficient (h) is derived by

$$h = \frac{q_w}{(T_w - T_b)} \tag{6.11}$$

where q_w is wall heat flux. T_w and T_b are wall and bulk temperatures, respectively.

Nusselt number is expressed as:

$$Nu = \frac{h \cdot D_h}{k_{nf}} \tag{6.12}$$

Fanning friction factor (f) is defined by

$$f = \frac{(\Delta P/L)\cdot D_h}{2\,\rho_{nf}\,u_{in}^2} \tag{6.13}$$

where ΔP is pressure drop. L is length of the channel.

6.3.3 NUMERICAL MODEL

The electric machine and the cooling jacket are meshed and analyzed by CFD simulations. Simulations are run for different volume fractions of nanoparticles. Heat transfer and fluid flow parameters such as heat transfer coefficient, Nusselt number, Reynolds number, Fanning friction factor, and pressure drop are calculated for each volume fraction of nanoparticles.

Figure 6.3 shows the CFD solution flowchart. The geometry creation, establishment of governing equations, boundary conditions determination, meshing, and mesh quality investigations are pre-processing steps. Then the CFD simulations are run based on control parameters. Obtained results are evaluated in the post-processing step.

Table 6. 3. Grid sensitivity analyses

Number of nodes	Computed heat transfer coefficient	Percentage variation
2×10^6	119.93	—
4×10^6	133.52	11.33
6×10^6	131.92	1.2%
8×10^6	131.78	0.11%

Table 6. 4. Thermo-physical properties of Al2O3-water

φ	ρ (kg/m³)	C_p (J/kg K)	k (W/m K)	μ (Pa s)
0.02	1056.6	3922.4	0.6691	9.37×10^{-4}
0.04	1116	3693.2	0.7014	9.86×10^{-4}
0.05	1140.15	3466.95	0.7205	9.96×10^{-4}
Al_2O_3	3970	765	40	—
Water	997.1	4179	0.613	8.91×10^{-4}

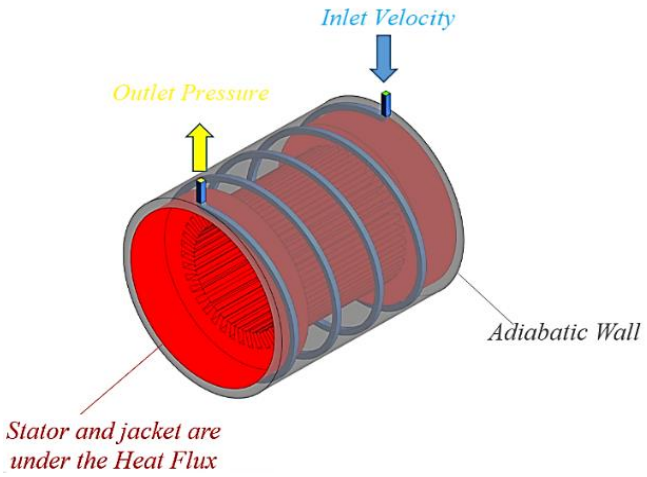

Figure 6. 4. Boundary conditions.

6.3.3.1 GRID INDEPENDENCE VALIDATION

As the accuracy of obtained numerical results is strongly affected by the number of nodes in the meshed model, as a preprocessing step, the accuracy and independence of results from the number of mesh nodes must be investigated. Different simulations were performed and computed heat transfer coefficients versus the number of nodes are listed in Table 6.3. As can be seen, as the number of nodes exceeds 6 × 106, the variation of the computed heat transfer coefficient is only 0.11%. Therefore, 6 × 106 nodes provide satisfactory numerical accuracy. According to the density of meshes, to overcome the high volume of calculations a computer server with 48 cores and 124GB of RAM is employed.

6.3.3.2 BOUNDARY CONDITIONS

Boundary conditions are the inlet velocity of the fluid with the temperature of 343 K and the outlet pressure. Stator and its cooling jacket are considered to be under a constant heat flux of 3500 W/m2. The wall in which the channels are located is considered insulated. Figure 6.4 shows applied boundary conditions. The determinant parameters for the CFD analysis are listed in Table 6.5.

Table 6. 5. Determinant parameters for different CFD analysis

CFD determinant parameters for different analysis	
Re	500 - 2000
Number of Turns	2, 4, 6, 8
Base Fluid	Pure Water
Inlet Fluid Temperature	343.15(K) / 70 (c°)
Heat Flux	3500 (W/m^2 K)

The employed nanofluid is Al_2O_3-water. Effects of adding nanoparticles on the fluid flow and thermal performance of the cooling system are studied for different volume fractions of the nanoparticles. Thermo-physical properties of the nanofluid and the base fluid (water) are listed in Table 6.4 [228].

6.4 RESULTS

The cooling system is analyzed by 3D CFD simulations. Numerical simulations are performed under the boundary conditions described in the previous section. The effect of different geometries of the cooling jacket and concentrations of nanoparticles are studied. The applied heat flux and thermophysical properties of nanofluids are considered constant. Fluid flow, thermal characteristics, and performance of the cooling system for different given concentrations of nanoparticles and different geometries of the cooling jacket are discussed and computed results are compared with the results obtained from the use of water as the coolant. Studied nanoparticle concentrations are ranged between 0 and 5%. Channel turns number are considered 4, 6, and 8 turns.

6.4.1 HEAT TRANSFER CHARACTERISTICS

Figure 6.5 shows a contour plot of heat transfer coefficient variations against variation of pumping power (Reynold number) and nanoparticle concentrations for nanofluids flowing in cooling channels with 8 turns. The contour plot shows that the heat transfer coefficient increases with the increase of Reynolds number. Also, at any pumping power, increasing the concentration of nanoparticles increases the heat transfer coefficient.

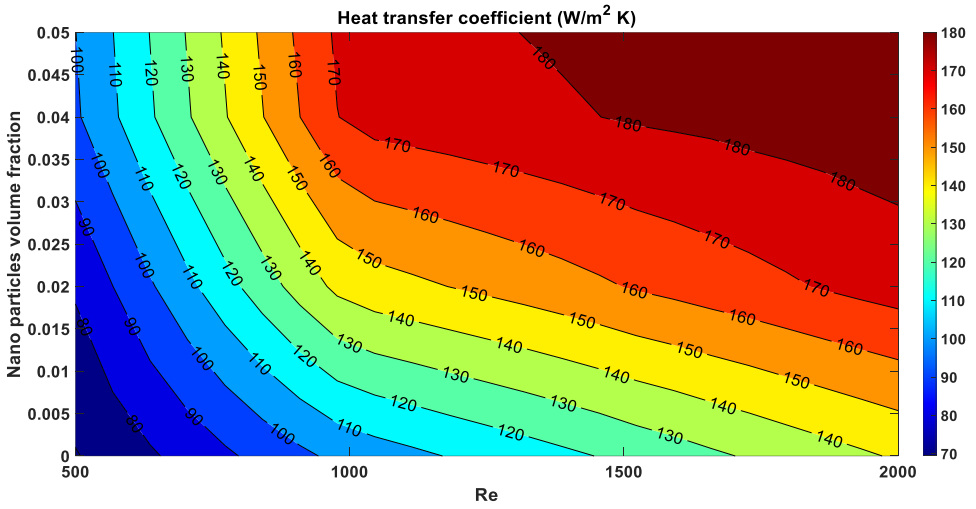

Figure 6. 5. Contour plot of heat transfer coefficient versus volume fraction and Reynolds number.

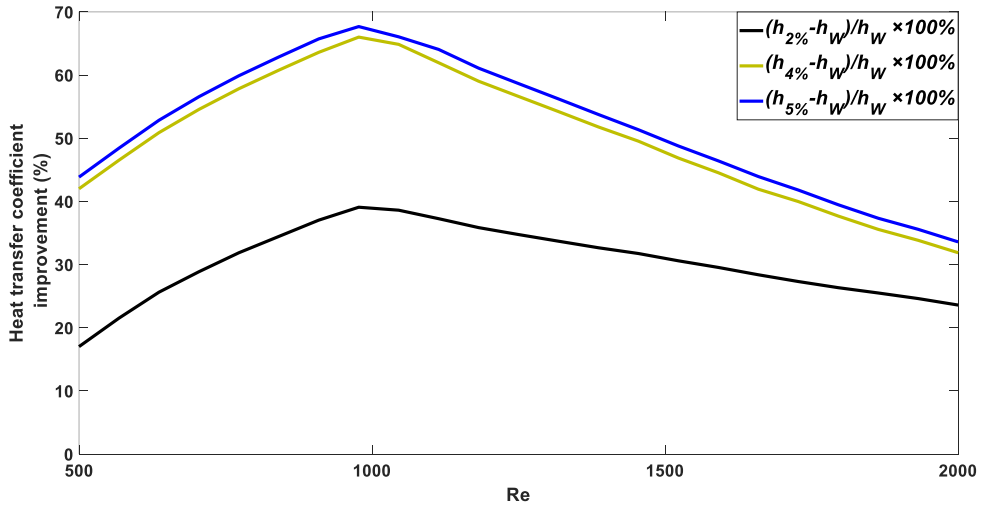

Figure 6. 6. Relative heat transfer coefficient changes for nanofluids with 2%, 4%, and 5% volume fraction with respect to water.

To better illustrate the effect of the Reynolds number and the concentration of nano-particles on changes in the heat transfer coefficient, relative heat transfer coefficient changes to water are plotted in Figure 6.6 for φ = 2%, φ = 4%, and φ = 5%. According to the results, compared to water, the maximum enhancement percentage of heat transfer coefficient occurs around Reynolds number of 1000 and its value is 39.1%, 66.02%, and 67.7% for nanoparticles volume fractions of 2%, 4%, and 5%, respectively.

The increase in heat transfer coefficient due to the adding of nanoparticles in the base fluid results from the fact that the addition of nanoparticles to the base fluid increases its thermal conductivity. This improves the thermal penetration depth of the coolant fluid. Also, according to Table 6.4, the presence of nanoparticles in the base fluid leads to a reduction in the specific heat capacity of the base fluid. This increases the amount of the absorbed heat flux by the coolant fluid. Therefore, the nanofluid with the nanoparticle concentration of 5% shows the largest heat transfer coefficient increase. However, the increase in the relative heat transfer coefficient enhancement for increasing the volume fraction from 4% to 5% is much smaller than the case of increasing the volume fraction from 2% to 4%. In fact, adding nanoparticles to a base fluid affects the heat transfer coefficient in two different ways. While increasing nanoparticle concentration enhances the heat transfer coefficient by increasing the thermal conductivity of the nanofluid, increasing the nano-particle concentration can lead to a reduction of the temperature gradient at the wall of the channels (increasing thickness of the boundary layer). Therefore, there are two factors that positively and negatively affect the heat transfer coefficient enhancement. Here, in the case of using the nanofluids with 5% volume fraction in 8 turns cooling jacket, the wall temperature gradient reduces significantly leading to a small heat transfer coefficient improvement.

As it was mentioned, the maximum enhancement percentage of heat transfer coefficient occurs around Reynolds number of 1000. This is because, by the increase of Reynolds number, friction resistance reduces leading to improvement of convective heat trans-fer. On the other hand, from a specific Reynolds number onward, due to viscosity, the slope of the friction resistance changes decreases. Therefore, while in the laminar flow regime, the heat transfer coefficient always increases with increasing Reynolds number, but at higher Reynolds numbers, the slope of increasing the heat transfer coefficient decreases.

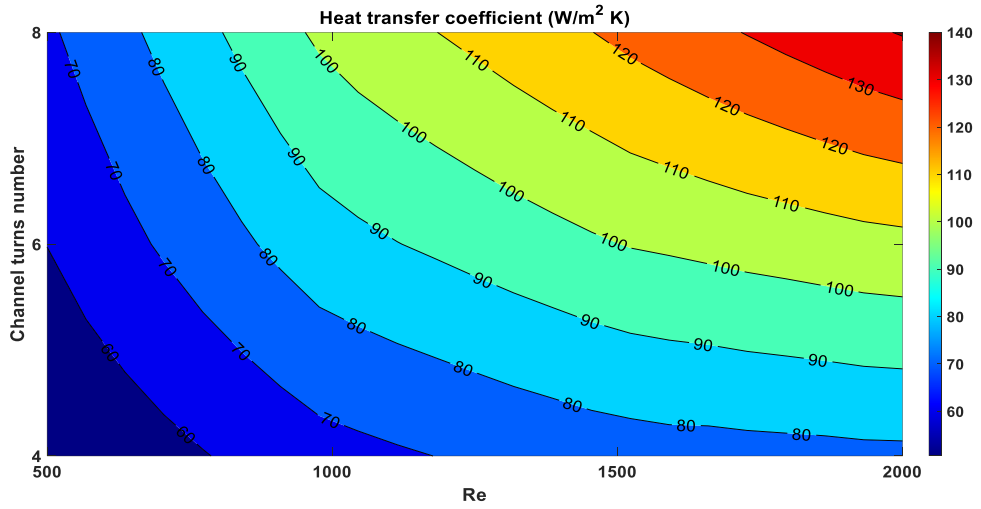

Figure 6. 7. Contour plot of heat transfer coefficient versus channel turns number and Reynolds number.

The effect of different channel turns numbers on the heat transfer coefficient for a cooling system using water as the coolant is shown in Figure 6.7. As is shown in Figure 6.7, due to the increase in the cooling cross-sectional area, increasing the turns number of the channel improves heat transfer from the electric motor to the coolant fluid, thus increasing the heat transfer coefficient.

To compare the amount of the increase in heat transfer coefficient due to the increase in the turn number of channels, Figure 6.8 shows the relative increase in heat transfer co-efficient for channels with 6 and 8 turns compared to the channel with 4 turns. According to Figure 6.8, as the Reynolds number increases, the heat transfer coefficient increases for both cases (6 and 8 turns), but in the case of the channel with 8 turns, this increase for larger Reynolds numbers is greater than in the case of the channel with 6 turns. This difference in the amount of improvement in heat transfer coefficient at larger Reynolds numbers is due to the fact that the pitch of the channel with 8 turns is smaller than the channel with 6 turns. The smaller pitch of spiral channels causes the friction factor to de-crease further by increasing the Reynolds number [229]. Further reduction of the friction factor at larger Reynolds numbers greater enhances the convective heat transfer.

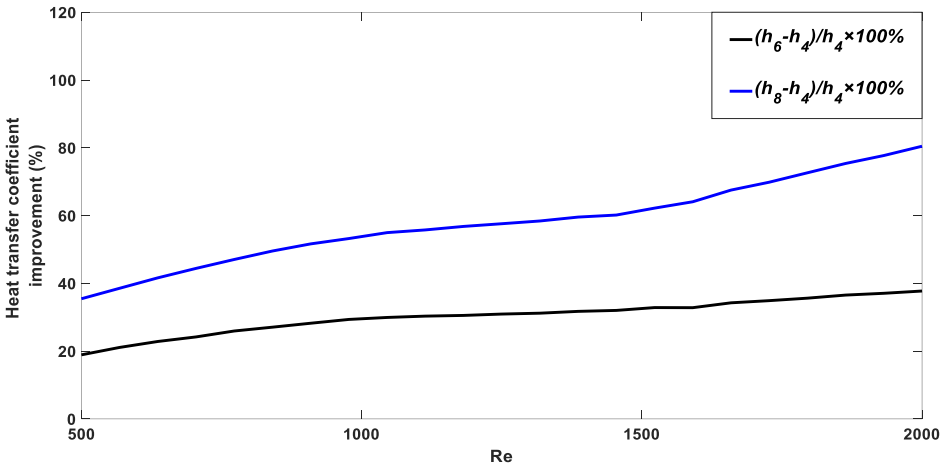

Figure 6. 8. Relative increase in heat transfer coefficient for channel turns numbers of 6 and 8 with respect to 4.

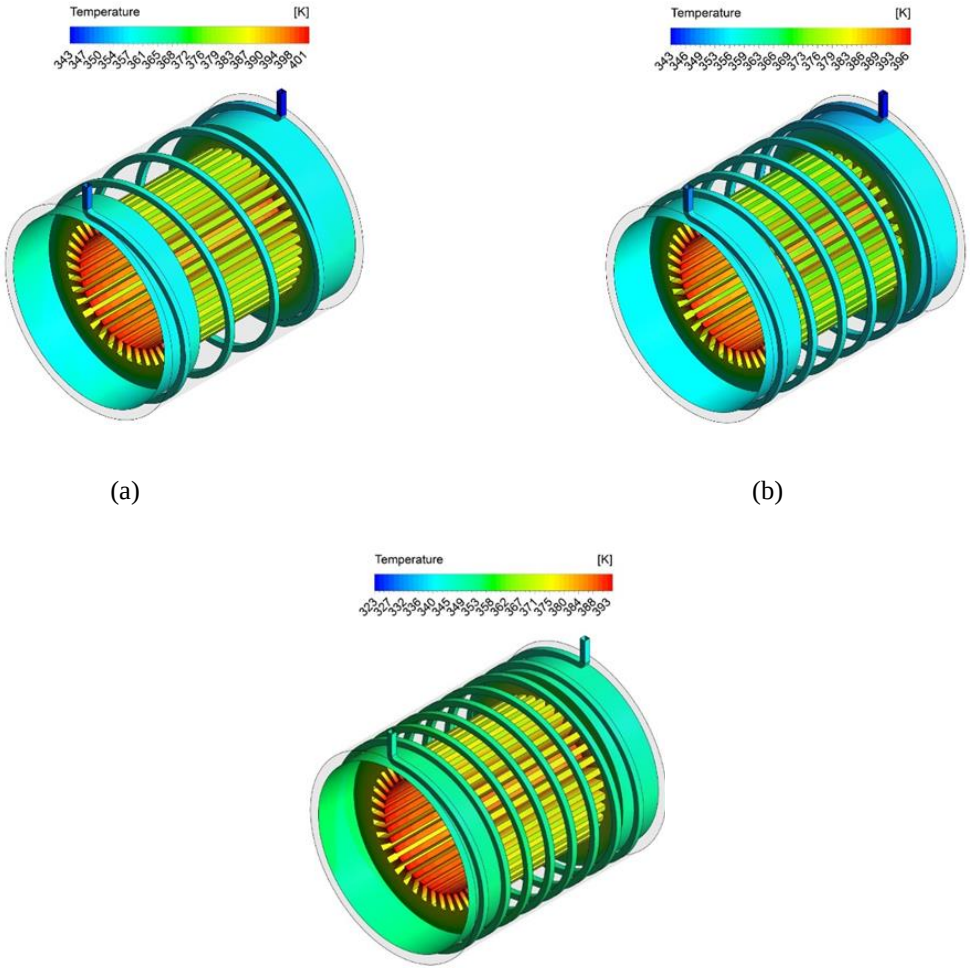

(a) (b)

(c)

Figure 6. 9. Temperature distribution contours of the cooling system using the nanofluid at Reynolds number of 2000 with (a) 4 turns, (b) 6 turns, and (c) 8 turns.

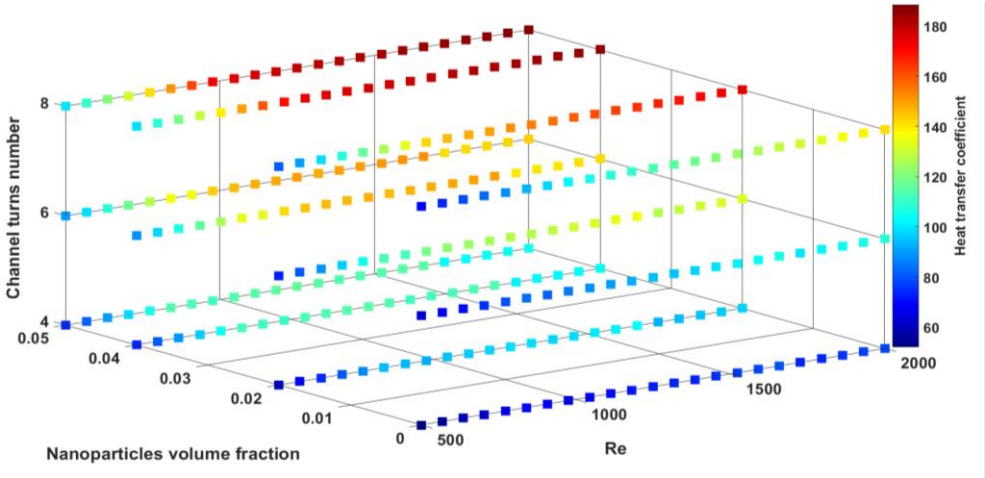

Figure 6. 10. Heat transfer coefficient versus Reynolds number, nanoparticles volume fraction, and channel turns number.

Temperature distribution contours of the cooling system using the nanofluid at Reynolds number of 2000 with 4, 6, and 8 turns are shown in Figure 6.9. As can be seen in Figure 6.9, the temperature of the electric motor has been increased due to the production of stator thermal flux and the temperature of the coolant fluid that flows through the spiral channels, as it approaches the outlet, is brought about by temperature rise. Investigating the effect of turns numbers shows that with the increase in the turns number of cooling channels, due to the increase of the cross-section in contact with the nanofluid, the maximum operating temperature has decreased.

Figure 6.10 shows the effect of these factors on the heat transfer coefficient for nanoparticle concentrations from 0 to 5% (where φ=0 refers to the base fluid, water) and channel turns numbers of 4, 6, and 8 at different Reynolds numbers. According to Figure 6.10, from the heat transfer perspective, it can be concluded that the highest heat transfer improvement at all pumping powers has been obtained for the case of using the channel with 8 turns and employing the nanofluid with higher nanoparticles concentration.

6.4.2 Fluid Flow characteristics

This subsection discusses the effect of geometry and fluid characteristics from the fluid flow perspective. Variations of the pressure drop at different Reynolds numbers for nanofluids with different nanoparticle concentrations are shown in Figure 6.11.

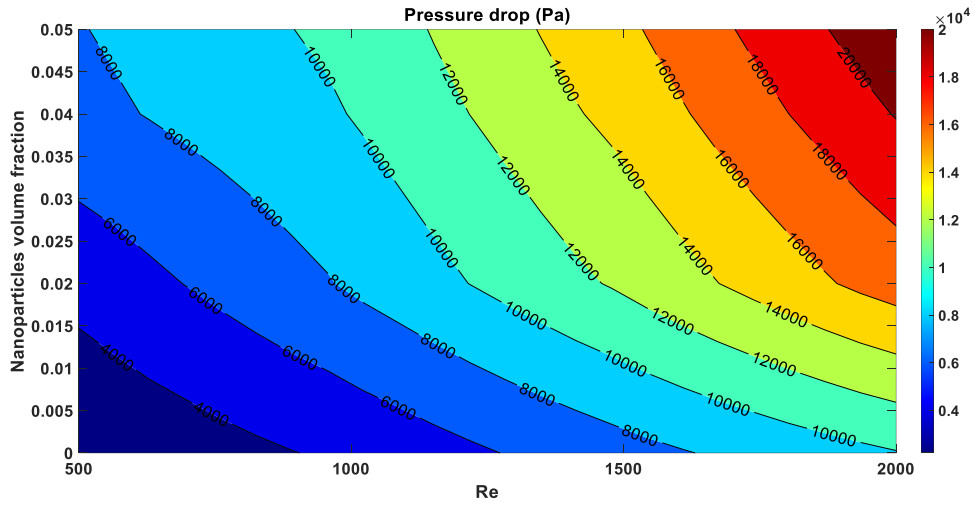

Figure 6. 11. Variation of the pressure drop at different Reynolds numbers for nanofluids with different nanoparticles concentrations.

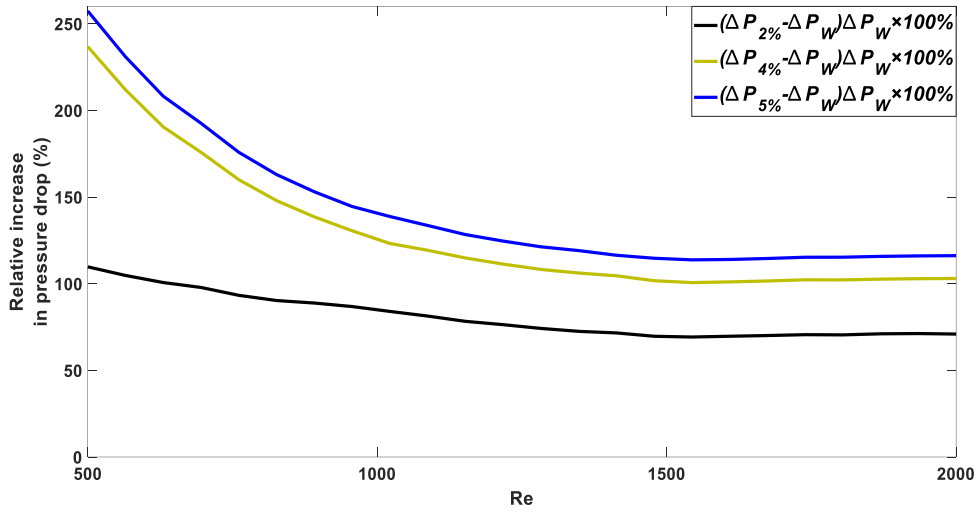

Figure 6. 12. Relative increase in pressure drop with respect to water.

As can be seen, increasing the concentration of nanoparticles increases the viscosity and increases the pressure drop. The percentage of the increase in pressure drop relative to the base fluid at different Reynolds numbers is depicted in Figure 6.12. According to the plot, at a smaller Reynolds number, the effect of increasing the nanoparticle concentration on the pressure drop is much greater than that at large Reynolds numbers. The reason for this phenomenon is that at small Reynolds numbers the friction factor is high and in large Reynolds numbers the friction factor decreases, especially this

reduction of the friction factor is greater for nanofluids with higher nanoparticle concentrations.

The contour plot of pressure drop variations versus Reynolds number due to different channel turns numbers is shown in Figure 6.13. This figure illustrates that for all Reynolds numbers, increasing turns number of channels increases the pressure drop because the channel length increases. The percentage of the relative increase of pressure drop for channels with turns numbers of 6 and 8 with respect to the pressure drop of the coolant flowing in the channel with 4 turns is shown in Figure 6.14. Due to the smaller pitch of the channel with 8 turns, at larger Reynolds numbers, the friction factor decreases more than in the channel with 6 turns, so the percentage of the relative increase in pressure drop decreases at larger Reynolds numbers for the case of the channel with 8 turns.

Figure 6.15 shows the contours of the pressure distribution inside the spiral channels with different turns numbers. As can be seen, with the increase in the number of turns, the pressure drop also increases due to the velocity gradient and the change in the flow field along the spiral channels.

To illustrate the effect of channel turns number and nanoparticle concentration, Figure 6.16 shows a 3D plot of pressure drop variations with respect to different channel turn numbers and different concentrations of nanoparticles at Reynolds numbers from 500 to 2000.

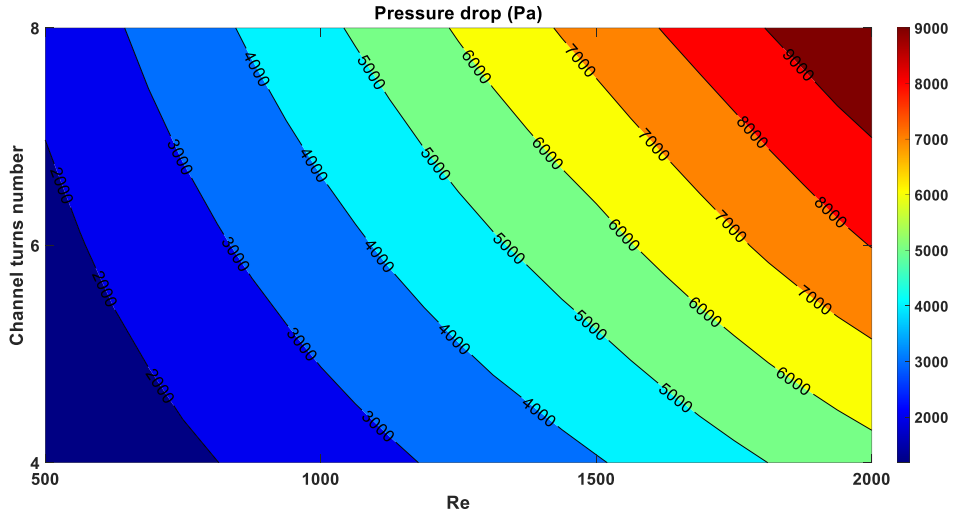

Figure 6. 13. Variations of pressure drop at different Reynolds numbers for channel turns number of 4, 6, and 8.

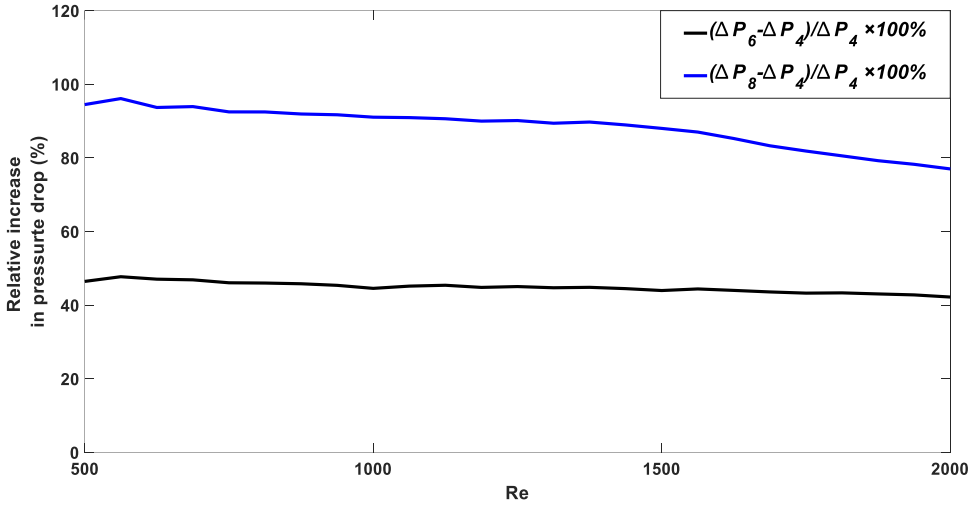

Figure 6. 14. Relative increase in heat transfer coefficient for channel turns numbers of 6 and 8 with respect to 4.

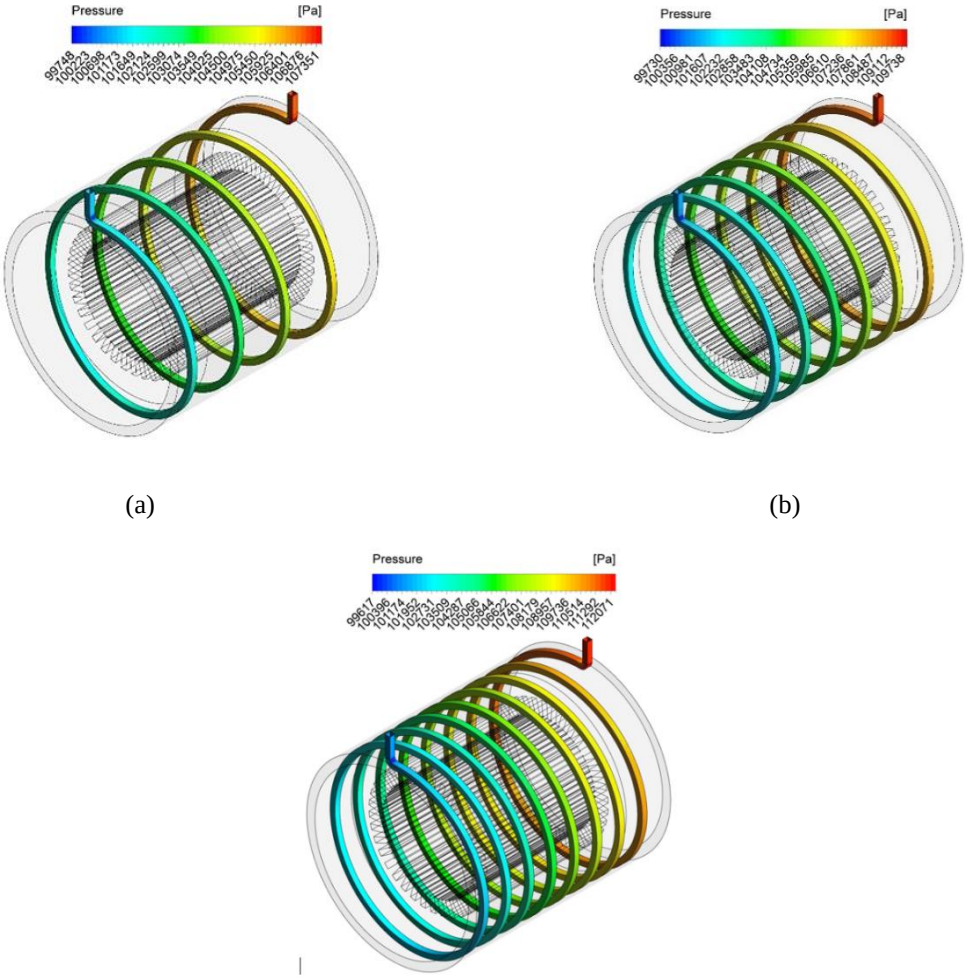

Figure 6. 15. Pressure distribution contours of the cooling system using the nanofluid with different turns numbers (a) 4 turns, (b) 6 turns, and (c) 8 turns.

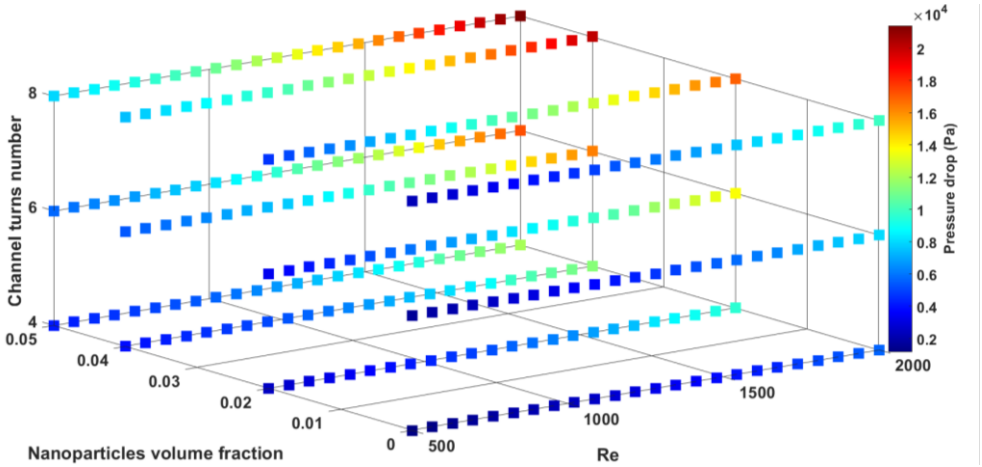

Figure 6. 16. Pressure drop versus Reynolds number, nanoparticles volume fraction, and channel turns number.

6.4.3 Overall Performance Evaluation

Since the addition of nanoparticles affects both heat transfer and fluid flow characteristics, the performance of the system should be evaluated from both aspects. In this study, enhancement of heat transfer and friction factor are considered as evaluation factors. In other words, cooling system performance is evaluated based on the ratio of heat transfer improvement to the increase in the required pumping power. Therefore, the best performance is achieved when the maximum amount of heat transfer improvement is obtained in exchange for the minimum need to increase the pumping power. To evaluate the performance of the cooling system based on the results obtained from the CFD analysis and considering both the heat transfer and the fluid flow performances of the cooling system, the Performance Evaluation Criteria (PEC) is defined as [230]:

$$PEC = \frac{\left(\frac{Nu_{nf}}{Nu_b}\right)}{\left(\frac{f_{nf}}{f_b}\right)^{(1/3)}} \tag{6.14}$$

where Nu_{nf} and f_{nf} are Nusselt number and Fanning friction factor computed for nanofluids. N_{ub} and f_b are Nusselt number and Fanning friction factor of the base fluid. In (14), Nusselt number represents the heat transfer performance factor and the Fanning factor signifies the fluid flow performance of the cooling system.

In order to provide a clear picture of the cooling system performance based on heat transfer and fluid flow indices, numerator value changes of PEC versus the denominator value changes for nanoparticles concentrations of 2%, 4% and 5% for the channel with 8 turns are plotted in Figure 6.17. According to the plot, for the case of using the nanofluid with 2% volume fraction, the performance of the cooling system at Reynolds numbers equal or smaller than 780 and larger than 1700 is worse than its performance when water is used. A similar condition occurs for the nanofluid with 4% volume fraction when the Reynolds number is smaller than 700 or larger than 1700. In the case of the nanofluid with 5% volume fraction, worse performances are noticed for Reynolds numbers smaller than 780 and larger than 1575.

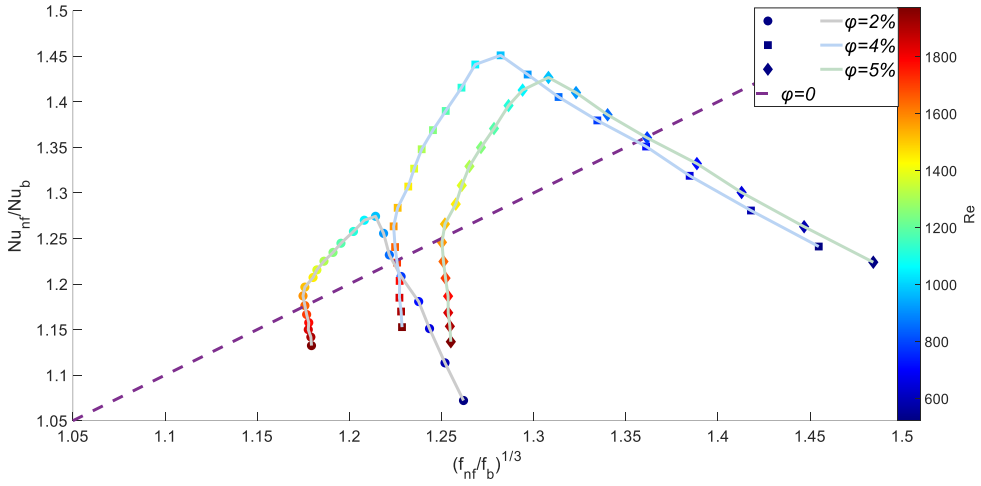

Figure 6. 17. Numerator value changes of PEC versus the denominator value changes for nanoparticles concentrations of 2%,4%, and 5%.

Therefore, compared to water, the use of nanofluid with the volume fraction of 4% in more cases improves the performance of the cooling system. In other words, with increasing the concentration of nanoparticles, the rate of heat transfer improvement exceeds the rate of increase in pressure losses. However, excessive increase of nanoparticle concentration (here 5%) leads to decreased heat transfer and fluid flow performances.

As mentioned before, heat transfer performance is impaired due to the dual effect of increasing the nanoparticle concentration which increases the thickness of the channel wall boundary layer.

Figures 6.18a, 6.18b, and 6.18c show PEC index values for nanofluids with nanoparticle concentrations of 2%, 4%, and 5%, respectively. For all cases, the highest value of the PEC index is obtained at Reynolds number of 1049. As can be seen in Figure 6.18, it can be concluded that the greatest improvement in the overall performance of the cooling system, for all nanoparticle concentrations, is obtained in the situation where the heat transfer performance enhancement due to the addition of nanoparticles is almost at its maximum value while the increase in pressure drop is moderate.

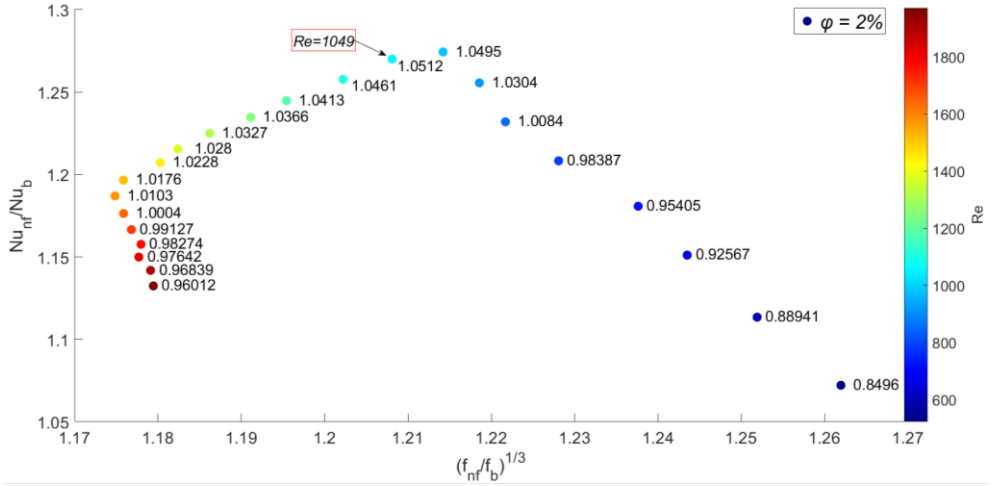

(a)

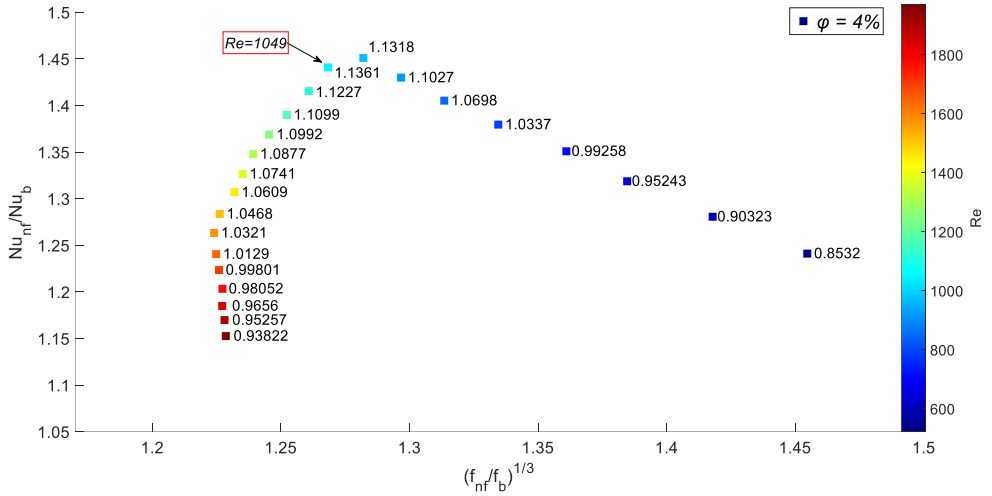

(b)

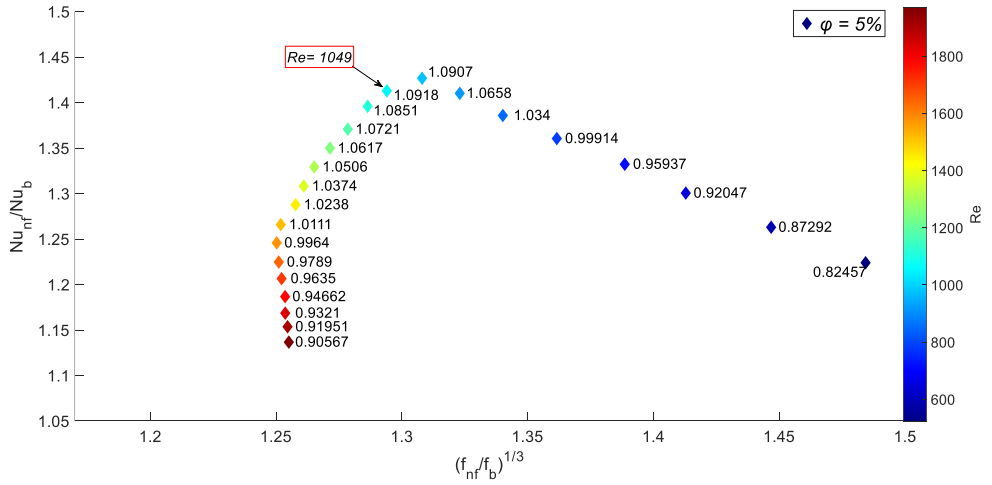

(c)

Figure 6. 18. PEC values, (a) for φ = 2%, (b) for φ = 4%, (c) for φ = 5%.

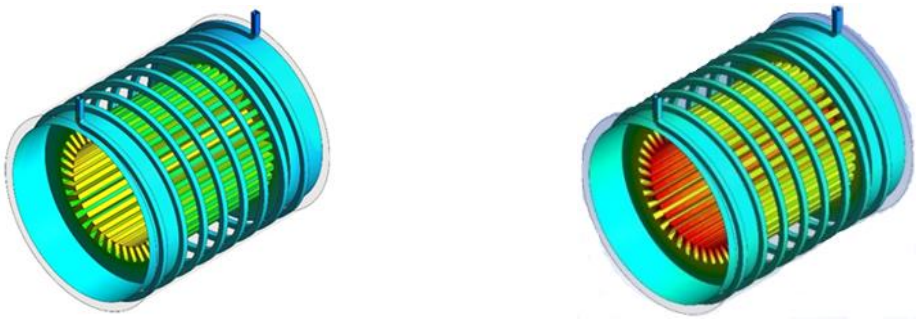

(a) (b)

Figure 6. 19. Temperature distribution contours at Reynolds number of 2000 with volume fractions of (a) 2% and (b) 4%.

This finding demonstrates that the main factor in improving the overall performance of the cooling system is improving its heat transfer performance. Therefore, the key factor that causes nanofluids with excessive nanoparticle concentrations to have a lower overall performance is the dual effect of adding nanoparticles on heat transfer rather than the negative effect of increasing pressure drop.

Finally, In Figure 6.19., contours of temperature distribution are shown at the Reynolds number of 2000 for the nanofluid with volume fractions of 2% and 4%. As can be seen, by increasing the volume fraction of nanoparticles in the fluid from 2% to 4%, the heat transfer from channel's walls to the cooling fluid increases and the motor temperature decreases. The improvement in cooling due to the use of nanoparticles in the base fluid results from the fact that the addition of nanoparticles to the base fluid increases its conduction heat transfer coefficient. This improves thermal penetration depth of the coolant fluid. Also, the presence of a nanoparticle in the base fluid leads to a reduction in specific heat capacity of the base fluid. This increases amount of the absorbed heat flux by the coolant fluid. These two factors reduce the operating temperature of the motor and improve heat transfer performance of the cooling system.

6.5 CONCLUSION

The effect of structural geometry of the cooling system and volume fraction of Al2O3 nanofluid on heat transfer and fluid flow performances of the cooling system for electric machine applications are analyzed in this chapter. The effect of adding nanoparticles to the base fluid and different geometries are examined on a cooling system based on the cooling jacket method. The core idea is to demonstrate these relationships so that the best combination of structural geometry and nanofluid volume fraction can be chosen to design a high-performance cooling system. Also, this study aimed at demonstrating and com-paring the importance of two factors of heat transfer and fluid flow on the overall performance of the cooling system. The main conclusions are as follows.

(a) For the same structural geometry, the heat transfer coefficient increases with the in-crease of Reynolds number. Also, at any pumping power, increasing the concentration of nanoparticles increases the heat transfer coefficient.

(b) In reference to (a), from a specific Reynolds number onward, due to the viscosity, the slope of the friction resistance changes decreases. Therefore, while in the laminar flow regime the heat transfer coefficient always increases with increasing Reynolds number, at higher Reynolds numbers, the slope of increasing the heat transfer coefficient decreases.

(c) Adding nanoparticles to a base fluid affects the heat transfer coefficient in two different ways. While increasing nanoparticle concentration enhances the heat transfer coefficient by increasing the thermal conductivity of the nanofluid, increasing the nanoparticle concentration can lead to a reduction of the temperature gradient at the wall of the channels. In this study, numerical results for the nanofluid with the volume fraction of 5% in cooling jacket channels with 8 turns show a very small heat transfer coefficient enhancement resulted from a significant decrease in temperature gradient at the channel walls.

(d) Due to the increase in the cooling cross-sectional area, increasing the turns number of the channel improves heat transfer from the electric motor to the coolant fluid, thus in-creasing the heat transfer coefficient.

(e) Increasing turn number of channels leads to a greater enhancement of heat transfer co-efficient at larger Reynolds numbers. This is due to the fact that the pitch of the channel decreases by increasing turns number. As the smaller pitch of spiral channels causes the friction factor to decrease further by increasing the Reynolds number, greater enhancement of the heat transfer coefficient is achieved.

(f) Due to the smaller pitch of the channel with a higher number of turns, at larger Reynolds numbers, the friction factor decreases more than in the channel with a lower number of turns, so the percentage of the relative increase in pressure drop decreases at larger Reynolds numbers for spiral channels with a higher number of turns.

(g) According to the results and discussions, it was demonstrated that the main factor in improving the overall performance of the cooling system is the increase in its heat transfer performance. Therefore, the key factor that causes nanofluids with excessive nanoparticle concentrations to have a lower overall performance is the dual effect of adding nanoparticles on heat transfer rather than the negative effect of increasing pressure drop.

7. ELECTRIC MACHINE COOLING SYSTEMS BASED ON PCM AND A HYBRID COOLING SYSTEM

7.1 INTRODUCTION

This chapter investigates the cooling performance of entirely passive cooling systems and hybrid (passive + active) cooling systems for electric machine cooling applications. Cooling systems are either active or passive. Although in active cooling systems, heat transfer coefficient is higher, the installation, repair, maintenance, and pump power are the problems associated with the employment of active cooling systems [231]. The use of cooling jackets is the most common cooling method for electric machine applications [232]. In a passive cooling system, in which the pump is not used in the cooling circuit, the heat generated by the electric machine should be adsorbed and transferred without engaging the pump [233].

Phase Change Materials (PCMs) are used as heat adsorbent agents to cool electronic components [234–236], electric motors [237], and thermal energy storage systems [238–240]. In the phase change process, the heat flux is dissipated as latent heat to melt down the material while its temperature does

not change until the phase change is complete. Among the relevant studies, Wang et al. studied the use of PCMs for cooling electric motor rotors [241]. They injected PCM paraffin into a Permanent Magnet Synchronous Motor (PMSM) and found that the use of PCMs increases the motor utilization time by 50% until it reaches the maximum allowed temperature. In another study, they used PCMs, along with a fin, and observed the improved PCM-based cooling system performance [242].

The use of PCMs for cooling of electric machines rotor/stator has recently attracted the attention of researchers. The majority of studies used oil-based PCMs, such as paraffin, in cooling systems. Also, metal-based phase change materials are used for cooling the electric machine and preventing its extensive temperature rise. As compared to oil-based phase change materials, these materials have a higher melting point and thermal conductivity. Therefore, in this chapter, a metal-based PCM that possess a higher thermal conductivity compared to Paraffin that is a common PCM studied in the literature was selected. The flow field and transient heat conduction are simulated using the finite volume method. The accuracy of numerical values obtained from the simulation of the phase change materials is validated. The sensitivity of the numerical results to the number of computational elements and time step values is assessed. The main goal of adopting the PCM-based passive cooling system is to maintain the operational electric machine temperature in the allowed range for applications with high and repetitive peak power demands such as electric vehicles.

PCM-based cooling systems take advantage of the high latent heat absorbance capability of PCMs during phase change processes. In the first study, PCM is employed in spiral channels with different channel turns. In the second study, entire the cooling jacket is filed by PCM. Both scenarios are based on the completely passive cooling system technique. Changes in the temperature of PCM, rotor and stator temperatures, and liquid phase volume fraction of PCM in different geometric arrangements are investigated.

Performance of passive PCM-based cooling systems strongly depends on the time duration of the PCM melting process. In fact, after the melting process

completed, the heat transfer capability of the cooling system significantly deteriorated. This makes PCM-based passive cooling systems suitable for short-time heat removal needs. Therefore, passive PCM-based cooling systems can be used for heat fluxes arising during short-time intervals. In other words, passive PCM-based cooling systems are not suitable for heat removal when a constant heat flux is applied. Therefore, in this chapter, combination of passive PCM-based cooling systems with active liquid-cooling systems are investigated. The idea is to remove the extra heat generated at repetitive peak power operating points of the electric machine and to employ a liquid-cooling system for removing the heat generated by more frequently operating points of the electric machine.

7.2 GOVERNING EQUATION AND NUMERICAL METHOD

The porous enthalpy method is used to simulate the phase change process in the cooling stage. The simulation is three-dimensional, and the flow is considered laminar, transient, and incompressible. The governing equations are Navier-Stokes and Energy equations:

$$\nabla.\vec{V} = 0 \tag{7.1}$$

$$\frac{\partial\vec{V}}{\partial t} + \vec{V}.\nabla.\vec{V} = \frac{1}{\rho}\left(-\nabla P + \mu\nabla^2\vec{V} + \rho\beta\vec{g}\left(T - T_{ref}\right)\right) + \vec{S} \tag{7.2}$$

$$\frac{\partial h}{\partial t} + \frac{\partial H}{\partial t} + \nabla.\left(\vec{V}h\right) = \nabla.\left(\frac{k}{\rho C_P}\nabla h\right) \tag{7.3}$$

where H is the enthalpy of PCM, containing nanoparticles, and equal to the sum of sensible enthalpy (h) and latent heat (ΔH).

$$H = h + \Delta H \tag{7.4}$$

The sensible enthalpy is calculated using the following equation:

$$h = h_{ref} + \int_{T_{ref}}^{T} C_P\, dT \tag{7.5}$$

where, h_ref is the original enthalpy, T_ref is the original temperature, and C_P is the specific heat capacity under constant pressure. The latent heat is calculated based on the latent heat of the material:

$$\Delta H = \alpha L \tag{7.6}$$

where, L and α are latent heat and liquid fraction, respectively. α is defined as follows:

$$\alpha = \begin{cases} 0 & if\ T < T_{solidus} \\ \frac{T - T_{solidus}}{T_{liquidus} - T_{solidus}} & if\ \ T_{liquidus} < T < T_{solidus} \\ 1 & if\ T > T_{liquidus} \end{cases} \tag{7.7}$$

The latent heat capacity can be zero (for solid) and equal to L for liquid. The Energy Equation is as follows for the melting or freezing problem:

$$\frac{\partial(\rho H)}{\partial t} + \nabla.(\rho \vec{v} H) = \nabla.(k \nabla T) + S \tag{7. 8}$$

where, v $\vec{}$ and S are the fluid velocity and source, respectively.

$$\vec{S} = \frac{(1-\lambda)^2}{\lambda^3} A_{mush} \vec{V} \tag{7.9}$$

In this equation, Amush is the Mushy factor and equal to 10^6 [243].

The governing equations are discretized using the second-order upwind method. The velocity and pressure equations are coupled using the SIMPLE method. The convergence criterion is considered 10^{-6} for all equations. The time step of the simulation is 10^{-3}.

7.3 PROBLEM STATEMENT AND BOUNDARY CONDITION

In the present study, the passive cooling system is designed for an electric motor. The specifications of the designed motor are presented in Table 7.1. The metal alloy-based PCMs are used for cooling. The thermophysical properties of PCMs are presented in Table 7.1.

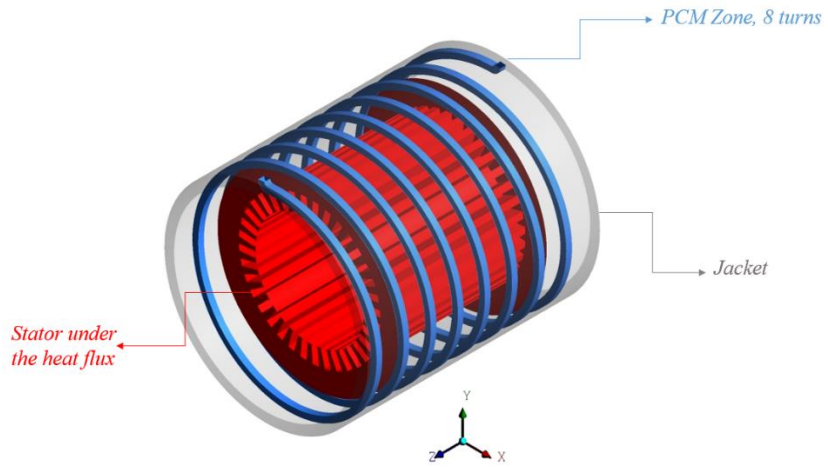

(a)

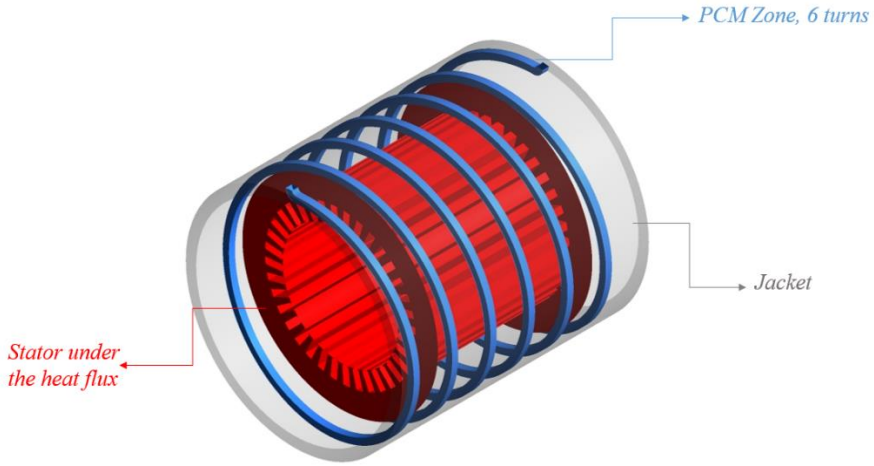

(b)

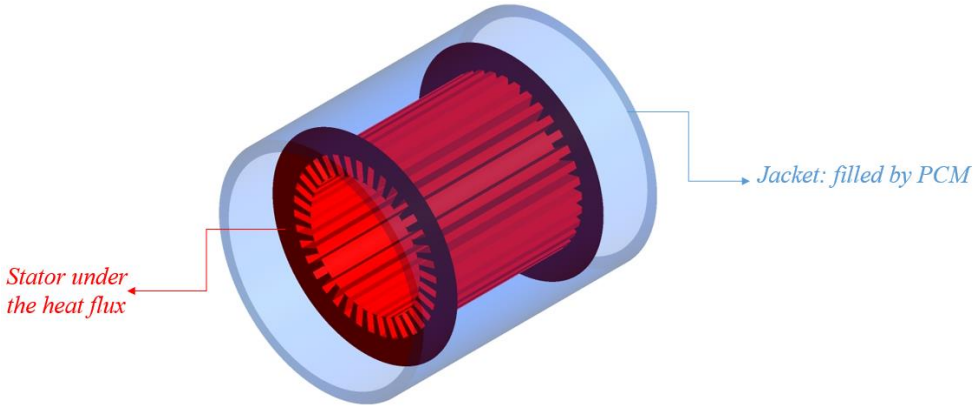

(c)

Figure 7. 1. Schematic of geometries under investigation.

Table 7. 1. Thermophysical properties of PCM in present study [244]

Metal based PCM	Melting Temperature (°C)	Conductivity $k(\frac{W}{m-K})$	Latent heat $h_{sf}(\frac{j}{kg})$	Specific heat $C_p(\frac{kj}{kg.K})$	Density $\rho(\frac{kg}{m^3})$
52BI/30PB/18SN	58	33.2	202000	3230	9079

Figure 7.1 shows the arrangement of the phase change material inside the motor's cooling jacket. As can be seen, PCMs have been used in a cooling system with a spiral arrangement of 6 (Figure 7.1 a) and 8 (Figure 7.1 b) turns and in the entire cooling jacket (Figure 7.1 c). The heat flux applied to the rotor wall is 3500 watts per square meter. All external walls are insulated. The motor temperature change over time is measured by transient simulation of the flow field and heat transfer.

7.4 Validation and Grid study

To validate the numerical method used in the simulation of the PCM melting process, the results are compared to the experimental data in [244], where the behavior of PCM (RT50) was investigated inside a shell and tube heat exchanger. Figure 7.2 compares changes in the temperature of the phase change materials based on the time obtained from the numerical solution with the results presented in this reference. As can be seen, the results of the study are in good agreement with [244], indicating that the employed numerical method is accurate.

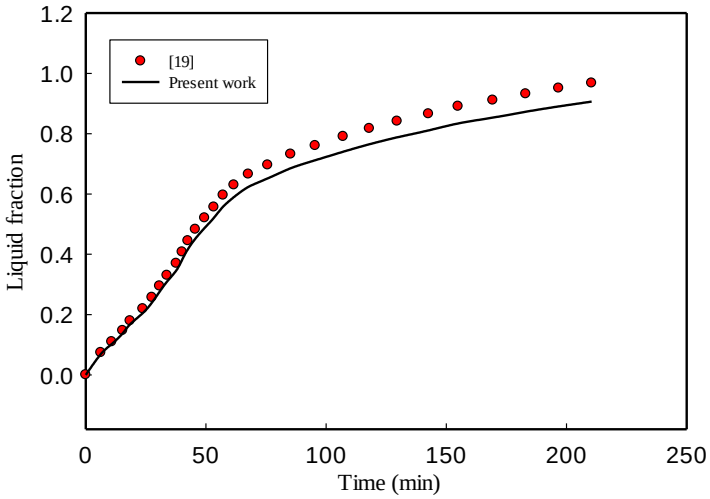

Figure 7. 2. Validation of results in Hosseini et al.'s study [244].

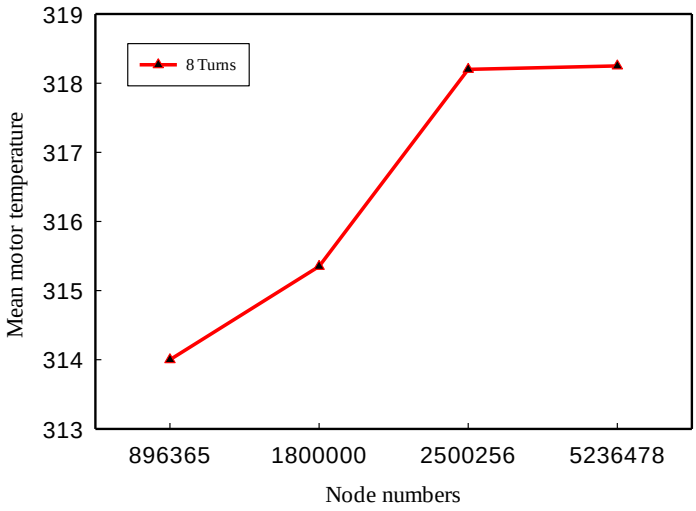

(a)

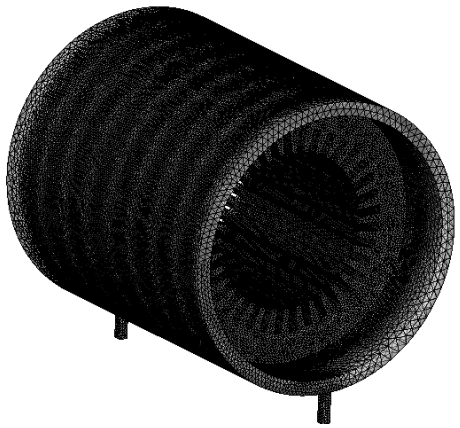

(b)

Figure 7. 3. Grid independency and computational grid, (a) Grid independency, (b) applied computational grid.

In the numerical simulation, the number of computational elements has a considerable effect on the numerical results. In the present study, the simulation was done for a different number of elements and the effect of the number of elements on the mean motor temperature after 500 seconds and eight PCM turns around the rotor is presented in Figure 7.3a. According to this figure, the results become independent of the number of the computational network with increasing the number of elements to more than 2,500,256. Figure 7.3b shows the applied computational mesh network.

7.5 RESULT AND DISCUSSION

This section presents the numerical results obtained from the transient simulation of the flow field and heat transfer. The results entail the distribution of the volume fraction of the liquid phase, temperature distribution of the PCM path, and temperature distribution of the motor body at different times.

Figure 7.4 shows the distribution contour of the volume fraction of the liquid phase at different times, representing the melting process. As can be seen, no phase change can be seen after 300s and with six turns; however, the phase change occurred at t = 500 s, and 0.4 of the PCMs changed to the liquid phase.

Comparison between the scenarios with six and eight turns at t=500 s showed that 0.25 of PCM changed to liquid phase under the scenario with eight turns. According to Figure 7.4, the volume fraction of the liquid phase reduces from 0.77 to 0.51 at t = 600 s with increasing the number of turns from six to eight. By increasing the number of turns around the PCM path, the latent heat capacity increases in the melting process, and more heat is needed for phase change. Therefore, the transition from solid to liquid phase takes longer to happen with increasing the number of turns in the passive cooling system under investigation.

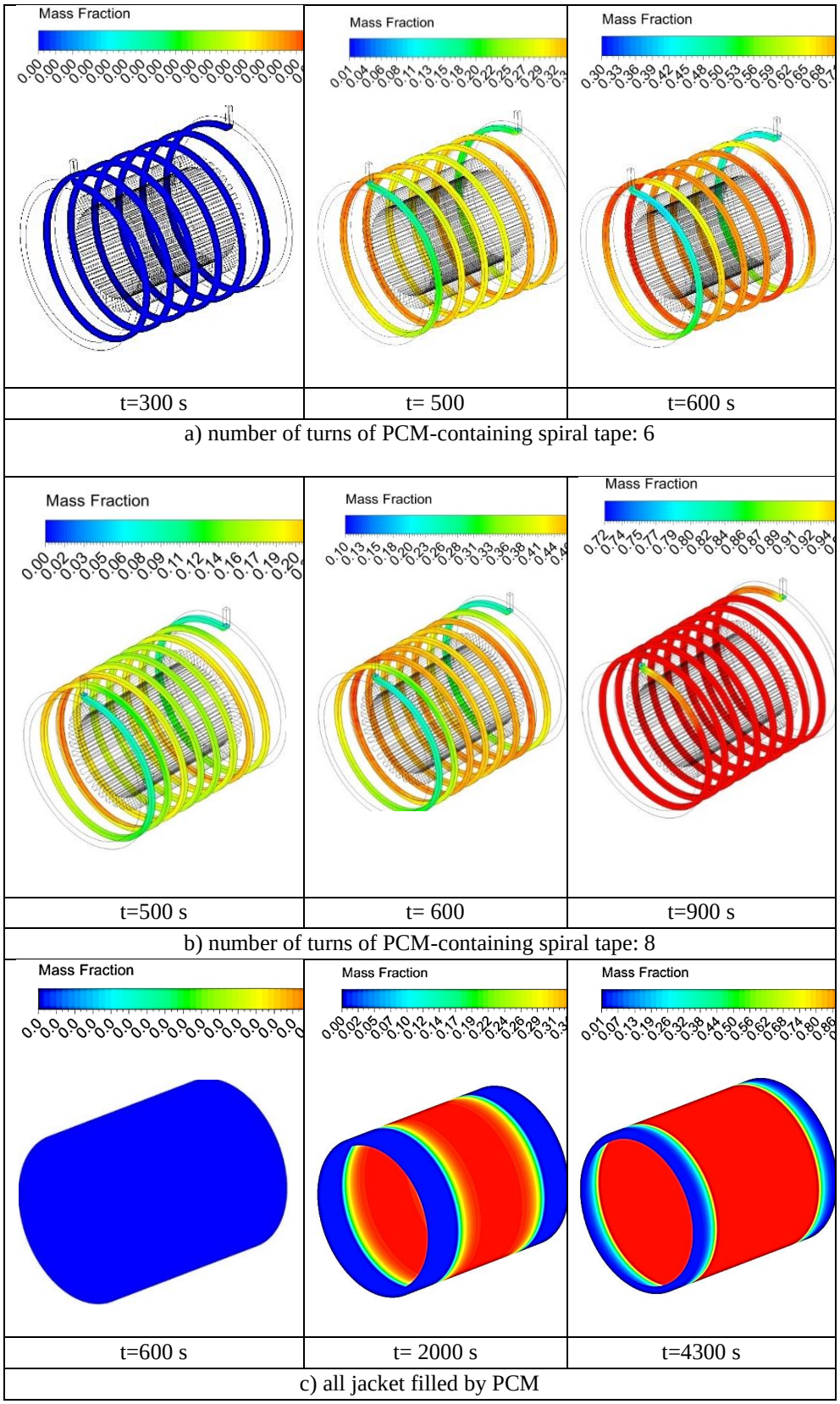

Figure 7. 4. Distribution of volume fraction of the liquid phase for three different PCM arrangements.

The prolongation of the melting process causes the longer adsorption of heat flux by PCM and the operating temperature is maintained for a longer time within the allowed temperature range. The utilization time of the active cooling system reduces with increasing the operating time of the passive cooling system within the allowed operating temperature. Reducing the operation time of the active cooling system in the electric motors of electric vehicles improves the discharge and operation time.

As seen in Figure 7.4.c in the case that the whole area of the cooling jacket volume is filled by PCM, at t = 600 s, the phase change material is in the solid phase and the phase change process has not yet begun. Over time at t = 200 s, the maximum value of the liquid phase is 0.38, which indicates that the phase change has occurred and part of the phase change material has been converted to the liquid phase. Finally, at t = 4000 s, the maximum mass fraction of the liquid phase is equal to 0.98, which indicates that over time and when the heat flux of the electric machine is applied to the phase change material, a sufficient latent heat for melting in the phase change process is provided.

To investigate the behavior of PCMs in the present study, Figure 7.5 shows the temperature changes at different times under both scenarios of six and eight turns. According to this figure, the maximum temperature at t=300 s, 500 s, and 600 s is 47°C, 54°C, and 57°C, respectively, in a jacket with six embedded turns of PCM. The maximum temperature for the scenario with eight turns at t = 500 s, 600 s, and 900 s is 53°C, 55°C, and 56.7°C, respectively. As can be seen, an increase in the cooling path temperature is higher than the central temperature where the stator is connected to the jacket on both sides. According to the results, the latent melting temperature increases with increasing the number of turns of the PCM-containing cooling path; in addition, the PCMs can maintain the allowed motor temperature for a longer time by absorbing the applied heat flux.

Figure 7.5.c shows the temperature distribution when the entire jacket is filled with phase-change material at 600, 2000 and 4300 seconds. As can be seen at t = 600s, the maximum temperature of the phase change material is 42 ° C

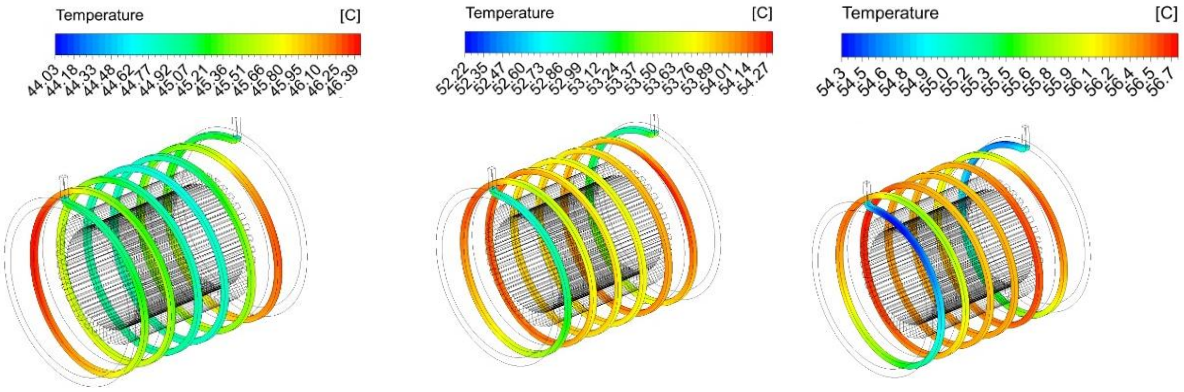

t=300 s t= 500 t=600 s

a) number of turns of PCM-containing spiral tape: 6

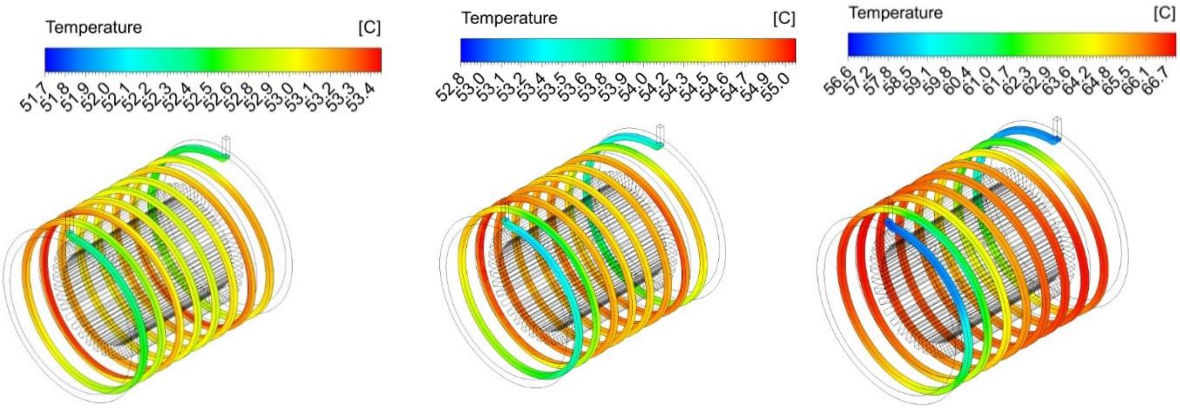

t=500 s t= 600 t=900 s

b) number of turns of PCM-containing spiral tape: 8

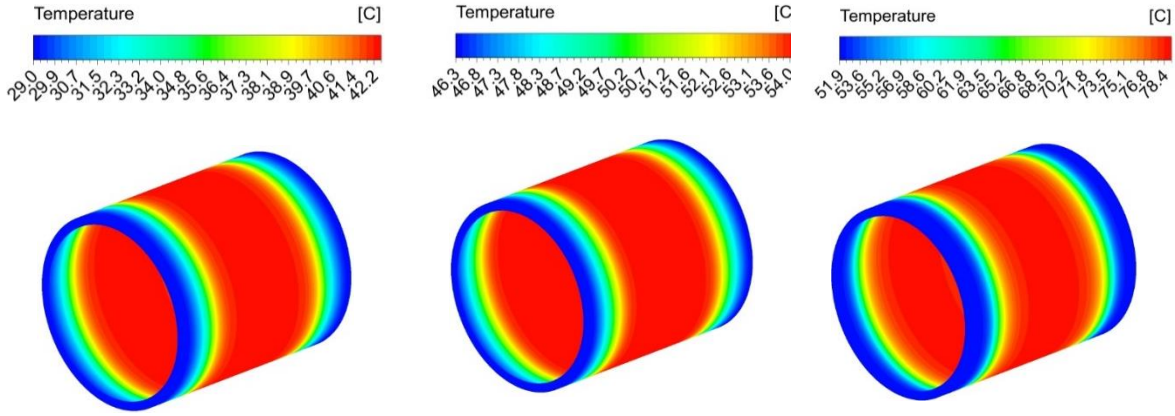

t=600 s t= 2000 s t=4300 s

c) all jacket filled by PCM

Figure 7. 5. Distribution of path filled with PCM in three different arrangements

and at t = 2000s, with the penetration of heat into it, the maximum temperature increases to 54 ° C and finally with continuing the phase change process and the predominance of the liquid phase, the temperature of the PCM-filled chamber increased to 78 °C. In the following, quantitative and qualitative changes of the electric machine temperature over time are presented and the thermal performance of the passive cooling system used in the present study is investigated.

Figure 7.6 shows the contour of the temperature distribution of the rotor and stator at different times and scenarios under investigation. According to Figure 7.6a, in the presence of six turns of PCM around the spiral path, the motor temperature increases over time in a gradual melting process. At t = 300 s, 500 s, and 600 s, the maximum temperature was 74.5°C, 87.7°C, and 91.7°C, respectively. The investigation into the degree of maximum temperature changes showed that the effectiveness of PCM in preventing temperature rise reduces with the progress of the melting process and domination of the liquid phase. In fact, PCM has the maximum efficiency when it is undergoing the phase change process. In addition, with the completion of the melting process, a sensible heat transfer occurs.

Figure 7.7 shows changes in the volume fraction of the liquid phase over time for two different conditions under study. As can be seen, the volume fraction of the liquid phase increased after 400 s. There is a slight delay of 50 seconds at the start of the melting process between the arrangements with eight and six turns. After the beginning of the melting process, the volume fraction of the liquid phase increases linearly; in addition, the process was longer at the arrangement with eight turns in that a complete phase transition to liquid occurred after 720 s in the arrangement with six turns and after 968 s in the arrangement with eight turns. The PCM mass and heat adsorption increase in the melting process by increasing the number of turns. This is why the melting process time has increased.

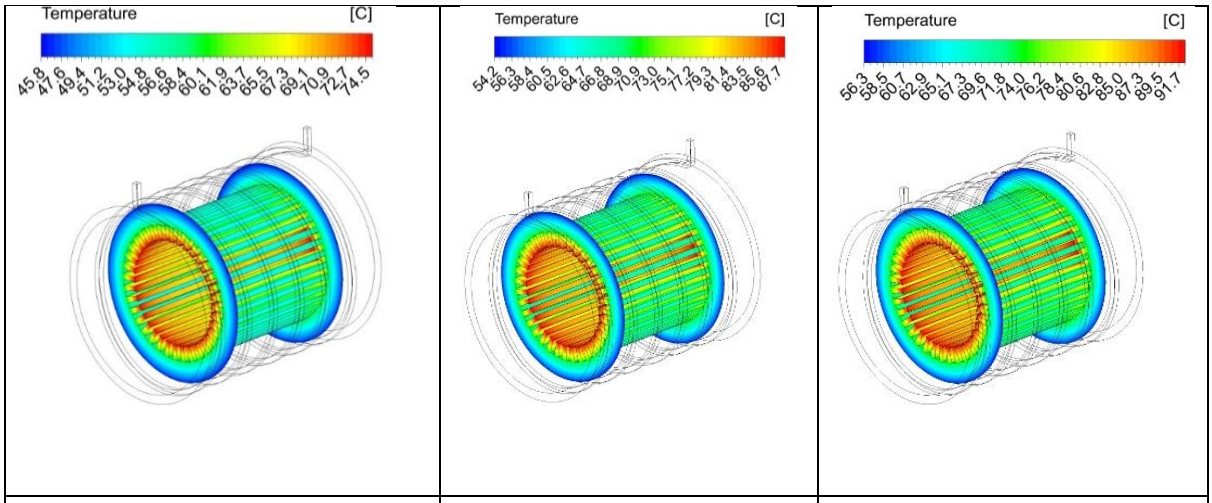

t=300 s	t= 500	t=600 s

a) number of turns of PCM-containing spiral tape: 6

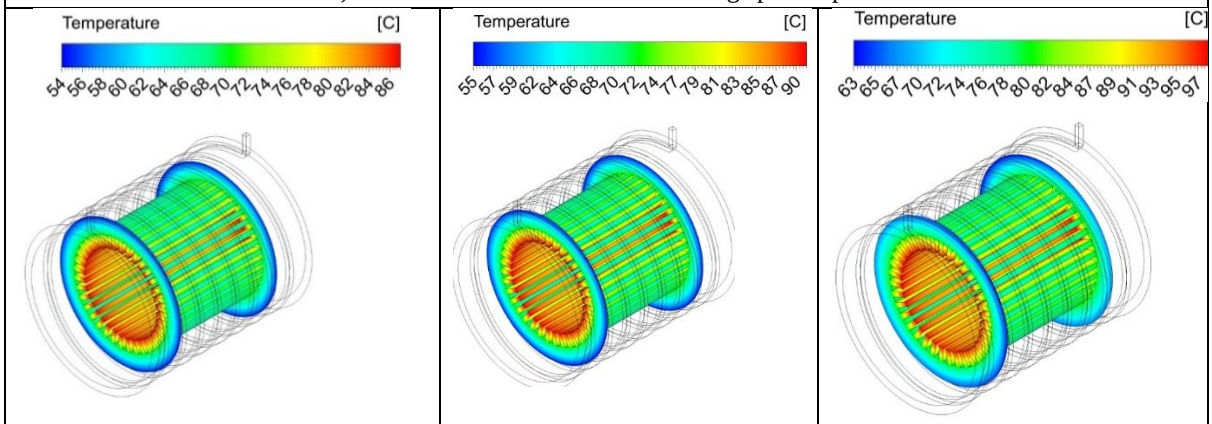

t=500 s	t= 600	t=900 s

b) number of turns of PCM-containing spiral tape: 8

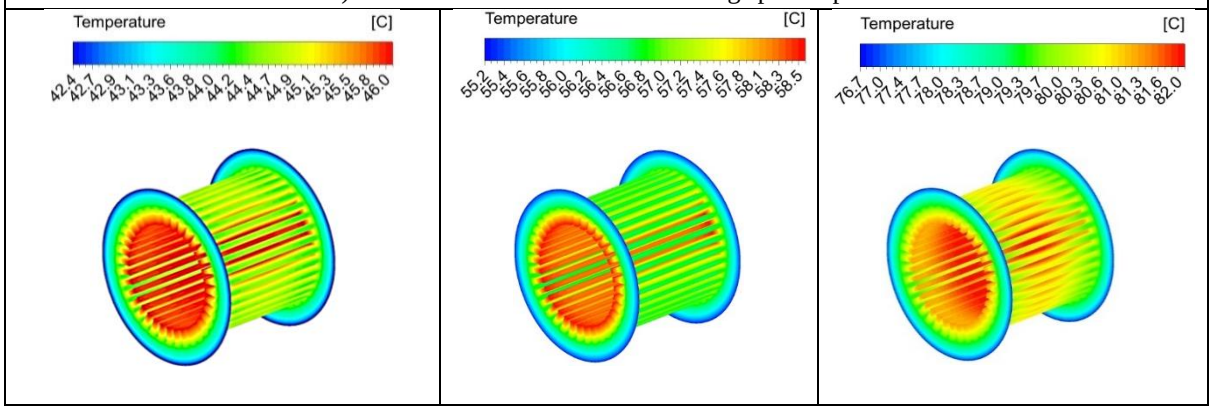

600 s	2000 s	4300 s

C) number of turns of PCM-containing spiral tape: 6

Figure 7. 6. Temperature distribution of motor at two different arrangements of the PCM-containing cooling system.

Changes in the volume fraction of the liquid phase of the phase change material when the entire jacket chamber is filled with the phase change material, show that after 1000 seconds, the melting process has started due to the increase in heat required for melting. Thus, in the case where the phase change material is used in the spiral path with 8 and 6 turns, the whole process of melting and conversion of the whole phase change material to liquid phase has occurred in 1000 seconds, but in the condition where the whole jacket chamber is filled with the phase change material, the process of phase change and conversion of the whole PCM to the liquid phase occurred during 6000 seconds. This study shows that the process of changing the amount of liquid phase of PCM shows that at about 1000 seconds, the melting process begins and the volume fraction of the liquid phase begins to increase.

By t = 3150 s, with a constant slope, the volume fraction of the liquid phase increases to 0.65, after which its slope changes, and finally, at t = 6000 s, all the phase change material transforms to the liquid phase. The reason for the change in slope at t = 3150 s can be due to the predominance of the liquid phase after that and the effect of heat is noticeable. In fact, based on the volume fraction distribution of PCM in the liquid phase, we can say; the best performance is achieved up to t = 3150 s, when the dominant mechanism of heat transfer is latent heat of melting. In the following, the electric machine temperature changes in three different conditions over time are investigated.

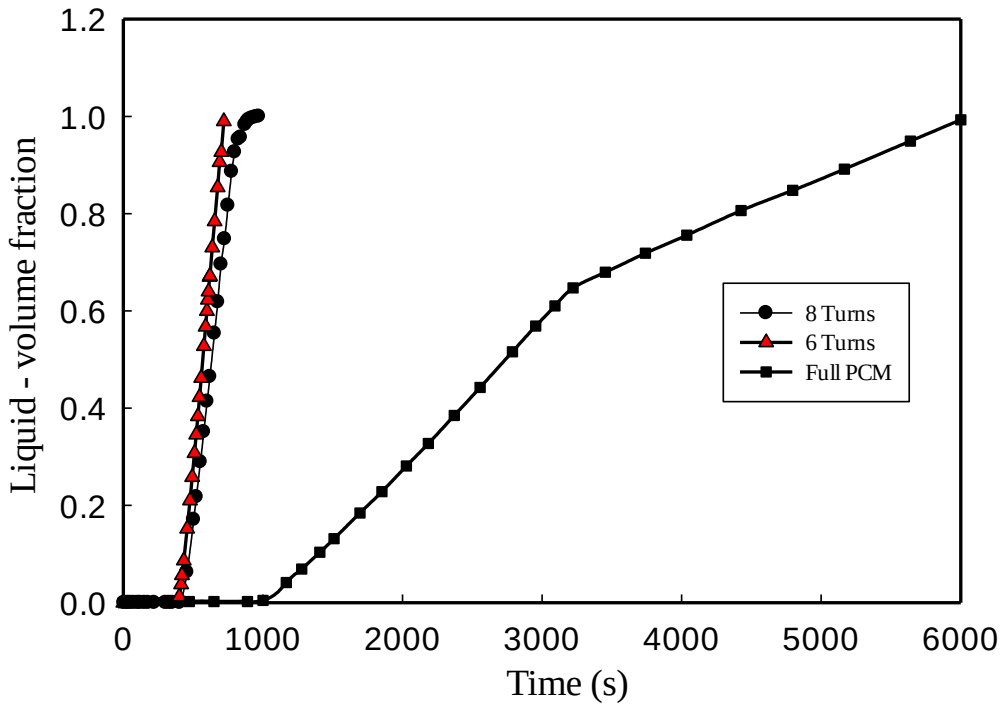

Figure 7. 7. Changes in volume fraction of liquid phase over time and effect of number of PCM-containing path's turns.

Figure 7.8 shows changes in the mean motor temperature based on time. As can be seen, the motor temperature increases linearly with time before the initiation of the melting process. This is because sensible heat is the dominant mechanism of heat transfer. With the beginning of the melting process, the gradient of temperature changes reduces as a part of the heat flux is adsorbed during the melting process (latent melting heat). Figure 7.8 shows that the motor temperature remains within the desired temperature (lower than 60) for a longer time with increasing the mass and space occupied by the PCM.

Also, the study of temperature changes in conditions where the jacket chamber is entirely filled with phase change material, shows that the cooling performance is acceptable. For up to 4000 seconds, the operating temperature is less than 80 ˚C using only the passive cooling system based on the phase change material. Maintaining the allowable temperature by the passive cooling system for more than one hour reduces the energy consumption in the cooling section, and this can increase the working life of hybrid/electric vehicles and increase their efficiency.

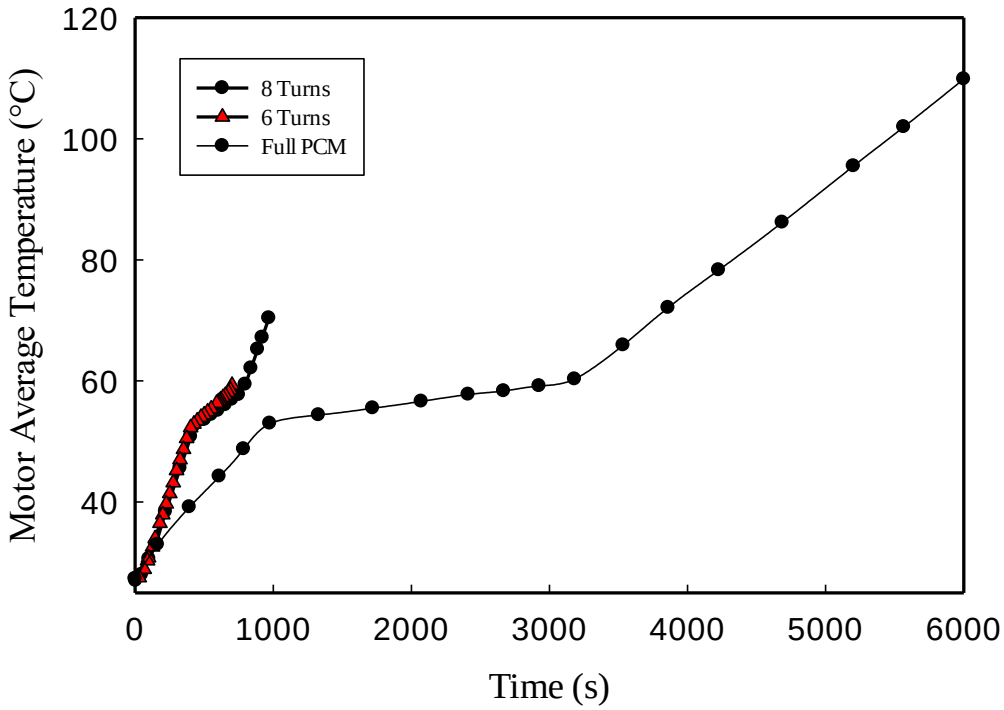

Figure 7. 8. Changes in mean motor temperature over time and effect of number of PCM-containing path's turns.

Examination of the change in the electric machine temperature gradient when the entire chamber is filled with the phase change material shows that the process of temperature changes is consistent with the process of liquid phase changes (Figure 7.7). As can be seen, up to t = 3150 s, due to the predominance of the latent heat, the temperature increased with a smaller slope, and this is the period when the best performance of the passive cooling system is achieved where the electric machine temperature is maintained below 60 ˚C without any energy consumption and the pumping power.

7.6 HYBRID COOLING SYSTEM

The combination of active and passive cooling methods that is called hybrid cooling system is investigated in this section. In this study, active cooling system is based on water-cooling and the passive one is based on using PCM. Figure 7.9 shows losses of an electric machine under three widely used driving cycles [245]. The driving cycles are Federal Test Procedure (FTP-75), New European Driving Cycle (NEDC), and Japanese test cycle (JC08).

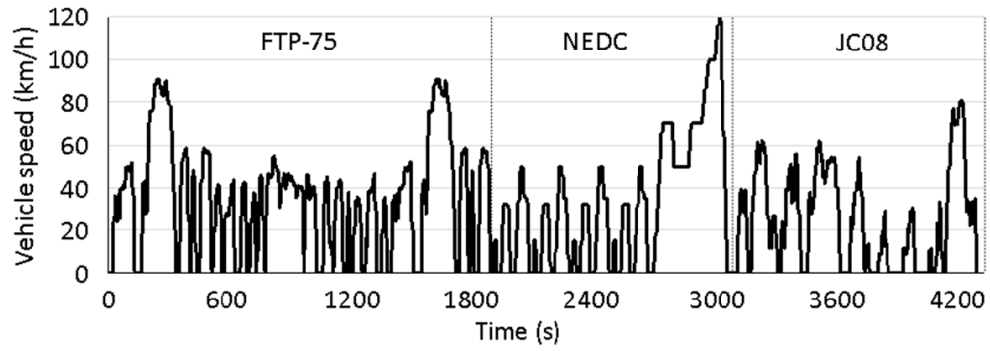

(a)

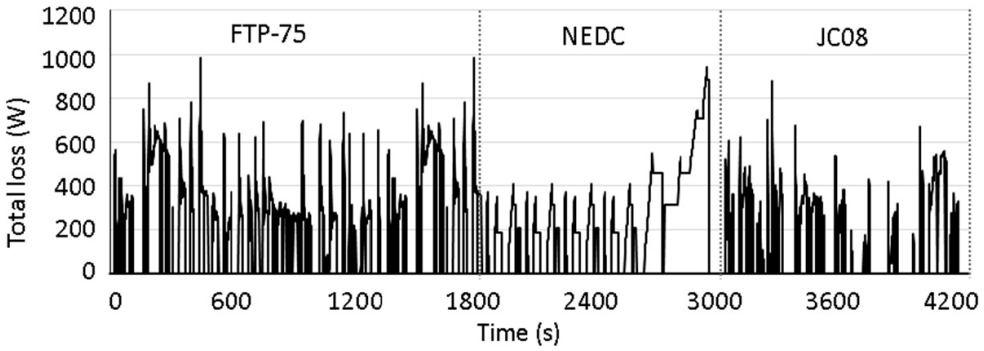

(b)

Figure 7. 9. Electric vehicle driving cycles and corresponding electric machine losses, (a) driving cycles, (b) corresponding electric machine losses [245].

As can be seen, part of losses are very repetitive but other parts are not frequent. So, the active cooling system can be designed for repetitive losses and the passive PCM-based cooling system can be responsible for less frequent peak losses. This adequately fits properties of PCM that can absorb high volume of heat but for a short time.

Figure 7.10 shows the model of hybrid cooling system consisting of spiral channels containing water as the active part of the cooling system and the cooling jacket filled by PCM as the passive part of the cooling system. The main purpose of implementing the hybrid cooling system is to reduce the temperature of the phase-change material and increase the melting time.

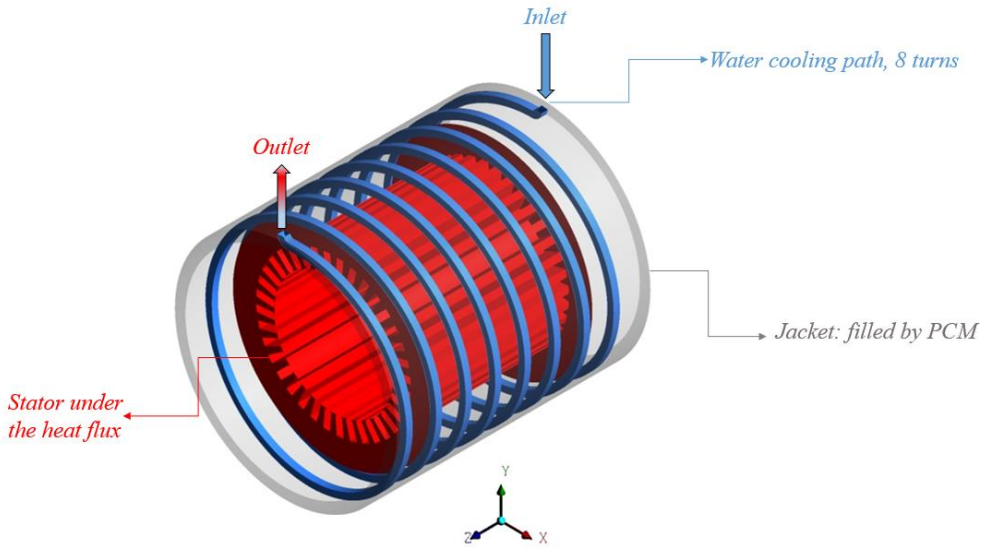

Figure 7. 10. Model of the under-study hybrid cooling system.

Figure 7.11 shows the average temperature of the electric machine when the hybrid cooling system as a combination of an active and a passive cooling system parts is used. As can be seen, employing the hybrid cooling system, the average temperature of the electric machine remains below 80 degrees up to more than 5000 seconds. According to Figure 7.11, temperature changes have shown three different behaviors, depending on time. First, with a steep slope, the temperature of the electric machine has increased. This is due to the tangible heat that is applied under the exposure of heat flux. After 1150 seconds, the slope of temperature changes has decreased because at this point, the phase change process has begun, and the heat flux of the electric machine is dissolved by the latent heat capacity of the PCM melting. After the melting process continues and the dominant volume fraction becomes liquid, the slope of the electric machine temperature increases.

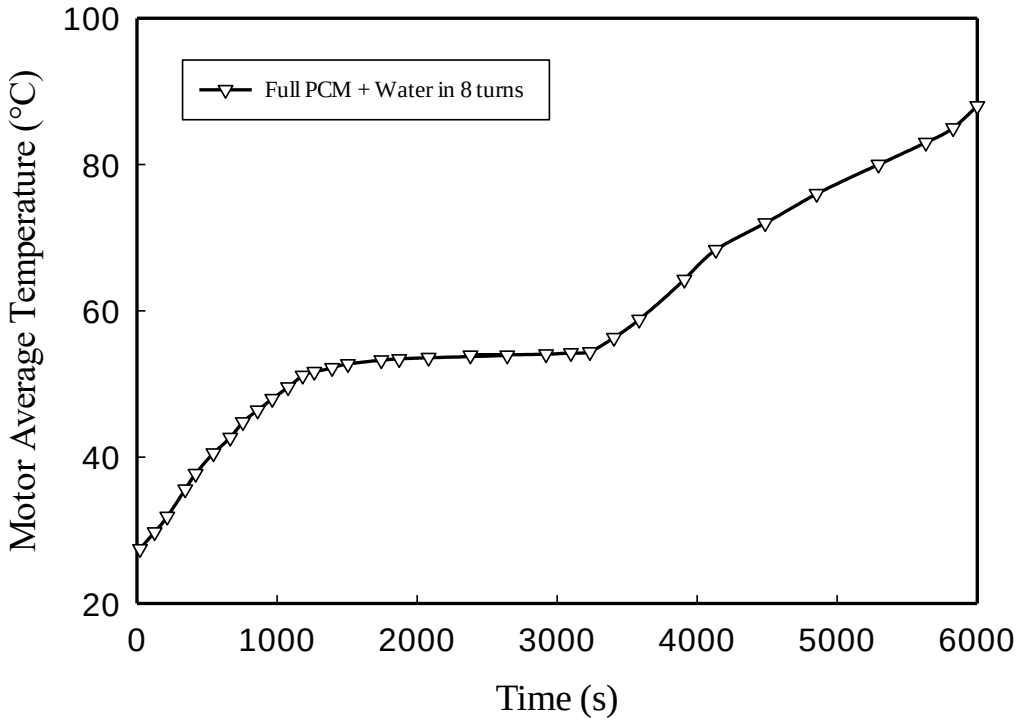

Figure 7. 11. Average temperature of the electric machine, using hybrid cooling system.

Changes in the volume fraction value of the liquid phase in terms of time is shown in Figure 7.12. As can be seen, the changes in the volume fraction of the liquid phase can be justified based on the trend of temperature increase. First, the volume fraction of the liquid phase is equal to zero and after 1150 seconds, by absorbing the heat flux generated by the electric machine, the volume fraction of the liquid phase increases until after 6000 seconds, it reaches to 0.85.

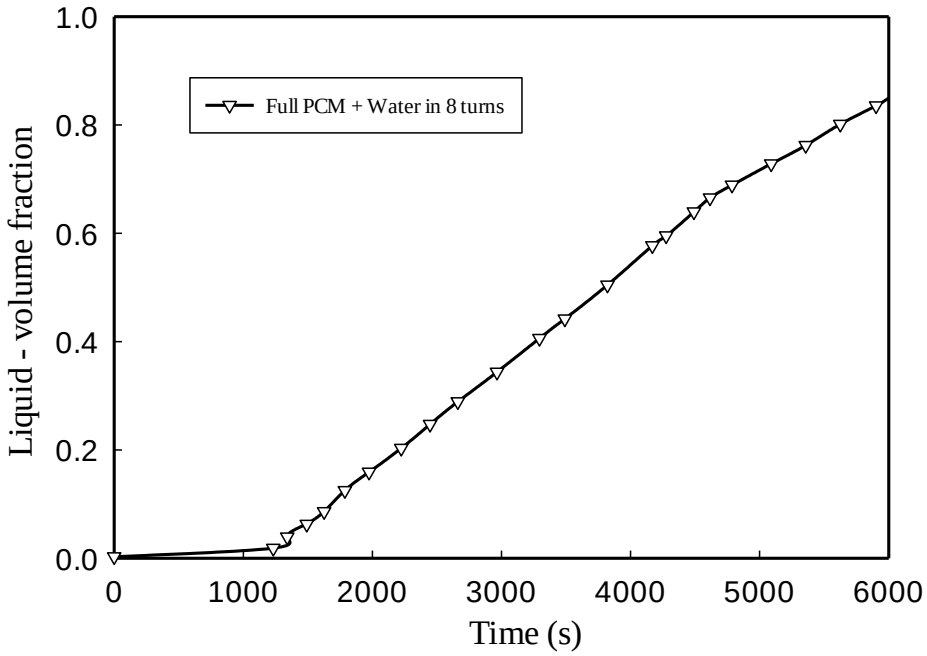

Figure 7. 12. Changes in volume fraction of liquid phase of the phase change material, using the hybrid cooling system.

7.7 COMPARISON OF DIFFERENT TYPES OF INVESTIGATED COOLING SYSTEMS

In this section, by comparing the electric machine operating temperature in terms of time in each of the studied conditions, the performance of the designed cooling systems has been investigated. In this regard, the average temperature changes for four different cooling systems in terms of time are shown in Figure 7.13. As mentioned above, three types of passive cooling systems have been studied with different layouts of the phase change material and a hybrid system employing both active and passive cooling methods. As it can be observed in Figure 7.13, when 6 and 8 turn channels containing phase change material have been used, it has no significant effectiveness and, in a short time, the temperature of the electric machine has increased. While, in the case where the entire cooling jacket surrounding the electric machine is filled with phase-change material, the temperature of the electric machine has been less than 70 degrees in a time interval of more than 4,000 seconds. These results indicate that if a passive cooling system based on phase change

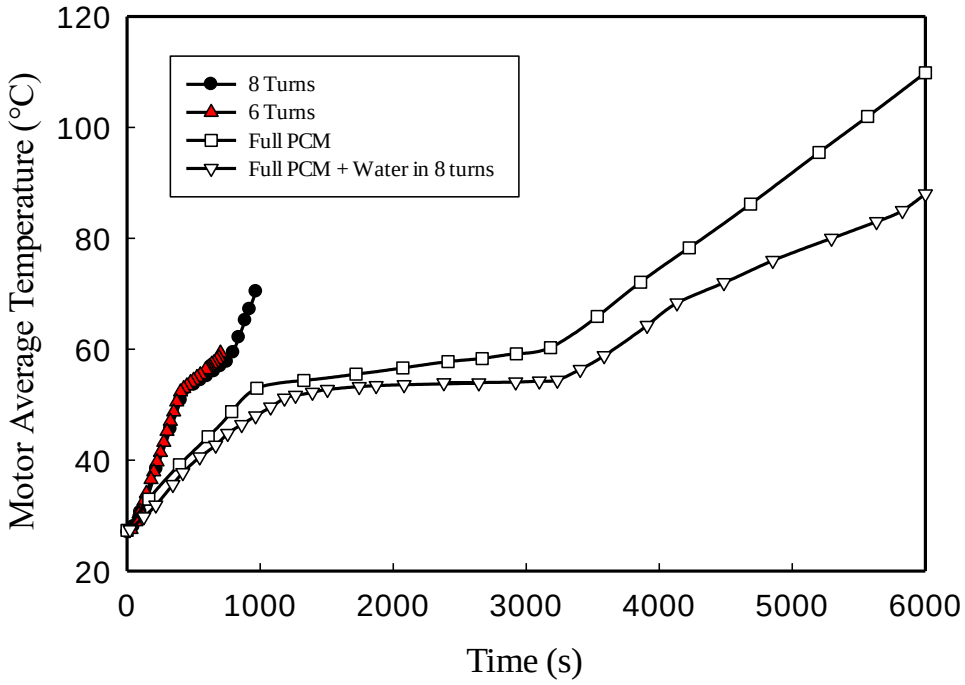

Figure 7. 13. The effect of different arrangements of the phase change material and the hybrid cooling system on the average temperature of the electric machine.

materials is used for cooling the electric machine, it is suggested that the entire cooling jacket be filled with the phase change material. The investigation of the average temperature of the electric machine in conditions where spiral channels containing water are used inside the area filled by the phase change material demonstrates that due to the heat transfer from the phase change material into the fluid, the average temperature of the electric machine has decreased. Employing the cooling fluid increases the ability to absorb heat in the phase change material and increases the melting time. By increasing the melting time, in fact the time of absorbing the heat flux of the electric machine by the phase change material will increase.

Figure 7.14 shows the effect of different arrangements of the phase change material as well as the effect of using the hybrid cooling system on the volume fraction value of the liquid phase indicating the phase change process from solid to liquid state in terms of time. As can be seen by increasing the volume of the phase change material as a result of increasing the turn number channels filled with the phase change material, the phase change process duration has

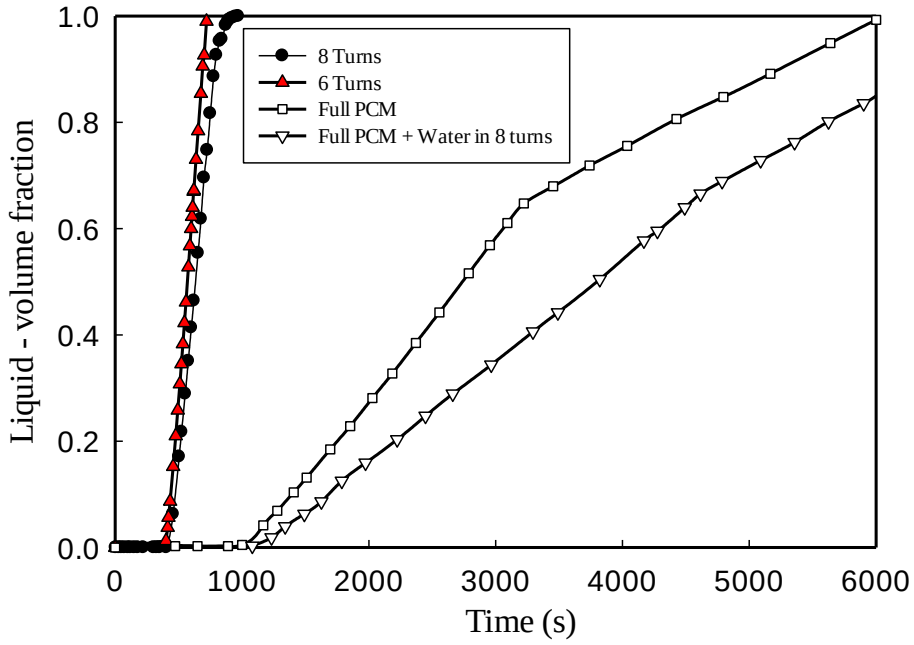

Figure 7. 14. The effect of different arrangements of the phase change material and the hybrid cooling system on the phase change process.

slightly increased. In the case of the entire cooling jacket filled with the phase change material, the melting time has increased significantly, and the melting process starts at 1020 seconds. From Figure 7.14, it can be seen that in the case of using the hybrid cooling system, due to the heat transfer from the phase change material to water, beginning of the phase change process has delayed and in 6000 seconds, 0.8 of the phase change material has been transformed into liquid phase.

7.8 Flow Physics

In this section, thermal performance of the under-study hybrid cooling system is investigated. For this purpose, the temperature distribution of the active part of the hybrid cooling system consisting of cooling channels containing the cooling fluid is shown at three different times in Figure 7.15. As can be seen, over time, the heat flux generated by the electric machine is absorbed by the cooling system and the temperature of the cooling fluid and the phase change material increase. Increasing the cooling fluid temperature in fact reduces the temperature of the phase change material and this increases the

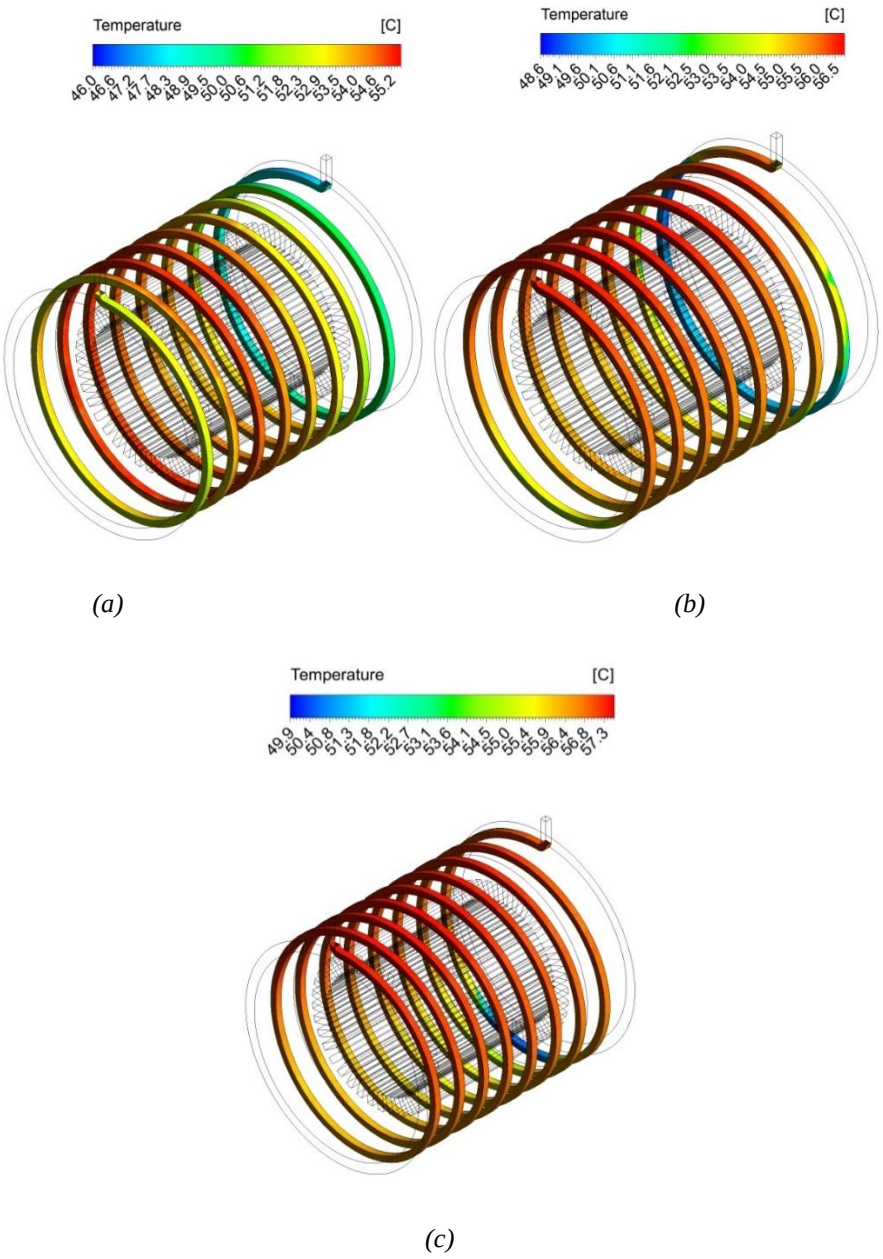

Figure 7. 15. Temperature distribution of the active cooling part of the hybrid cooling system, (a) *at t= 2000 s, (*b*) at t=* 3*000 s, (*c*) at t=* 6*000 s.*

melting time. The investigation of temperature distribution contour at three different times in figure 7.15 shows that the inlet cooling fluid temperature is at its minimum value and along the way by absorbing heat flux, its temperature has increased at the outlet point. The temperature distribution contour of the electric machine stator is shown in Figure 7.16. As can be seen,

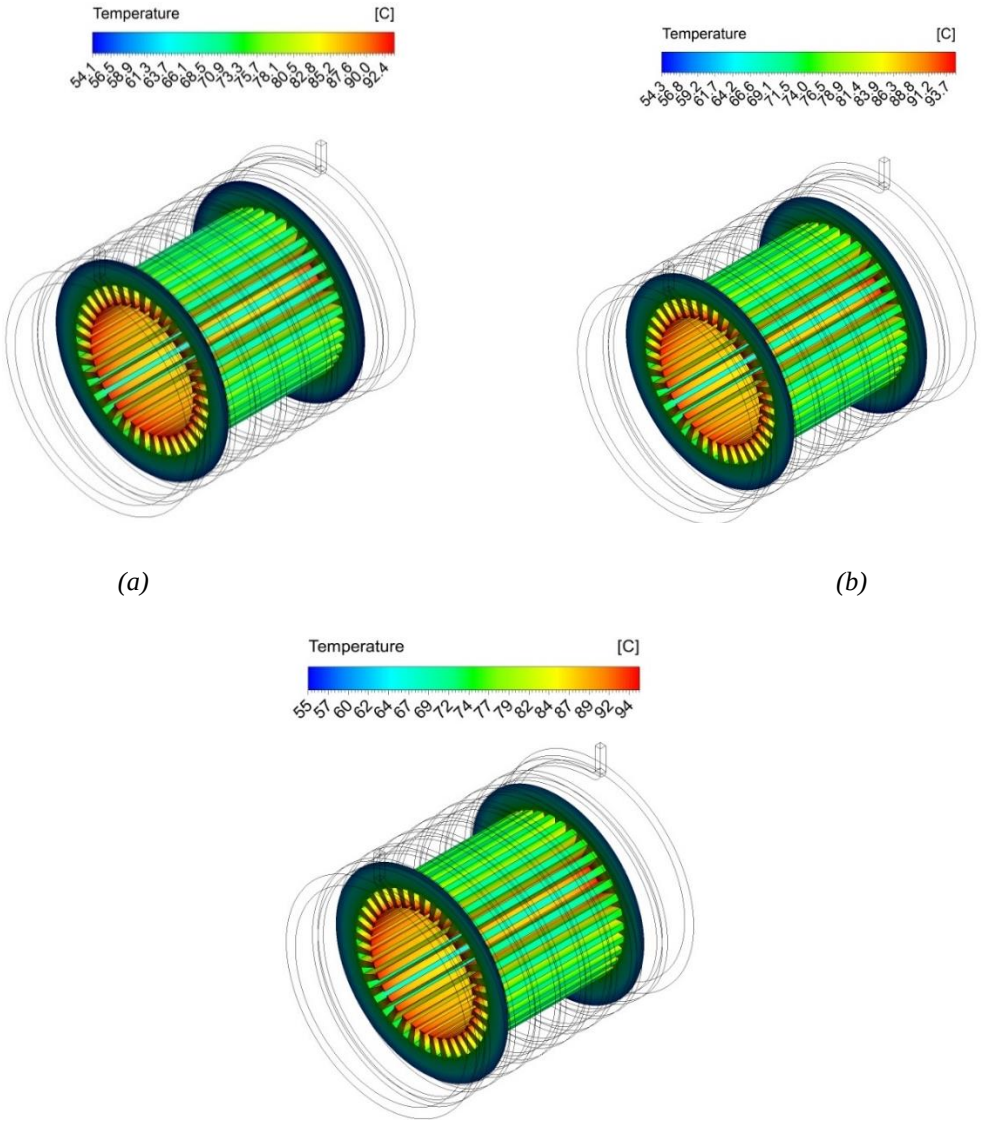

Figure 7. 16. Temperature distribution of the electric machine stator when the hybrid cooling system is used, (a) *at t= 2000 s, (*b) *at t= 3000 s, (*c) *at t= 6000 s.*

over time, the temperature of the electric machine increases and the cross sections with higher temperatures have increased (this has increased the average temperature in terms of time). According to Figure 7.16, at 6000 seconds, the maximum temperature of the electric machine is 94°C. Liquid mass fraction of PCM inside the cooling jacket at t= 2000 s, t= 3000 s, and t= 6000 s are shown in Figure 7.17. As can be seen, at t = 6000s large amount

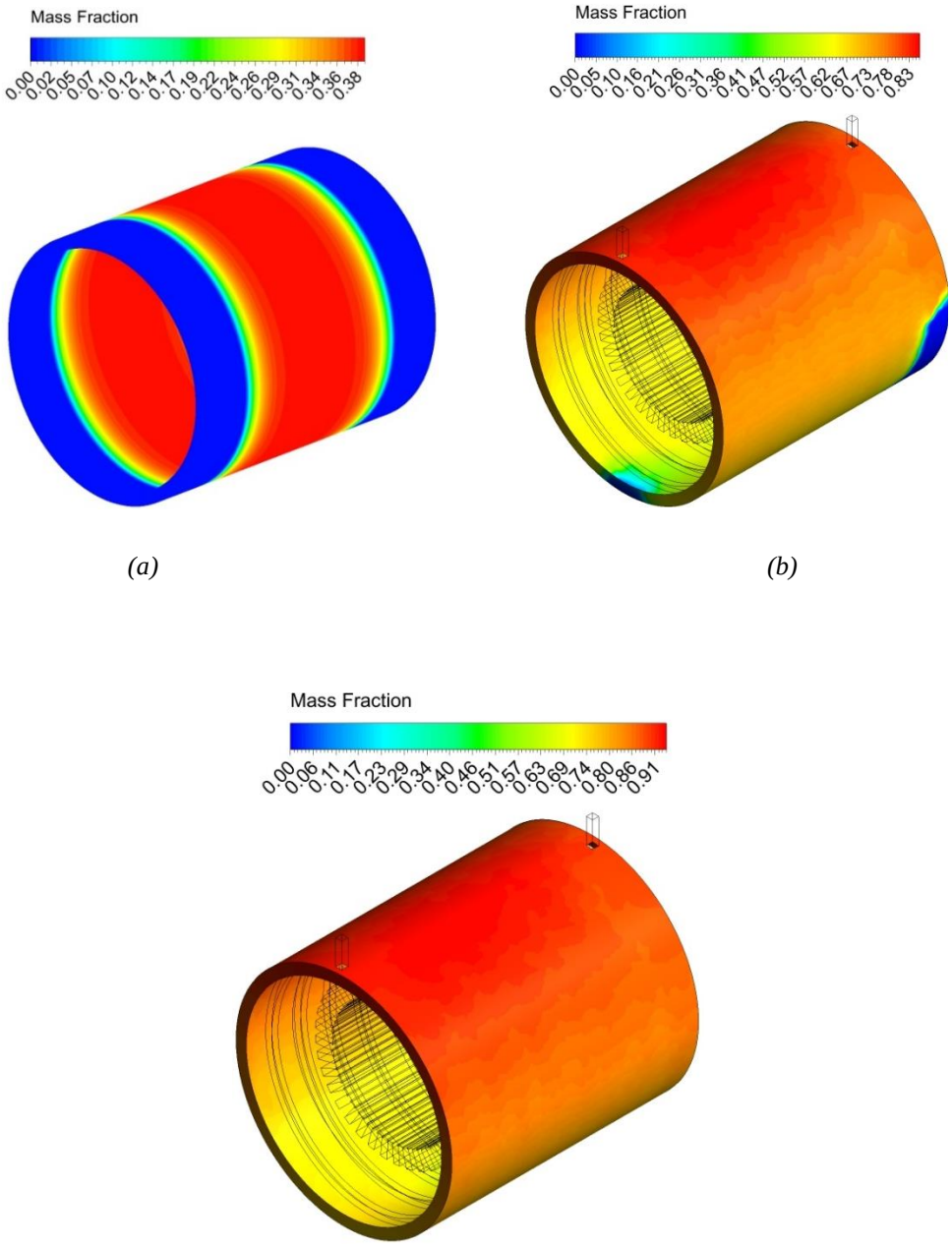

Figure 7. 17. Temperature distribution of the cooling jacket when the hybrid cooling system is used, (a) *at t= 2000 s, (*b*) at t= 3000 s, (*c*) at t= 6000 s.*

of PCM is transformed to the liquid phase indicating the highest limit of PCM effectiveness.

7.9 CONCLUSION

In this chapter, the flow field and heat transfer for cooling an electric motor were investigated based on the finite volume method. In this study, the passive cooling method was implemented and PCM, as the cooling agent were adopted. PCM was used in the spiral path with different turns. Changes in the temperature of PCM, rotor and stator temperature, and volume fraction of liquid phase in different geometric arrangements at different times were investigated. The accuracy of the results was also validated. According to the results, the use of a passive PCM-based cooling system with a spiral arrangement can maintain the motor's operating temperature within the allowed range in 900 s without consuming external power. The results indicate that the complete melting time increases by 200 s with increasing the number of PCM-containing path's turns from six to eight. According to the results, the optimal arrangement of the PCM-containing path to maintain the operating temperature within the allowed range and the design of an active cooling system for the post-phase change process are good recommendations for future studies.

In addition to the spiral channels containing PCM, the entire jacket compartment is also filled with PCM material. The results show that in this case, for 3150 seconds, the passive cooling system used was able to maintain the operating temperature of the electric machine below 60 ˚C. Based on the results, the passive cooling system, which does not require any cooling fluid, without pumping power, is able to have a good cooling performance and decreases the electric machine temperature.

According to the results, the effectiveness of the hybrid cooling system with the PCM-containing path to maintain the operating temperature within the allowed range and the water-cooling active cooling system for the post-phase change process is demonstrated.

8. CONCLUSIONS AND FUTURE WORK

8.1 SUMMARY AND CONCLUSIONS

The main focus of this study was to investigate the effectiveness of employing advanced coolants and phase change materials in cooling systems of electric machines. Regarding the advanced coolants, nanofluids were adopted. The reason behind this adoption lies in the significantly improved heat transfer performance of nanofluids compared to conventional cooling fluids. Besides the enhanced heat transfer of nanofluids, other properties of nanofluids affect their overall performance. Therefore, both heat transfer and fluid flow properties of nanofluids were evaluated in this thesis.

Regarding phase changed materials, high latent heat as their most distinctive property makes them suitable to be used as thermal energy storage medium. In this thesis, the employment of phase change materials in improving efficiency of electric machine cooling systems was investigated.

In Chapter 2, various cooling methods for electric machine cooling applications were described. Moreover, general and specific requirements of electric machine cooling systems for electric/hybrid vehicle applications were investigated.

Knowing the requirements, the motivations behind the research were determined by investigating potential areas for improving the performance of

electric machine cooling systems in order to meet the requirements of this application. According to the discussion, it was concluded that removing heat from the surface of the stator using common cooling jackets is a cost-effective and proper approach. Generated heat in different parts of electric machines can be transferred to the cooling jacket by means of convection, heat pipes, etc. Therefore, the focus of the research was set on improving heat transfer performance of cooling systems based on cooling jackets with minimal changes in the structure of the cooling system.

The heat transfer and fluid flow properties of nanofluids were studied in **Chapter 3.** Moreover, the most effective mechanisms of nanofluids heat transfer were described. It was found that high thermal conductivity of nanoparticles plays a key role in heat transfer enhancement of nanofluids. In line with this property of nanoparticles, Al_2O_3 nanoparticles were selected for this research. Various modelling approaches were described in this chapter. According to pros and cons the multiphase modelling method was selected for simulations.

Various properties of phase change materials were studied in Chapter 4. Also, applications of phase change materials and their potential benefits in cooling systems were described. It was concluded that the use of phase change materials alone is not suitable for cooling systems in applications where rapid heat flux changes occur because the phase change processes need time to complete and return to the previous state.

In Chapter 5, employing Ethylene-Glycol coolant in spiral channels inside the cooling jacket, effects of some structural changes were investigated. Moreover, the effects of volume fraction and pumping power on heat transfer and fluid flow of the coolant were studied. It was observed that increasing turn number of channels, the volume fraction of ethylene glycol, and the Reynolds number all increase the heat transfer coefficient. The defined performance evaluating parameter in this study, PEC, was used to evaluate the thermal and fluid flow performances of the cooling system.

According to the simulation results, it was concluded that in comparison with pure water with turn number of 8, at volume fraction of 60:40, and at Reynolds number of 5000, the highest PEC can be obtained.

The effect of structural geometry of the cooling system and volume fraction of Al_2O_3 nanofluid on heat transfer and fluid flow performances of the cooling system for electric machine applications are analyzed in **Chapter 6**. The effect of adding nanoparticles to the base fluid and different geometries are examined for a cooling system based on the cooling jacket method. According to results, it was concluded that increase of Reynolds number and concentration of nanoparticles increase the heat transfer coefficient. It was observed that because increasing the nanoparticle concentration can lead to a reduction of the temperature gradient at the wall of the channels, from a specific nanoparticle concentration onward, the rate of heat transfer enhancement decreases significantly. This is the dual effect of adding nanoparticle into base fluids.

Two fully passive cooling systems based on phase change materials were studied in **Chapter7.** One arrangement was employing phase change materials inside spiral channels and the other was based on filling entire the cooling jacket with phase change materials. In the case of phase change materials in spiral channels it was found that this configuration is no effective and even by increasing turn number of spiral channels no remarkable improvement was observed.

Examining the losses caused by the operation of electric machines in the application of electric vehicles under standard driving cycles, it was observed that due to the large number of starters and stops that require frequent acceleration and deceleration, peak loss values are much larger than the average loss. Exploiting high latent heat capacity of phase change materials and fast heat transfer ability of the active cooling method, a hybrid cooling system was investigated. The hybrid cooling system consists of a passive cooling part based on phase change materials and an active cooling part based on liquid cooling approach. The passive cooling part is responsible to absorb high heat fluxes generated during peak load demands by the cooling jacket filled with a metal-based phase change material. On the other hand, the active cooling part removes the excess heat flux from the phase change material preparing it for the next peak heating cycle. Analyses, demonstrated the

effectiveness of the hybrid cooling system for electric machines used in electric/hybrid vehicle applications.

8.2 FUTURE WORKS

Following on from this study, future works should be developed and continued in some directions suggested as follows.

Developing and analysing couplings between analytical model of cooling systems and electric machine thermal models. These coupled models can be used for evaluation and design purposes.

Investigating application of the hybrid cooling system to other applications with high power cycling. For example, power electronics energy conversion systems in traction applications, where there is high power cycling due to high traction and regenerative braking power flows.

Investigation of efficient heat transfer methods to transfer heat from inner parts of electric machine to the cooling jacket such as employing heat pipes. In this way, temperature distribution on the stator surface becomes more uniform.

REFERENCES

1. M. Naidu, T. W. Nehl, S. Gopalakrishnan and L. Wurth, "Keeping cool while saving space and money: a semi-integrated, sensorless PM brushless drive for a 42-V automotive HVAC compressor," in *IEEE Industry Applications Magazine*, vol. 11, no. 4, pp. 20-28, July-Aug. 2005.
2. Q. Chen, H. Shao, J. Huang, H. Sun and J. Xie, "Analysis of Temperature Field and Water Cooling of Outer Rotor In-Wheel Motor for Electric Vehicle," in IEEE Access, vol. 7, pp. 140142-140151, 2019.
3. P. Lindh et al., "Performance of a Direct-Liquid-Cooled Motor in an Electric Bus Under Different Load Cycles," in IEEE Access, vol. 7, pp. 86897-86905, 2019.
4. Edison Gundabattini, Ravi Kuppan, Darius Gnanaraj Solomon, Akhtar Kalam, D.P. Kothari, Rosli Abu Bakar, A review on methods of finding losses and cooling methods to increase efficiency of electric machines, Ain Shams Engineering Journal, Volume 12, Issue 1, 2021, Pages 497-505.
5. J. Huang et al., "A Hybrid Electric Vehicle Motor Cooling System—Design, Model, and Control," in IEEE Transactions on Vehicular Technology, vol. 68, no. 5, pp. 4467-4478, May 2019.
6. Canders, W.-R.; Hoffmann, J.; Henke, M. Cooling Technologies for High Power Density Electrical Machines for Aviation Applications. Energies 2019, 12, 4579.
7. Rehman, Z.; Seong, K. Three-D Numerical Thermal Analysis of Electric Motor with Cooling Jacket. Energies 2018, 11, 92.
8. Colin Richmond, Ramesh Kuppuswamy, Azeem Khan, The Effect of Coolant Velocity for Enhancing the High-Speed Permanent Magnet Generator Efficiency, Procedia CIRP, Volume 91, 2020, Pages 21-26.

9. Michele De Gennaro, Jonathan Jürgens, Alessandro Zanon, Johannes Gragger, Erwin Schlemmer, Antonio Fricassè, Luca Marengo, Bernd Ponick, Elena Trancho Olabarri, Jutta Kinder, Andrea Cavallini, Paolo Mancinelli, Maria Hernandez, Maarten Messagie, Designing, prototyping and testing of a ferrite permanent magnet assisted synchronous reluctance machine for hybrid and electric vehicles applications, Sustainable Energy Technologies and Assessments, Volume 31, 2019, Pages 86-101.
10. Silwal, B.; Mohamed, A.H.; Nonneman, J.; De Paepe, M.; Sergeant, P. Assessment of Different Cooling Techniques for Reduced Mechanical Stress in the Windings of Electrical Machines. *Energies* 2019, *12*, 1967.
11. Yang, Yinye; Bilgin, Berker; Kasprzak, Michael; Nalakath, Shamsuddeen; Sadek, Hossam; Preindl, Matthias; Cotton, James; Schofield, Nigel; Emadi, Ali: 'Thermal management of electric machines', IET Electrical Systems in Transportation, 7, (2), 2017, pp. 104-116.
12. "*Electric Motor Failure Causes*," https://electricalacademia.com/motor-control/electric-motor-failure-causes/.
13. Patrick K. Schelling, Li Shi, Kenneth E. Goodson, "Managing heat for electronics," *Materials Today*, Vol 8, Issue 6, 2005, pp 30-35.
14. "Thermal Management Market by Material (Adhesives, Nonadhesive), Device (Conduction, Convection, Advanced, and Hybrid), Thermal Management Service, End-Use Industry, and Region - Global Forecast to 2024, " RESEARCH AND MARKETS, Report, ID: 4808171, July 2019, 181 Pages.
15. G. E. Luke, "The Cooling of Electric Machines," in Transactions of the American Institute of Electrical Engineers, vol. XLII, pp. 636-652, January-December 1923, doi: 10.1109/T-AIEE.1923.5060903.
16. Edison Gundabattini, Ravi Kuppan, Darius Gnanaraj Solomon, Akhtar Kalam, D.P. Kothari, Rosli Abu Bakar, "A review on methods of finding losses and cooling methods to increase efficiency of electric machines," *Ain Shams Engineering Journal*, Vol 12, Issue 1, 2021, pp 497-505.
17. H.A. Nasef, S.A. Nada, Hamdy Hassan, "Integrative passive and active cooling system using PCM and nanofluid for thermal regulation of concentrated photovoltaic solar cells," *Energy Conversion and Management*, Vol 199,2019, pp112065.
18. Yuanlong Wang, Yi Yu, Zhiqiang Jing, Chunyan Wang, Guan Zhou, Wanzhong Zhao, "Thermal performance of lithium-ion batteries applying forced air cooling with an improved aluminium foam heat sink design," *International Journal of Heat and Mass Transfer*, Vo. 167, 2021, pp. 120827.
19. Hitensinh Vaghela, Vikas J. Lakhera, Biswanath Sarkar, "Forced flow cryogenic cooling in fusion devices: A review," *Heliyon*, Vol. 7, Issue 1, 2021, e06053, ISSN 2405-8440.

20. Li, B., Kuo, H., Wang, X. et al. Thermal Management of Electrified Propulsion System for Low-Carbon Vehicles. Automot. Innov. 3, 299–316, 2020.
21. Yi Man, Hongxing Yang, Yunxia Qu, Zhaohong Fang, "A Novel Nocturnal Cooling Radiator Used for Supplemental Heat Sink of Active Cooling System," *ProcediaEngineering*, Vol 121, 2015, pp300-308.
22. Mohamed R. Gomaa, Hegazy Rezk, "Passive cooling system for enhancement the energy conversion efficiency of thermo-electric generator," Energy Reports, Volume 6, Supplement 9, Pages 687-692, 2020.
23. Jose J. Corona, Kamal A. Kaddoura, Augustine A. Kwarteng, Osama Mesalhy, Louis C. Chow, Quinn H. Leland, John P. Kizito, Comparison of two axial fans for cooling of electromechanical actuators at variable pressure, Thermal Science and Engineering Progress, Volume 20, 2020.
24. A. Lindner and I. Hahn, "Practical evaluation of a passive stator cooling concept without thermal stacking," 2017 IEEE Workshop on Electrical Machines Design, Control and Diagnosis (WEMDCD), 2017, pp. 132-139, doi: 10.1109/WEMDCD.2017.7947736.
25. Soubhik Kumar Bhaumik, Rashmita Behera, CFD Optimization of free Convective Cooling of Finned Heat Sinks: Effect of Fin Spacing, Procedia Engineering, Vol 127, 2015, pp 155-161.
26. P. S. Nasab, R. Perini, A. Di Gerlando, G. M. Foglia and M. Moallem, "Analytical Thermal Model of Natural-Convection Cooling in Axial Flux Machines," in *IEEE Transactions on Industrial Electronics*, vol. 67, no. 4, pp. 2711-2721, April 2020.
27. Y. Gai *et al.*, "Cooling of Automotive Traction Motors: Schemes, Examples, and Computation Methods," in *IEEE Transactions on Industrial Electronics*, vol. 66, no. 3, pp. 1681-1692, March 2019.
28. D. A. Staton and A. Cavagnino, "Convection Heat Transfer and Flow Calculations Suitable for Electric Machines Thermal Models," in *IEEE Transactions on Industrial Electronics*, vol. 55, no. 10, pp. 3509-3516, Oct. 2008.
29. X. Huang, C. Gerada, A. Goodman, K. Bradley, He Zhang and Youtong Fang, "A Brushless DC motor design for an aircraft electro-hydraulic actuation system," *2011 IEEE International Electric Machines & Drives Conference (IEMDC)*, 2011, pp. 1153-1158.
30. G. M. Gilson, T. Raminosoa, S. J. Pickering, C. Gerada and D. B. Hann, "A combined electromagnetic and thermal optimisation of an aerospace electric motor," *The XIX International Conference on Electrical Machines - ICEM 2010*, 2010, pp. 1-7.
31. S. Ulbrich, J. Kopte and J. Proske, "Cooling Fin Optimization on a TEFC Electrical Machine Housing Using a 2-D Conjugate Heat Transfer Model," in *IEEE Transactions on Industrial Electronics*, vol. 65, no. 2, pp. 1711-1718, Feb. 2018.

32. D. A. Staton and E. So, "Determination of optimal thermal parameters for brushless permanent magnet motor design," *Conference Record of 1998 IEEE Industry Applications Conference. Thirty-Third IAS Annual Meeting (Cat. No.98CH36242)*, 1998, pp. 41-49 vol.1.
33. A. Bernot, "A high reliability natural convection airliner actuator permanent magnet motor," *2016 XXII International Conference on Electrical Machines (ICEM)*, 2016, pp. 46-52.
34. J. Li, Da-Woon Choi and Yun-Hyun Cho, "Development of a natural cooled axial flux permanent magnet generator for wind turbine," *2012 IEEE International Symposium on Industrial Electronics*, 2012, pp. 635-640.
35. C. Yung, "Cool facts about cooling electric motors," *Industry Applications Society 60th Annual Petroleum and Chemical Industry Conference*, 2013, pp. 1-10.
36. Fang Qi, Daniel Scharfenstein, Claude Weiss, Clemens Müller, Ulrich Schwarzer, "Motor Handbook, " Institute for Power Electronics and Electrical Drives, RWTH Aachen University & Infineon Technologies AG, Version: 2.1, 2019.
37. Z. Xu *et al*., "Thermal management of a permanent magnet motor for an directly coupled pump," *2016 XXII International Conference on Electrical Machines (ICEM)*, 2016, pp. 2738-2744.
38. C. Yung, "Cool Facts About Cooling Electric Motors: Improvements in Applications That Fall Outside the Normal Operating Conditions," in *IEEE Industry Applications Magazine*, vol. 21, no. 6, pp. 47-56, Nov.-Dec. 2015.
39. C. A. Cezario and A. A. M. Oliveira, "CFD electric motor external fan system validation," *2008 18th International Conference on Electrical Machines*, 2008, pp. 1-6.
40. L. Kung, U. Bikle, O. Popp and R. Jakoby, "Improvement of the cooling performance of symmetrically self-ventilated induction machines in the 2-15 MW range," *IEMDC 2001. IEEE International Electric Machines and Drives Conference (Cat. No.01EX485)*, 2001, pp. 673-680.
41. T. Nakahama, D. Biswas, K. Kawano and F. Ishibashi, "Improved cooling performance of large motors using fans," in *IEEE Transactions on Energy Conversion*, vol. 21, no. 2, pp. 324-331, June 2006.
42. S. Mizuno, S. Noda, M. Matsushita, T. Koyama and S. Shiraishi, "Development of a Totally Enclosed Fan-Cooled Traction Motor," in *IEEE Transactions on Industry Applications*, vol. 49, no. 4, pp. 1508-1514, July-Aug. 2013.
43. T. Nakahama, F. Ishibashi, K. Sato and K. Kawano, "Effects of Fan Blade Forward-Swept and Inclined Amounts in Electric Motors," in *IEEE Transactions on Energy Conversion*, vol. 25, no. 2, pp. 457-464, June 2010.
44. E. Galloni, P. Parisi, F. Marignetti, G. Volpe, CFD analyses of a radial fan for electric motor cooling, Thermal Science and Engineering Progress, Vol 8, 2018, pp 470-476.

45. Ming Kang, Huimin Wang, Liyan Guo, Tingna Shi, Changliang Xia, Self-circulation cooling structure design of permanent magnet machines for electric vehicle, Applied Thermal Engineering, Vol 165, 2020, 114593..
46. S. L. Rocca, S. J. Pickering, C. N. Eastwick, C. Gerada and K. Ronnberg, "Numerical Study on the Impact of End Windings Porosity on the Fluid Flow and Heat Transfer in a Totally Enclosed Fan-Cooled Electrical Machine," *2019 IEEE International Electric Machines & Drives Conference (IEMDC)*, 2019, pp. 2138-2143.
47. C. Micallef, S. J. Pickering, K. A. Simmons and K. J. Bradley, "Improved Cooling in the End Region of a Strip-Wound Totally Enclosed Fan-Cooled Induction Electric Machine," in *IEEE Transactions on Industrial Electronics*, vol. 55, no. 10, pp. 3517-3524, Oct. 2008.
48. W. Tong, S. Wu and R. Tang, "Research on the Airflow and Thermal Performance in a Large Forced Air-Cooled Permanent Magnet Synchronous Machine," IEEE Access, vol. 7, pp. 162343-162352, 2019.
49. L. Ye, D. Li, Y. Ma and B. Jiao, "Design and Performance of a Water-cooled Permanent Magnet Retarder for Heavy Vehicles," in IEEE Transactions on Energy Conversion, vol. 26, no. 3, pp. 953-958, Sept. 2011.
50. Z. Huang, S. Nategh, V. Lassila, M. Alaküla and J. Yuan, "Direct oil cooling of traction motors in hybrid drives," *2012 IEEE International Electric Vehicle Conference*, 2012, pp. 1-8.
51. Q. Lu, X. Zhang, Y. Chen, X. Huang, Y. Ye and Z. Q. Zhu, "Modeling and Investigation of Thermal Characteristics of a Water-Cooled Permanent-Magnet Linear Motor," in *IEEE Transactions on Industry Applications*, vol. 51, no. 3, pp. 2086-2096, May-June 2015.
52. P. Zheng, R. Liu, P. Thelin, E. Nordlund and C. Sadarangani, "Research on the Cooling System of a 4QT Prototype Machine Used for HEV," in *IEEE Transactions on Energy Conversion*, vol. 23, no. 1, pp. 61-67, March 2008.
53. Michal Sikora, Radek Vlach, Petr Navr´atil, "The unusual water cooling applied on small asynchronous motor," *Engineering MECHANICS, Vol. 18, 2011, No. 2, p. 143–153*.
54. Marco Cavazzuti, Gloria Gaspari, Stefano Pasquale, Enrico Stalio, Thermal management of a Formula E electric motor: Analysis and optimization, Applied Thermal Engineering, Vol 157, 2019, 113733.
55. X. Fan, D. Li, R. Qu, C. Wang and H. Fang, "Water Cold Plates for Efficient Cooling: Verified On A Permanent-Magnet Machine with Concentrated Winding," in *IEEE Transactions on Industrial Electronics*, vol. 67, no. 7, pp. 5325-5336, July 2020.
56. Sarit K. Das, Stephen U.S. CHOI, "A Review of Heat Transfer in Nanofluids", *Advances in Heat Transfer, Elsevier*, Vol 41, 2009, pp 81-197.

57. M. Usman Sajid, Hafiz Muhammad Ali, “Recent advances in application of nanofluids in heat transfer devices: A critical review”, *Renewable and Sustainable Energy Reviews*, Vol 103, 2019, pp 556-592.
58. S. Rashidi, F. Hormozi, N. Karimi, Waqar Ahmed, “Chapter 14 - Applications of nanofluids in thermal energy transport, In Micro and Nano Technologies”,*Emerging Nanotechnologies for Renewable Energy*,*Elsevier*, 2021, pp 345-368.
59. N. A. Che Sidik, M. N. A. Witri Mohd Yazid, R. Mamat, “A review on the application of nanofluids in vehicle engine cooling system”, *International Communications in Heat and Mass Transfer*, Vol 68, 2015, pp 85-90.
60. N. A. Che Sidik, M. N. A. Witri Mohd Yazid, R. Mamat, “Recent advancement of nanofluids in engine cooling system”, *Renewable and Sustainable Energy Reviews*, Vol 75, 2017, pp 137-144.
61. S.M. Peyghambarzadeh, S.H. Hashemabadi, S.M. Hoseini, M. Seifi Jamnani, “Experimental study of heat transfer enhancement using water/ethylene glycol based nanofluids as a new coolant for car radiators”, *International Communications in Heat and Mass Transfer*, Vol 38, Issue 9, 2011, pp 1283-1290.
62. D. G. Subhedar, Bharat M. Ramani, A. Gupta, “Experimental investigation of heat transfer potential of Al2O3/Water-Mono Ethylene Glycol nanofluids as a car radiator coolant”, *Case Studies in Thermal Engineering*, Vol 11, 2018, pp 26-34.
63. J. L. Routbort, D. Singh, and G. Chen, “Heavy vehicle systems optimization merit review and peer evaluation,” *Annu. Report, Argonne Natl. Lab. Chicago, Illinois, USA*, 2006.
64. H.A. Mohammed, A.A. Al-aswadi, N.H. Shuaib, R. Saidur, “Convective heat transfer and fluid flow study over a step using nanofluids: A review,” *Renewable and Sustainable Energy Reviews*, Vol 15, Issue 6, 2011, pp 2921 2939.
65. P. Kumar, R.M. Sarviya, “Recent developments in preparation of nanofluid for heat transfer enhancement in heat exchangers: A review,” *Materials Today: Proceedings*, 2021, ISSN 2214-7853.
66. Berger Bioucas, F.E., Rausch, M.H., Schmidt, J. et al. Effective Thermal Conductivity of Nanofluids: Measurement and Prediction. Int J Thermophys 41, 55, 2020.
67. M. K. Bhatnagar, M. Rai, M. Ashraf, Om Kapoor, T.G. Mamatha, M. Vishnoi, “Efficiency enhancement of heat exchanger using inserts and nano-fluid - A review,” *Materials Today: Proceedings*, 2020, ISSN 2214-7853.
68. Kumar D., Choi. S. U. S., Patel, H. E., “Heat Transfer in nanofluids-A Review,” *J.Heat Transfer Engineering*, Vol 21, No.10, 2006, pp 3-19.
69. Lin Qiu, Ning Zhu, Yanhui Feng, Efstathios E. Michaelides, Gaweł Żyła, Dengwei Jing, Xinxin Zhang, Pamela M. Norris, Christos N. Markides, Omid Mahian, “A review of recent advances in thermophysical properties at the nanoscale: From solid state to colloids,” *Physics Reports*,Vol 843, 2020, pp 1-81.

70. Ehsan, M. M. and Shafi Noor. “Study of Heat Transfer Performance and Pumping Power Improvement of Nanofluid Through a Rough Circular Tube.” International Research Journal of Engineering and Technology, Vol 03, pp 1709-1717, 2016.
71. S. Rahmanian, A. Hamzavi, “Effects of pump power on performance analysis of photovoltaic thermal system using CNT nanofluid,” *Solar Energy*, Vol 201, 2020,pp 787-797.
72. Hussein A. Mohammed, F. Fathinia, Hari B. Vuthaluru, Shaomin Liu, “CFD based investigations on the effects of blockage shapes on transient mixed convective nanofluid flow over a backward facing step,” *Powder Technology*, Vol 346, 2019, pp 441-451.
73. Pawel Keblinski, Jeffrey A. Eastman, David G. Cahill, Nanofluids for thermal transport, Materials Today, Volume 8, Issue 6, 2005, Pages 36-44.
74. J.J. Wang, R.T. Zheng, J.W. Gao, G. Chen, Heat conduction mechanisms in nanofluids and suspensions, Nano Today, Volume 7, Issue 2, 2012, pp 124-136.
75. P Keblinski, S.R Phillpot, S.U.S Choi, J.A Eastman, Mechanisms of heat flow in suspensions of nano-sized particles (nanofluids), International Journal of Heat and Mass Transfer, Volume 45, Issue 4, 2002, pp 855-863.
76. Machrafi, H., Lebon, G. The role of several heat transfer mechanisms on the enhancement of thermal conductivity in nanofluids. Continuum Mech. Thermodyn. 28, 2016, pp 1461–1475.
77. Touloukian, Y. S. Powell, R. W. Ho, C. Y. Klemens, P. G., "Thermophysical Properties of Matter," The TPRC Data Series. Volume 2, 1970.
78. Pawel Keblinski and David G. Cahill, "Comment on "Model for Heat Conduction in Nanofluids", " Phys. Rev. Lett. 95, 209401, 2005.
79. Seok Pil Jang and Stephen U. S. Choi, " Role of Brownian motion in the enhanced thermal conductivity of nanofluids, " Appl. Phys. Lett. 84, 4316, 2004.
80. Henry, Asegun S.; Chen, Gang, "Spectral Phonon Transport Properties of Silicon Based on Molecular Dynamics Simulations and Lattice Dynamics, “ Journal of Computational and Theoretical Nanoscience, Volume 5, Number 2, 2008, pp. 141-152(12).
81. G. Chen, Nanoscale Energy Transport and Conversion a Parallel Treatment of Electrons, Molecules, Phonons and Photons, Oxford University Press, New York/Oxford, 2005.
82. Steven L. Fiedler, Sergei Izvekov, Angela Violi, "The effect of temperature on nanoparticle clustering," *Carbon,*Vol 45, Issue 9, 2007, pp 1786-1794.
83. M. Agop, V. Paun, Anca Harabagiu, "El Naschie’s ε(∞) theory and effects of nanoparticle clustering on the heat transport in nanofluids," *Chaos, Solitons & Fractals*, Vol 37, Issue 5, 2008, pp 1269-1278.
84. Wu, Chunwei and Cho, Tae Joon and Xu, Jiajun and Lee, Donggeun and Yang, Bao and Zachariah, Michael R., "Effect of nanoparticle clustering on the effective thermal

conductivity of concentrated silica colloids" *American Physical Society*, Vol 81, pp 011406, 2010.

85. Jahar Sarkar, "A critical review on convective heat transfer correlations of nanofluids," *Renewable and Sustainable Energy Reviews*, Vol 15, Issue 6, 2011, pp 3271-3277.
86. S. Javed, Hafiz Muhammad Ali, H. Babar, M. S. Khan, Muhammad Mansoor Janjua, M. Anser Bashir, "Internal convective heat transfer of nanofluids in different flow regimes: A comprehensive review," *Physica A: Statistical Mechanics and its Applications*, Vol 538, 2020, pp 122783.
87. W. Daungthongsuk, Somchai Wongwises, "A critical review of convective heat transfer of nanofluids," *Renewable and Sustainable Energy Reviews*, Vol 11, Issue 5, 2007, pp 797-817.
88. Senthilraja, S.; Vijayakumar, K.; Gangadevi, R, "A comparative study on thermal conductivity of Al2O3/water, CuO/water and Al2O3–CuO/water nanofluids," *Dig. J. Nanomat*, Biol. 2015, 10, 1449–1458.
89. Min-Sheng Liu, Mark Ching-Cheng Lin, I-Te Huang, Chi-Chuan Wang, Enhancement of thermal conductivity with carbon nanotube for nanofluids, International Communications in Heat and Mass Transfer, Volume 32, Issue 9, 2005, Pages 1202-1210.
90. Yashawantha, K.M., Vinod, A.V, "ANN modelling and experimental investigation on effective thermal conductivity of ethylene glycol:water nanofluids," *Journal of Thermal Analysis and Calorimetry*, 2020.
91. P. Anand, Rajesh Kumar Gadekula, Uppada Venkata Ramana, Raja Sekhar Dondapati, "Effect of Diameter of Nanoparticles on the thermophysical properties of LN2 based Cryocoolants," *Materials Today: Proceedings*, Vol 5, Issue 14, Part 2, 2018, pp 28279-28287.
92. Dongsheng Wen, Guiping Lin, Saeid Vafaei, Kai Zhang, "Review of nanofluids for heat transfer applications," *Particuology*, Vol 7, Issue 2, 2009, pp 141-150.
93. Okonkwo, E.C., Wole-Osho, I., Almanassra, I.W. *et al.* "An updated review of nanofluids in various heat transfer devices," *Journal of Thermal Analysis and Calorimetry*, 2020, SN-1588-2926.
94. P. Yesodha, M. Bhuvaneswari, S. Sivasankaran, K. Saravanan, "Convective heat and mass transfer of chemically reacting fluids with activation energy along with Soret and Dufour effects," *Materials Today: Proceedings*, Vol 42, Part 2, 2021, pp 600-606.
95. Koji Miyoshi, Masayuki Kamaya, Yoichi Utanohara, Akira Nakamura, "Heat transfer coefficient suitable for thermal fatigue assessment at a T-junction," *Nuclear Engineering and Design*, Vol 370, 2020, pp110916.
96. Nishant Kumar, Shriram S. Sonawane, Shirish H. Sonawane, "Experimental study of thermal conductivity, heat transfer and friction factor of Al2O3 based nanofluid," *International Communications in Heat and Mass Transfer*, Vol 90, 2018, pp 1-10.

97. Meisam Asadi, Amin Asadi, Sadegh Aberoumand, "An experimental and theoretical investigation on the effects of adding hybrid nanoparticles on heat transfer efficiency and pumping power of an oil-based nanofluid as a coolant fluid," *International Journal of Refrigeration*, Vol 89, 2018, pp 83-92.
98. K. Abdul Hamid, W.H. Azmi, M.F. Nabil, Rizalman Mamat, K.V. Sharma, "Experimental investigation of thermal conductivity and dynamic viscosity on nanoparticle mixture ratios of TiO2-SiO2 nanofluids," *International Journal of Heat and Mass Transfer*, Vol 116, 2018, pp 1143-1152.
99. Zafar Said, L. Syam Sundar, Hegazy Rezk, Ahmed M. Nassef, Hafiz Muhammad Ali, Mohsen Sheikholeslami, "Optimizing density, dynamic viscosity, thermal conductivity and specific heat of a hybrid nanofluid obtained experimentally via ANFIS-based model and modern optimization," *Journal of Molecular Liquids*, Vol 321, 2021, pp 114287.
100. Kriti Singh, S.K. Sharma, Shipra Mital Gupta, "An experimental investigation of hydrodynamic and heat transfer characteristics of surfactant-water solution and CNT nanofluid in a helical coil-based heat exchanger," *Materials Today: Proceedings*, 2021, ISSN 2214-7853.
101. Tae Jong Choi, Myeong Soo Park, Sung Hyoun Kim, Seok Pil Jang, Experimental Study on the Effect of Nanoparticle Migration on the Convective Heat Transfer Coefficient of EG/Water-based Al2O3 Nanofluids, International Journal of Heat and Mass Transfer, Volume 169, 2021.
102. Min Yang, Changhe Li, Liang Luo, Runze Li, Yunze Long, Predictive model of convective heat transfer coefficient in bone micro-grinding using nanofluid aerosol cooling, International Communications in Heat and Mass Transfer, Volume 125, 2021.
103. Seshu Kumar Vandrangi, Sampath Emani, Suhaimi Hassan, K.V. Sharma, Fluid dynamic simulations of EG-W (ethylene glycol–water) mixtures to predict nanofluid heat transfer coefficients, Environmental Technology & Innovation, Volume 20, 2020.
104. Sedong Kim, Baasandulam Tserengombo, Soon-Ho Choi, Jungpil Noh, Sunchul Huh, Byeongkeun Choi, Hanshik Chung, Junhyo Kim, Hyomin Jeong, Experimental investigation of heat transfer coefficient with Al2O3 nanofluid in small diameter tubes, Applied Thermal Engineering, Volume 146, 2019, pp 346-355.
105. K. Logesh, Reetesh Tiwari, R. Harish, S. Ajay, Netragaonkar adesh sunilrao, Experimental Studies On Convective Heat Transfer Coefficient of Al203/Ethylene Glycol-Carbon Nano Tube Nanofluids, Materials Today: Proceedings, Volume 18, Part 7, 2019, pp 4738-4744.
106. M. Naraki, S.M. Peyghambarzadeh, S.H. Hashemabadi, Y. Vermahmoudi, Parametric study of overall heat transfer coefficient of CuO/water nanofluids in a car radiator, International Journal of Thermal Sciences, Volume 66, 2013, pp 82-90.
107. Majid Zarringhalam, Arash Karimipour, Davood Toghraie, Experimental study of the effect of solid volume fraction and Reynolds number on heat transfer coefficient and

pressure drop of CuO–Water nanofluid, Experimental Thermal and Fluid Science, Volume 76, 2016, pp 342-351.

108. Amirhossein Zamzamian, Shahin Nasseri Oskouie, Ahmad Doosthoseini, Aliakbar Joneidi, Mohammad Pazouki, Experimental investigation of forced convective heat transfer coefficient in nanofluids of Al2O3/EG and CuO/EG in a double pipe and plate heat exchangers under turbulent flow, Experimental Thermal and Fluid Science, Volume 35, Issue 3, 2011, pp 495-502.
109. W.H. Azmi, K.V. Sharma, P.K. Sarma, Rizalman Mamat, Shahrani Anuar, Comparison of convective heat transfer coefficient and friction factor of TiO2 nanofluid flow in a tube with twisted tape inserts, International Journal of Thermal Sciences, 2014, pp 84-93.
110. K.V. Sharma, L. Syam Sundar, P.K. Sarma, Estimation of heat transfer coefficient and friction factor in the transition flow with low volume concentration of Al2O3 nanofluid flowing in a circular tube and with twisted tape insert, International Communications in Heat and Mass Transfer, Volume 36, Issue 5, 2009, pp 503-507.
111. R. Martínez-Cuenca, R. Mondragón, L. Hernández, C. Segarra, J.C. Jarque, T. Hibiki, J.E. Juliá, Forced-convective heat-transfer coefficient and pressure drop of water-based nanofluids in a horizontal pipe, Applied Thermal Engineering, Volume 98, 2016, pp 841-849.
112. D. Cabaleiro, L. Colla, F. Agresti, L. Lugo, L. Fedele, Transport properties and heat transfer coefficients of ZnO/(ethylene glycol+water) nanofluids, International Journal of Heat and Mass Transfer, Volume 89, 2015, pp 433-443.
113. Weerapun Duangthongsuk, Somchai Wongwises,Effect of thermophysical properties models on the predicting of the convective heat transfer coefficient for low concentration nanofluid, International Communications in Heat and Mass Transfer, Volume 35, Issue 10, 2008, pp 1320-1326.
114. Jubair A. Shamim, Palash K. Bhowmik, Chen Xiangyi, Kune Y. Suh, A new correlation for convective heat transfer coefficient of water–alumina nanofluid in a square array subchannel under PWR condition, Nuclear Engineering and Design, Volume 308, 2016, pp 194-204.
115. Manish Dadhich, Om Shankar Prajapati, Vikas Sharma, Investigation of boiling heat transfer of titania nanofluid flowing through horizontal tube and optimization of results utilizing the desirability function approach, Powder Technology, Volume 378, Part A, 2021, pp 104-123.
116. Alireza Banisharif, Patrice Estellé, Alimorad Rashidi, Stephan Van Vaerenbergh, Masoud Aghajani, Heat transfer properties of metal, metal oxides, and carbon water-based nanofluids in the ethanol condensation process, Colloids and Surfaces A: Physicochemical and Engineering Aspects, Volume 622, 2021, pp 126720.

117. Ming-jie Bai, Jin-long Liu, Jiang He, Wen-jun Li, Jun-jun Wei, Liang-xian Chen, Jian-yin Miao, Cheng-ming Li, Heat transfer and mechanical friction reduction properties of graphene oxide nanofluids, Diamond and Related Materials, Volume 108, 2020.
118. Aditya Jayanthi, John Peddieson, "Formulation of multiphase mixture models for fragmenting flows," *European Journal of Mechanics - B/Fluids*, Vol 46, 2014, pp 118-125.
119. A. De Santis, M. Colombo, B.C. Hanson, M. Fairweather, "A generalized multiphase modelling approach for multiscale flows," *Journal of Computational Physics*, Vol 436, 2021, 110321.
120. M. Akbari, N. Galanis, A. Behzadmehr, "Comparative analysis of single and two-phase models for CFD studies of nanofluid heat transfer," *International Journal of Thermal Sciences*, Vol 50, Issue 8, 2011, pp 1343-1354.
121. Mustafa Turkyilmazoglu, "Fully developed slip flow in a concentric annuli via single and dual phase nanofluids models," *Computer Methods and Programs in Biomedicine*, Vol 179, 2019, 104997.
122. Khalil Khanafer, Kambiz Vafai, "Analysis of turbulent two-phase flow and heat transfer using nanofluid," *International Communications in Heat and Mass Transfer*, Vol 124, 2021, 105219.
123. Thomas Barberon, Philippe Helluy, Finite volume simulation of cavitating flows, Computers & Fluids, Volume 34, Issue 7, 2005, pp 832-858.
124. Faccanoni, Gloria; Kokh, Samuel; Allaire, Grégoire. Modelling and simulation of liquid-vapor phase transition in compressible flows based on thermodynamical equilibrium. ESAIM: Mathematical Modelling and Numerical Analysis - Modélisation Mathématique et Analyse Numérique, Tome 46 (2012) no. 5, pp. 1029-1054.
125. Hamed Safikhani, Abbas Abbassi, "A new dispersion model for thermal properties of nanofluids in flat tubes," *International Journal of Thermal Sciences*, Vol 109, 2016, pp 114-122.
126. Shailesh Kumar, Santosh Kumar Prasad, Jyotirmay Banerjee, Analysis of flow and thermal field in nanofluid using a single phase thermal dispersion model, Applied Mathematical Modelling, Volume 34, Issue 3, 2010, pp573-592.
127. Ambreen T, Saleem A, Park CW. Homogeneous and Multiphase Analysis of Nanofluids Containing Nonspherical MWCNT and GNP Nanoparticles Considering the Influence of Interfacial Layering. Nanomaterials (Basel). 2021;11(2):277.
128. M. Sanjosé, J.M. Senoner, F. Jaegle, B. Cuenot, S. Moreau, T. Poinsot, Fuel injection model for Euler–Euler and Euler–Lagrange large-eddy simulations of an evaporating spray inside an aeronautical combustor, International Journal of Multiphase Flow, Volume 37, Issue 5, 2011, pp 514-529.
129. Jigar Parekh, Roland Rzehak, Euler–Euler multiphase CFD-simulation with full Reynolds stress model and anisotropic bubble-induced turbulence, International Journal of Multiphase Flow, Volume 99, 2018, pp 231-245.

130. Saman Rashidi, Shima Akar, Masoud Bovand, Rahmat Ellahi, Volume of fluid model to simulate the nanofluid flow and entropy generation in a single slope solar still, Renewable Energy, Volume 115, 2018, pp 400-410.
131. Leina Hua, Hu Zhao, Jun Li, Junwu Wang, Qingshan Zhu, Eulerian–Eulerian simulation of irregular particles in dense gas–solid fluidized beds, Powder Technology, Volume 284, 2015, pp 299-311.
132. Manninen M, Taivassalo V, Kallio S. On the mixture model for multiphase flow. Espoo: VTT Technical Research Centre of Finland, 1996. 67 p. (VTT Publications; No. 288).
133. Mohammad Hesam Toosi, Majid Siavashi, Two-phase mixture numerical simulation of natural convection of nanofluid flow in a cavity partially filled with porous media to enhance heat transfer, Journal of Molecular Liquids, Volume 238, 2017, pp 553-569.
134. Guangli He, Yohtaro Yamazaki, Abuliti Abudula, A droplet size dependent multiphase mixture model for two phase flow in PEMFCs, Journal of Power Sources, Volume 194, Issue 1, 2009, Pages 190-198.
135. C.Y. Wang, P. Cheng, A multiphase mixture model for multiphase, multicomponent transport in capillary porous media—I. Model development, International Journal of Heat and Mass Transfer, Volume 39, Issue 17, 1996, Pages 3607-3618.
136. Maxwell, J.C., "Treatise on Electricity and Magnetism", Oxford, Clarendon Press, 1873.
137. W. Yu and S.U.S. Choi, "The Role of Interfacial Layers in the Enhanced Thermal Conductivity of Nanofluids: A Renovated Maxwell Model, " Journal of Nanoparticle Research volume 5, 2003, pp167–171.
138. Hamilton, R.L., Crosser O. K., "Thermal Conductivity of Heterogeneous Two Component Systems", *Industrial&Engineering Chemistry Fundumentals*, Vol 1, 1963, pp 187-191.
139. Elena V. Timofeeva, Alexei N. Gavrilov, James M. McCloskey, Yuriy V. Tolmachev, Samuel Sprunt, Lena M. Lopatina, and Jonathan V. Selinger, 'Thermal conductivity and particle agglomeration in alumina nanofluids: Experiment and theory,' Phys. Rev, Vol. 76, Iss. 6, 2007.
140. Pak, B.B., Cho, Y.I., "Hydrodynamic and Heat Transfer Study of Dispersed Fluids with Submicron Metallic Oxide Particles", *J. Experimental Heat Transfer*, Vol 11, 1998, pp 151-170.
141. Buongiorno, J. (August 15, 2005). "Convective Transport in Nanofluids." ASME. J. Heat Transfer. March 128(3), 2006, pp 240–250.
142. Sheng-Qi Zhoua, and Rui Ni, "Measurement of the specific heat capacity of water-based Al_2O_3 nanofluid, " Appl. Phys. Lett. 92, 093123, 2008.
143. Einstein, A., "Eine neue Bestimmung der Molekuldimensionen", Annalen der Physik, Vol 19, 1906, pp 289-306.

144. Gabriela Huminic, Angel Huminic, Claudiu Fleacă, Florian Dumitrache, Ion Morjan, Experimental study on viscosity of water based Fe–Si hybrid nanofluids, Journal of Molecular Liquids, Volume 321, 2021, 114938.
145. Goodwin J W, Colloids and Interfaces with Surfactants and Polymers—An Introduction, 2004, John Wiley & Sons.
146. Brinkman, H. C., "The Viscosity of Concentrated Suspensions and Solution", J. Chem. Phys, Vol 20, 1952, pp. 571-581.
147. Frankel, N. A., Acrivos A., "On the Viscosity of a Concentrat Suspension of Solid Spheres", *Chem. Engrg. Sci*, Vol 22, 1967, pp 847-853.
148. Irvin M. Krieger and Thomas J. Dougherty, "A Mechanism for Non-Newtonian Flow in Suspensions of Rigid Spheres, " Transactions of the Society of Rheology 3, 137, 1959.
149. Batchelor, G. K., "The Effect of Brownian Motion on The Bulk Stress in a Suspension of Spherical Particles", *J. Fluid Mech*, Vol 83, 1977, pp 97-117.
150. Haisheng Chen, Yulong Ding, and Chunqing Tan, "Rheological behaviour of nanofluids, " New Journal of Physics, Volume 9, 2007.
151. Rudyak, V.Y., Minakov, A.V., Guzey, D.V. et al. On laminar-turbulent transition in nanofluid flows. Thermophys. Aeromech. 23, 2016, pp 773–776.
152. Sunil Kumar, Alok Darshan Kothiyal, Mangal Singh Bisht, Anil Kumar, Turbulent heat transfer and nanofluid flow in a protruded ribbed square passage, Results in Physics, Volume 7, 2017, Pages 3603-3618.
153. Abdulrazzaq, T., Togun, H., Goodarzi, M. et al. Turbulent heat transfer and nanofluid flow in an annular cylinder with sudden reduction. J Therm Anal Calorim 141, 373–385 (2020).
154. Alina Adriana Minea, Numerical studies on heat transfer enhancement and synergy analysis on few metal oxide water based nanofluids, International Journal of Heat and Mass Transfer, Volume 89, 2015, pp 1207-1215.
155. Doohyun Kim, Younghwan Kwon, Yonghyeon Cho, Chengguo Li, Seongir Cheong, Yujin Hwang, Jaekeun Lee, Daeseung Hong, Seongyong Moon, Convective heat transfer characteristics of nanofluids under laminar and turbulent flow conditions, Current Applied Physics, Volume 9, Issue 2, Supplement, 2009, pp 119-123.
156. Wilcox, D. C., "Turbulence Modeling for CFD, " DCW Industries, Inc., 5354 Palm Drive, La Canada, Calif., 2006.
157. Patel, H. E., Sundararajan T., Pradeep T., Dasgupta A., Dasgupta N., Das, S. K., "A Micro-Convection Model for Thermal Conductivity of Nanofluids", Pramana — *J. Phys*, Vol 65, no. 5, 2005, pp 863–869.
158. Ioan Sarbu, Calin Sebarchievici, "A Comprehensive Review of Thermal Energy Storage," *Journal Sustainability*, 2018, 10(1), 191.
159. Alvaro de Gracia, Luisa F. Cabeza, Phase change materials and thermal energy storage for buildings, Energy and Buildings, Volume 103, 2015, pp 414-419.

160. F.S. Javadi, H.S.C. Metselaar, P. Ganesan, Performance improvement of solar thermal systems integrated with phase change materials (PCM), a review, Solar Energy, Volume 206, 2020, pp 330-352.
161. Leonard Wagner, " Overview of energy storage methods, " Research report, Mora Associates Ltd, 2007.
162. V. Zipf, A. Neuhäuser, C. Bachelier, R. Leithner, W. Platzer, Assessment of Different PCM Storage Configurations in a 50 MWel CSP Plant with Screw Heat Exchangers in a Combined Sensible and Latent Storage – Simulation Results, Energy Procedia, Volume 69, 2015, Pages 1078-1088.
163. Innovation Outlook: Thermal Energy Storage, IRENA, International Renewable Energy Agency, 2020.
164. J. Sarwar, B. Mansoor, Characterization of thermophysical properties of phase change materials for non-membrane based indirect solar desalination application, Energy Conversion and Management, Volume 120, 2016, pp 247-256.
165. Jahangiri A, Ahmadi O, "Numerical investigation of enhancement in melting process of PCM by using internal fins," *J Therm Anal Calorim*, 2019;137(6):1–8.
166. Usman H, Ali HM, Arshad A, Ashraf MJ, Khushnood S, Janjua MM, et al, "An experimental study of PCM based finned and un-finned heat sinks for passive cooling of electronics," *Heat Mass Transf*, 2018,54:3587–98.
167. Vasu A, Hagos FY, Noor MM, Mamat R, Azmi WH, Abdullah AA, Ibrahim TK, "Corrosion effect of phase change materials in solar thermal energy storage application," *Renew Sustain Energy Rev*, 2017,76:19–33.
168. Shili H, Fahem K, Harmand S, Ben Jabrallah S, "The effect of water's presence around the Phase Change Material," *Therm Sci*, 2019,OnLine-First (00):301-301.
169. Mohammad Irfan Lone, Ravindra Jilte, "A review on phase change materials for different applications," *Materials Today: Proceedings*, 2021, ISSN 2214-7853.
170. J.P. Sharma, R. Jilte, "A review on pure fatty acid-based phase change materials for energy storage applications," *J. Emerg. Technol. Innov. Res*., 5 (10), 2018, pp. 270-276.
171. A. Sharma, V.V. Tyagi, C.R. Chen, D. Buddhi, "Review on thermal energy storage with phase change materials and applications," 13, 2009, 318–345,
172. D. Zhou, C.Y. Zhao, Y. Tian, "Review on thermal energy storage with phase change materials (PCMs) in building applications," *Appl. Energy*, 92 (2012), pp. 593-605.
173. A.S. Fleischer, "Thermal energy storage using phase change materials: Fundamentals and applications," *SpringerBriefs Appl. Sci. Technol*., no. 9783319209210, 2015.
174. Giménez P, et al, "Effect of an increased thermal contact resistance in a salt PCM graphite foam composite TES system," *Renew Energy*, 2017, 106:321–34.
175. Ianniciello L, Biwolé P H, "Achard P Electric vehicles batteries thermal management systems employing phase change materials," *J Power Sources*, 2018, 378:383–403.

176. C. Suresh, R.P. Saini, “Experimental study on combined sensible-latent heat storage system for different volume fractions of PCM,” *Solar Energy*, Vol 212, 2020, pp 282-296.
177. Ahmed, N. & Elfeky, K.E. & Lu, Lin & Wang, Q.W., "Thermal performance analysis of thermocline combined sensible-latent heat storage system using cascaded-layered PCM designs for medium temperature applications," Renewable Energy, Elsevier, vol. 152(C), 2020, pp 684-697.
178. Bazri S, Badruddin IA, Naghavi MS, Bahiraei M. “A review of numerical studies on solar collectors integrated with latent heat storage systems employing fins or nanoparticles,” *Renew Energy*, 2018,118:761–78.
179. Helbing, T.B., Schmitz, G. “Experimental and numerical analysis of composite latent heat storage in cooling systems for power electronics,” *Heat Mass Transfer*, 2019, 55**,** 2949–2958.
180. Qudama Al-Yasiri, andMárta Szabó, “Performance Assessment of Phase Change Materials Integrated with Building Envelope for Heating Application in Cold Locations,” *European Journal of Energy Research*, 2021, ISSN: 2736-5506.
181. Wei Tian, Shuo Dang, Gang Liu, Zengxu Guo, Xiaohu Yang, “Thermal transport in phase change materials embedded in metal foam: evaluation on inclination configuration,” *Journal of Energy Storage*, Vol 33, 2021, 102166.
182. Yang G, Yim Y-J, Lee JW, Heo Y-J, Park S-J. “Carbon-Filled Organic Phase-Change Materials for Thermal Energy Storage: A Review,” *Molecules*. 2019; 24(11):2055.
183. Yinxu Zhao, Xuelai Zhang, Weisan Hua, “Review of preparation technologies of organic composite phase change materials in energy storage,” *Journal of Molecular Liquids*, 2021, 115923, ISSN 0167-7322.
184. Fei Xue, Xiao-dong Qi, Ting Huang, Chang-yu Tang, Nan Zhang, Yong Wang, “Preparation and application of three-dimensional filler network towards organic phase change materials with high performance and multi-functions,” *Chemical Engineering Journal*, Vol 419, 2021, 129620, ISSN 1385-8947.
185. Kalidasan B, A.K. Pandey, Syed Shahabuddin, Mathew George, Kamal Sharma, M. Samykano, V.V. Tyagi, R. Saidur, “Synthesis and characterization of conducting Polyaniline@cobalt-Paraffin wax nanocomposite as nano-phase change material: Enhanced thermophysical properties,” *Renewable Energy*, Vol 173, 2021, pp 1057-1069, ISSN 0960-1481.
186. Anna W. Kuziel, Grzegorz Dzido, Roman Turczyn, Rafał G. Jędrysiak, Anna Kolanowska, Anna Tracz, Wojciech Zięba, Aleksandra Cyganiuk, Artur P. Terzyk, Sławomir Boncel, “Ultra-long carbon nanotube-paraffin composites of record thermal conductivity and high phase change enthalpy among paraffin-based heat storage materials,” *Journal of Energy Storage*, Vol 36, 2021, 102396, ISSN 2352-152X.

187. Ukrainczyk, N., Kurajica, S., & Šipušić, J. "Thermophysical Comparison of Five Commercial Paraffin Waxes as Latent Heat Storage Materials," *Chemical and Biochemical Engineering Quarterly 24*, 2010, 129-137.
188. Ali Bashiri Rezaie, Majid Montazer, "Shape-stable thermo-responsive nano Fe3O4/fatty acids/PET composite phase-change material for thermal energy management and saving applications," *Applied Energy*, Vol 262, 2020, 114501, ISSN 0306-2619.
189. Yana Galazutdinova, Svetlana Ushak, Mohammed Farid, Said Al-Hallaj, Mario Grágeda, "Development of the inorganic composite phase change materials for passive thermal management of Li-ion batteries: Application," *Journal of Power Sources*, Vol 491, 2021, 229624, ISSN 0378-7753.
190. Zhenghui Shen, Kyudeok Oh, Soojin Kwon, Martti Toivakka, Hak Lae Lee, "Use of cellulose nanofibril (CNF)/silver nanoparticles (AgNPs) composite in salt hydrate phase change material for efficient thermal energy storage," *International Journal of Biological Macromolecules*, Vol 174, 2021, pp 402-412, ISSN 0141-8130.
191. Jiaming Bao, Deqiu Zou, Sixian Zhu, Qun Ma, Yinshuang Wang, Yunping Hu, "A medium-temperature, metal-based, microencapsulated phase change material with a void for thermal expansion," *Chemical Engineering Journal*, Vol 415, 2021, 128965, ISSN 1385-8947.
192. T.J. Lu, "Thermal management of high-power electronics with phase change cooling," *International Journal of Heat and Mass Transfer*, Vol 43, Issue 13, 2000, pp 2245-2256.
193. Sachin Rana, Mohammad Zunaid, Rajesh Kumar, "CFD simulation for heat transfer enhancement in phase change materials," *Materials Today: Proceedings*, 2021, ISSN 2214-7853.
194. Takashi Morimoto, Motoki Sugiyama, Hiroyuki Kumano, "Experimental study of heat transfer characteristics of phase change material emulsions in a horizontal circular tube," *Applied Thermal Engineering*, Vol 188, 2021, 116634, ISSN 1359-4311.
195. S. KumarSahoo, M. K. Das, P. Rath, "Application of TCE-PCM based heat sinks for cooling of electronic components: A review," *Renewable and Sustainable Energy Reviews*, Vol. 59, pp. 550–582, 2016.
196. M. Telkes, E. Raymond. "Storing solar heat in chemicals—a report on the Dover house," *Heat Vent* 46 (11) (1949) 80–6.
197. EM. Sparrow, ED. Larson, JW. Ramsey, "Freezing on a finned tube for either conduction-controlled or natural-convection-controlled heat transfer," *International Journal of Heat and Mass Transfer*, Vol. 24, 1981, pp. 273–84.
198. DJ. Morison, SI. Abdel-Khalik, "Effects of phase-change energy storage on the performance of air-based and liquid-based solar heating systems," *Solar Energy*, Vol. 20,1978, pp. 57–67.

199. R. Marshal, C. Dietsche, "Comparisons of paraffin wax storage subsystem models using liquid heat transfer media," *Solar Energy*, Vol.29,1982, pp.503–511.
200. U. Stritih, "An experimental study of enhanced heat transfer in rectangular PCM thermal storage," *International Journal of Heat and Mass Transfer*, Vol.47, 2004, pp. 2841–7.
201. KAR. Ismail, JR. Henriquez, LFM. Moura, MM. Ganzarolli. "Ice formation aroundisothermal radial finned tubes," *Energy Conversion and Management*, Vol.41, 2000, pp.585–605.
202. F. Agyenim, P. Eames, M. Smyth. "A comparison of heat transfer enhancement in medium temperature thermal energy storage heat exchanger using fins and multitubes," *ISES Solar World Congress*, Vol.13, 2007, pp.2726–30.
203. M.J. Hosseini, M. Rahimi, R. Bahrampouri, "Experimental and computational evolution of a shell and tube heat exchanger as a PCM thermal storage system," *International Communication in Heat and Mass Transfer*, Vol.50, 2014, pp. 128–136.
204. M. Rahimi, A.A. Ranjbar, D.D. Ganji, K. Sedighi, M.J. Hosseini, R. Bahrampoury, "Analysis of geometrical and operational parameters of PCM in a fin and tube heat exchanger," *International Communications in Heat and Mass Transfer*, Vol.53, 2014, pp. 109–115.
205. M.J. Hosseini, A.A. Ranjbar, K. Sedighi, M. Rahimi, "A combined experimental and computational study on the melting behavior of a medium temperature phase change storage material inside shell and tube heat exchanger," *International Communication in Heat and Mass Transfer*, vol.9, 2012, pp.1416–1424.
206. Z. Liu, X. Sun, C. Ma, "Experimental study of the characteristics of solidification of stearic acid in an annulus and its thermal conductivity enhancement," *Energy Conversion and Management*, vol.46, 2005, pp. 971–984.
207. M.J. Hosseini, A.A. Ranjbar, M. Rahimi, R. Bahrampouri, "Experimental and numerical evaluation of longitudinally finned latent heat thermal storage systems," *Energy and Buildings*,Vol.99, 2015, pp. 263–272.
208. AG. Bathelt, R. Viskanta. "Heat transfer at the solid–liquid interface during melting from a horizontal cylinder," *International Journal of Heat and Mass Transfer*, Vol.23, 1980, pp.1493–503.
209. H.M. Ettouney, I. Alatiqi, M. Al-Sahali, S.A. Al-Ali, "Heat transfer enhancement by metal screens and metal spheres in phase change energy storage systems," *Renewable Energy*, Vol.29, 2004, pp.841–860.
210. M. Akgün, O. Aydın, K. Kaygusuz, "Experimental study on melting/solidification characteristics of a paraffin as PCM," *Energy Conversion and Management*, Vol.48,2007, pp.669–678.
211. R. Vyshak, G. Jilani, "Numerical analysis of latent heat thermal energy storage system," *Energy Conversion and Management*, Vol. 48, 2007, pp. 2161–2168.

212. Y. Pahamli, M.J. Hosseini, A.A. Ranjbar, R. Bahrampoury, "Analysis of the effect of eccentricity and operational parameters in PCM-filled single-pass shell and tube heat exchangers," *Renewable Energy*, Vol. 97, 2016, pp.344-357.
213. N. Pradeep, K. Paramasivam, T. Rajesh, V. Subash Purusothamanan, S. Iyahraja, "Silver nanoparticles for enhanced thermal energy storage of phase change materials," *Materials Today: Proceedings*, Vol.17, 2020, pp 256-304.
214. Suraju Olawale Kasali, Jose Ordonez-Miranda, Karl Joulain, "Conductive thermal diode based on two phase-change materials," *International Journal of Thermal Sciences*, Vol. 153,2020, pp 178-190.
215. C. Selvam, S. Manikandan, N. Vijay Krishna, Ravita Lamba, S.C. Kaushik, Omid Mahian, "Enhanced thermal performance of a thermoelectric generator with phase change materials," *International Communications in Heat and Mass Transfer*, Vol 114, 2020, pp. 365-372.
216. . Baudot, V. Odagescu,Thermal properties of ethylene glycol aqueous solutions, Cryobiology,Volume 48, Issue 3, 2004, Pages 283-294.
217. Hairong Yue, Yujun Zhao, Xinbin Maa and Jinlong Gong, Ethylene glycol: properties, synthesis, and applications, Chem. Soc. Rev., 2012,41, 4218-4244.
218. Bohne, D., Fischer, S., Obermeier, E., 1984. Thermal conductivity, density, viscosity, and prandtl-numbers of ethylene glycol-water mixtures. Berichte der Bunsengesellschaft/Phys. Chem.Chem. Phys. 88, 739–742.
219. Sarafraz, M.M.; Safaei, M.R.; Leon, A.S.; Tlili, I.; Alkanhal, T.A.; Tian, Z.; Goodarzi, M.; Arjomandi, M. Experimental Investigation on Thermal Performance of a PV/T-PCM (Photovoltaic/Thermal) System Cooling with a PCM and Nanofluid. *Energies* 2019, *12*, 2572.
220. Almurtaji S, Ali N, Teixeira JA, Addali A. On the Role of Nanofluids in Thermal-hydraulic Performance of Heat Exchangers-A Review. Nanomaterials (Basel). 2020;10(4):734. Published 2020 Apr 11. doi:10.3390/nano10040734.
221. Shah, T.R.; Ali, H.M.; Janjua, M.M. On Aqua-Based Silica (SiO2–Water) Nanocoolant: Convective Thermal Potential and Experimental Precision Evaluation in Aluminum Tube Radiator. *Nanomaterials* 2020, *10*, 1736.
222. Benedict, F.; Kumar, A.; Kadirgama, K.; Mohammed, H.A.; Ramasamy, D.; Samykano, M.; Saidur, R. Thermal Performance of Hybrid-Inspired Coolant for Radiator Application. *Nanomaterials* 2020, *10*, 1100.
223. Li, Z.; Li, W.; Chen, Z. Performance Analysis of Thermoelectric Based Automotive Waste Heat Recovery System with Nanofluid Coolant. *Energies* 2017, *10*, 1489.
224. Deriszadeh, A.; de Monte, F. On Heat Transfer Performance of Cooling Systems Using Nanofluid for Electric Motor Applications. *Entropy* 2020, *22*, 99.
225. Parsaiemehr M, Pourfattah F, Ali Akbari O, Toghraie D, Sheikhzadeh G 2018 Turbulent flow and heat transfer of Water/Al_2O_3 nanofluid inside a rectangular ribbed channel, Physica E: Low-dimensional Systems and Nanostructures, pp 73-84.
226. Kedar N. Shukla, Thomas M. Koller, Michael H. Rausch, Andreas P. Fröba, Effective thermal conductivity of nanofluids – A new model taking into consideration Brownian motion, International Journal of Heat and Mass Transfer, Volume 99, 2016, Pages 532-540.
227. S. K. Das, S. U. S. Choi, W. Yu, and T. Pradeep, Nanofluids Science and Technology, John Wiley & Sons, Hoboken, NJ, USA, 2008.

228. Akbari OA, Toghraie D, Karimipour A. Impact of ribs on flow parameters and laminar heat transfer of water–aluminum oxide nanofluid with different nanoparticle volume fractions in a three-dimensional rectangular microchannel. Advances in Mechanical Engineering. 2015.

229. Tang L, Tang Y, Parameswaran S. A numerical study of flow characteristics in a helical pipe. Advances in Mechanical Engineering. July 2016.

230. Ping Li, Di Zhang, Yonghui Xie, Heat transfer and flow analysis of Al_2O_3–water nanofluids in microchannel with dimple and protrusion, International Journal of Heat and Mass Transfer, Volume 73, 2014, Pages 456- 67.

231. Pourfattah, F. and Sabzpooshani, M., 2020, "Thermal management of a power electronic module employing a novel multi-micro nozzle liquid-based cooling system: A numerical study", Int. J. Heat Mass Transf., Vol. 147 pp. 118928.

232. Kulkarni, D.P., Rupertus, G., Chen, E., 2012, "Experimental Investigation of Contact Resistance for Water Cooled Jacket for Electric Motors and Generators", IEEE Trans. Energy Convers., Vol. 27, pp. 204–210.

233. Kandasamy, R., Wang, X.-Q., Mujumdar, A.S., 2008, "Transient cooling of electronics using phase change material (PCM)-based heat sinks", Appl. Therm. Eng., Vol. 28, pp. 1047–1057.

234. Pakrouh, R., Hosseini, M.J., Ranjbar, A.A., Bahrampoury, R., 2015, "A numerical method for PCM-based pin fin heat sinks optimization", Energy Convers. Manag., Vol. 103, pp. 542–552.

235. Dammak, K. and El Hami, A., 2021, "Thermal reliability-based design optimization using Kriging model of PCM based pin fin heat sink", Int. J. Heat Mass Transf., Vol. 166, pp. 120745.

236. Yousef, M.S., Hassan, H., Kodama, S., Sekiguchi, H., 2019, "An experimental study on the performance of single slope solar still integrated with a PCM-based pin-finned heat sink", Energy Procedia., Vol. 156, pp. 100–104.

237. Tikadar, A., Johnston, D., Kumar, N., Joshi, Y., Kumar, S., 2021, "Comparison of electro thermal performance of advanced cooling techniques for electric vehicle motors", Appl. Therm. Eng, Vol. 183, pp. 116182.

238. Sharma, A., Chauhan, R., Ali Kallioğlu, M., Chinnasamy, V., Singh, T., 2020, "A review of phase change materials (PCMs) for thermal storage in solar air heating systems", Mater. Today Proc.

239. Ran, F., Chen, Y., Cong, R., Fang, G., 2020, "Flow and heat transfer characteristics of microencapsulated phase change slurry in thermal energy systems: A review", Renew. Sustain. Energy Rev., Vol., pp. 110101.

240. Guo, Y., Yang, H., Fu, W., Bai, L., Miao, J., 2021, "Temperature control of star sensor baffle using 3D printing and PCM thermal energy storage technology", Int. J. Heat Mass Transf., Vol. 165, pp. 120644.

241. Wang, J.-X., Li, Y.-Z., Wang, S.-N., Zhang, X. Ning, H.-S., Guo, W., 2016, "Experimental investigation of the thermal control effects of phase change material based packaging strategy for on-board permanent magnet synchronous motors", Energy Convers. Manag., Vol. 123, pp. 232–242.

242. Wang, S., Li, Y., Li, Y.-Z., Wang, J., Xiao, X. , Guo, W., 2016, "Transient cooling effect analyses for a permanent-magnet synchronous motor with phase-change-material packaging", Appl. Therm. Eng., Vol. 109, pp. 251–260.

243. Hosseini, M.J., Ranjbar, A.A., Sedighi, K., Rahimi, M., 2012, " A combined experimental and computational study on the melting behavior of a medium temperature phase change storage material inside shell and tube heat exchanger", Int. Commun. Heat Mass Transf., Vol. 39, pp. 1416–1424.

244. Hosseinizadeh, S.F., Tan, F.L., Moosania, S.M., 2011, "Experimental and numerical studies on performance of PCM-based heat sink with different configurations of internal fins", Appl. Therm. Eng., Vol. 31, pp. 3827–3838.

245. Yang, Y.P.; Shih, G.Y. Optimal Design of an Axial-Flux Permanent-Magnet Motor for an Electric Vehicle Based on Driving Scenarios. ***Energies*** **2016**, ***9***, 285.

UNIVERSITÀ DEGLI STUDI DELL'AQUILA

DIPARTIMENTO DI INGEGNERIA INDUSTRIALE E DELL'INFORMAZIONE E DI ECONOMIA

La borsa di dottorato è stata cofinanziata con risorse del Programma Operativo Nazionale 2014-2020 (CCI 2014IT16M2OP005), Fondo Sociale Europeo, Azione I.1 "Dottorati Innovativi con caratterizzazione industriale"